INTERROGATION OF THE CARDIAC ELECTROANATOMICAL SUBSTRATE

by

Joshua Jacob Evans Blauer

A dissertation submitted to the faculty of
The University of Utah
in partial fulfillment of the requirements for the degree of

Doctor of Philosophy

Department of Bioengineering

The University of Utah

December 2015

The University of Utah Graduate School

STATEMENT OF DISSERTATION APPROVAL

The dissertation of **Joshua Jacob Evans Blauer**

has been approved by the following supervisory committee members:

Robert S. MacLeod	, Chair	**7/8/2015** Date Approved
Ravi Ranjan	, Member	**7/8/2015** Date Approved
Nassir F. Marrouche	, Member	**7/8/2015** Date Approved
Frank Sachse	, Member	**7/10/2015** Date Approved
Edward Hsu	, Member	**7/8/2015** Date Approved

and by **Patrick A. Tresco**, Chair/Dean of

the Department/College/School of **Bioengineering**

and by David B. Kieda, Dean of The Graduate School.

ABSTRACT

Atrial fibrillation (AF) is the leading cause of ischemic stroke and is the most commonly observed arrhythmia in clinical cardiology. Catheter ablation of AF, in which specific regions of cardiac anatomy associated with AF are intenionally injured to create scar tissue, has been honed over the last 15 years to become a relatively common and safe treatment option. However, the success of these anatomically driven ablation strategies, particularly in hearts that have been exposed to AF for extended periods, remains poor. AF induces changes in the electrical and structural properties of the cardiac tissue that further promotes the permanence of AF. In a process known as electroanatomical (EAM) mapping, clinicians record time signals known as electrograms (EGMs) from the heart and the locations of the recording sites to create geometric representations, or maps, of the electrophysiological properties of the heart. Analysis of the maps and the individual EGM morphologies can indicate regions of abnormal tissue, or substrates that facilitate arrhythmogenesis and AF perpetuation. Despite this progress, limitations in the control of devices currently used for EAM acquisition and reliance on suboptimal metrics of tissue viability appear to be hindering the potential of treatment guided by substrate mapping.

In this research, we used computational models of cardiac excitation to evaluate parameters of EAM that affect the performance of substrate mapping. These models, which have been validated with experimental and clinical studies, have yielded new insights into the limitations of current mapping systems, but more importantly, they guided us to develop new systems and metrics for robust substrate mapping. We report here on the progress in these simulation studies and on novel measurement approaches that have the potential to improve the robustness and precision of EAM in patients with arrhythmias.

Appropriate detection of proarrhythmic substrates promises to improve ablation of AF beyond rudimentary destruction of anatomical targets to directed targeting of complicit tissues. Targeted treatment of AF sustaining tissues, based on the substrate mapping approaches described in this dissertation, has the potential to improve upon the efficacy of current AF treatment options.

For all those who have inspired and supported me.

CONTENTS

ACKNOWLEDGMENTS

The call of science can be exhilarating. Fascination with the mechanisms that underpin nature and our very own bodies drives men and women to lofty aspirations. The quest to learn more, solve pervasive problems, and to simply sate one's curiosity are the lifeblood of scientific endeavor. With lofty aims, and a sense of a noble pursuit, it is then easy for one to become carried away. Occasionally, our otherwise worthy goals exceed feasibility, individual capabilities, and especially our own personal resolve. Through the course of this modest body of work, I have encountered each of these obstacles and, but for a tremendous network of support, would have surely been undone. For those who have facilitated, enlightened, and encouraged me through this process, I am incredibly grateful.

I am grateful to my mentors. I am grateful to Dr. Rob MacLeod for support, guidance, lots of patience, and especially the willingness to help clean up messes I have made along the way. I am thankful to Dr. Nassir Marrouche for believing in me and accepting me into his group. I am thankful to Dr. Ravi Ranjan for mentorship and a sense of partnership in our work. For sharing their collective knowledge and experience, I give my sincere appreciation.

I am grateful for my lab mates, colleagues, and coauthors with whom I have had the opportunity to associate. I thank Darrell, Brett, Jess, Kedar, Josh, Nathan, Gernot, Anders, Eugene, Sathya, Gene, Nelly, Koji, Jose, Jayne, and many others. I am thankful for the students I have had the opportunity to mentor and learn from, including Chris, Swati, Greg, Andrew, Jesse, and Shawn.

Most of all I am thankful to my family. My wife and children have been so patient and supportive of their husband and father who has had a little too much of an affinity for school. I am thankful to parents and siblings and friends who have also provided significant support, especially the babysitting crew of Mom, Janet, Sarah, and Michelle. We could not have done it without you.

Finally, I am eternally grateful for the Architect of all that we seek to uncover with science. For the beauty, power, and possibility of this world that inspires us to seek knowledge.

CHAPTER 1

MULTISCALE MODELS OF SUBSTRATE MAPPING

The presence of cardiac scarring or fibrosis is a topic of great interest and study in cardiac electrophysiology, primarily because it can lead to and exacerbate life-threatening arrhythmias, such as atrial fibrillation or ventricular tachycardia [1, 2]. Normal cardiac conduction depends on organized propagation of excitation waterfronts. The presence of inexcitable scar tissue or regions of fibrosis—which we define very broadly as pathological changes in the nature and volume of the extracellular matrix (see Section 3.4.2)—can slow, disrupt, and detour normal activation sequences and may create a substrate in which an arrhythmia can initiate. For example, in cases of cell death incurred following myocardial infarction, scar tissues can form an anatomical substrate conducive to what is known as macroreentrant ventricular tachycardia (VT) [3]. Fibrosis does not generally render tissue completely inexciatable, but partially decouples myocytes, which increases intracellular resistance and renders conduction pathways more tortuous. The effect of these changes is slower and less uniform spread of activation impulses, which creates an ideal substrate for arrhythmogenesis, as seen, for example, in atrial fibrillation [4, 5]. Regardless of whether the diseased substrate is in the ventricles or atria, these arrhythmias may present as paroxysmal episodes that resolve quickly, or they may persist and require medical intervention, in the form of drugs or electrical cardioversion, to restore sinus rhythm. The mechanisms by which scarred and fibrotic substrates facilitate reentry may differ, but they share the common feature of an abnormal substrate disrupting normal impulse propagation in a manner that increases the propensity for arrhythmogenesis. Consequently, efforts to improve the treatment of persistent VT and atrial fibrillation (AF) have focused on the identification and targeted treatment of diseased, fibrotic substrates [6, 7].

Identification of abnormal cardiac substrates currently occurs by means of two orthogonal imaging modalities: magnetic resonance imaging (MRI) and electroanatomical mapping (EAM). Various groups, including ours, have shown that late gadolinium-enhanced (LGE)

MRI can identify scarring and fibrosis in both the ventricles and atria (Fig. 1.1 A and B) [8, 9, 10, 11]. These studies indicate that the location, extent, and presentation of these abnormal substrates contribute to the initiation and entrenchment of cardiac arrhythmias. As yet, however, analysis of MRI images cannot characterize the specific triggers, pathways of reentry, or mechanisms that are critical to arrhythmogenesis in an individual heart.

The current gold standard for identifying and targeting proarrhythmic cardiac substrates is electroanatomical mapping (EAM). A type of EAM known as substrate mapping is tailored to the identification of proarrhythmic substrate based on electrical signals recorded from the cardiac tissue. Specifically, electrodes are navigated to the surface of the heart (both the more typical inner surface, endocardium, or the outer surface, epicardium) to record the local electric potentials (Fig. 1.1 C). Numerous studies have shown that disruption of normal cardiac tissue affects the conduction of excitation wavefronts through the myocardium and consequently changes the morphology of electric potentials in the vicinity of that disruption [12, 13, 14, 15, 10]. When the spatial positions of these electrodes are recorded and the morphology of electrograms (EGM) is captured, a map of cardiac tissue health can be constructed. Maps generated during sinus rhythm, i.e., regular activation of the heart, or during arrhythmia have been used to identify regions with arrhythmogenic

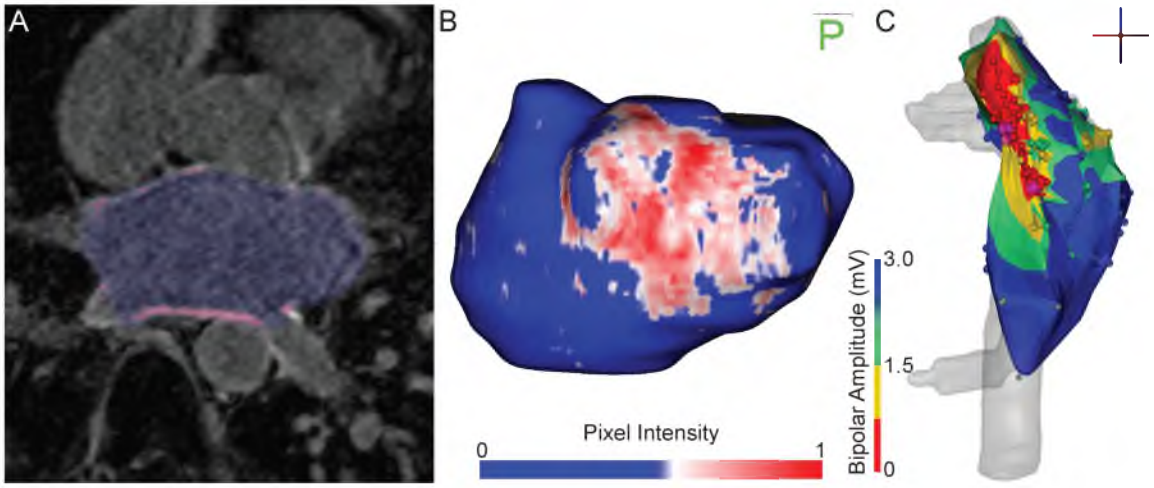

Fig. 1.1. Examples of cardiac substrate characterization using MRI and EAM. A. Late gadolinium-enhanced (LGE) MRI of a human left atrium shows the formation of scar tissue 3 months following an ablation procedure for atrial fibrillation. B. Segmentation and image analysis of the MRIs allows visualization of regions of scarring or structural remodeling (red and white regions in this image). C. Voltage map of swine right atrium shows the creation of two point lesions by radio frequency ablation (purple spheres). Electrograms acquired in regions surrounding the ablation lesions contain low bipolar amplitude activation signals (< 1.5 mV), indicating that normal cardiac conduction has been disrupted.

properties and to propose targets for ablation to restore and maintain sinus rhythm. However, various challenges limit the efficacy of clinical substrate mapping, and a major goal of this research was to combine experimental and simulation approaches to address some of these challenges.

As an example of the challenges of EAM, little is known about the impact of electrode size, configuration, or orientation on the accuracy of EAM-based assessment of the myocardium. Furthermore, robust experimental characterization of these parameters is limited due to challenges associated with controlling the interaction of recording devices, cardiac tissue, and activation wavefronts. However, emerging clinical technologies, combined with the ability to create realistic computational models of cardiac propagation and measurement, have the potential to overcome many of the current limitations associated with substrate mapping. The role of computational modeling is of special interest in this research. The National Institute of Health (NIH), Food and Drug Administration (FDA), and National Science Foundation (NSF) are committed to the development of "predictive, computational models that encompass multiple biological and behavior scales" in order to "efficiently and effectively address the challenges of understanding multiscale biological and behavioral systems" [16]. According to the FDA "[the] development of predictive models ... that advance our understanding of the performance of medical products in humans are of greatest interest" [16]. These ambitions apply especially well to the use of simulation in cardiac electrophysiology, which is a rapidly evolving field that depends heavily on medical devices and drugs. For example, specific features of intracardiac EGMs acquired during EAM procedures, e.g., low bipolar voltage, high dominant frequency, etc., have been associated with diseased cardiac substrate that causes life-threatening cardiac arrhythmias [13, 17]. However, the devices used to acquire these signals are often optimized for tasks other than the detection of diseased tissue, e.g., radio-frequency energy delivery for ablation therapy. Thus, there is a need to identify weaknesses in current measurement approaches and design new instrumentation and interpretation of measured signals from the heart. Multiscale computational models of mapping systems used for substrate characterization can help improve the selection of the most appropriate tools for a given substrate mapping application and predict the consequences of suboptimal choices.

Multiscale simulation of cardiac electrical activity is a relatively well-evolved approach with many tools and techniques that enable the modeling of a wide range of scenarios. For example, with an approximation and numerical scheme known as the bidomain [18, 19], it is possible to create computational models of both the diseased myocardium and rep-

resentations of mapping devices, proposed or in current clinical use. Results from such studies can efficiently and effectively enhance our understanding and the performance of mapping technologies [20, 21, 22]. The cardiac bidomain model has been widely adopted in cardiac research for its ability to translate phenomena that occur on a cellular level to the tissue and whole organ levels. Bidomain simulations of cardiac excitation and propagation can incorporate relevant features of both the cellular ionic currents and the myocardial substrate to produce realistic waves of excitation and extracellular electric potentials that reflect the biophysics of proarrhythmic substrates (Fig. 1.2). The bidomain formulation is a mathematical description of the relationship between the transmembrane potential (Φ_m) and electric potential in the extracellular domain (Φ_e). In this formulation, conductivity values are assigned to the intracellular and extracellular domains to form a framework in which solving the Φ_m for every element in the model allows for calculation of Φ_e. Φ_m is first calculated using models of ion channel kinetics in the cellular membrane. These models simulate action potentials based on the behavior of ion channels in different tissue types, for instance, Luo-Rudy (ventricular myocyte) or Coutemanche-Ramirez-Nattel (atrial myocyte) [23, 24]. Once Φ_e has been computed, it is used as the initial conditions from which the next iteration of Φ_m can be solved using the membrane model. In this

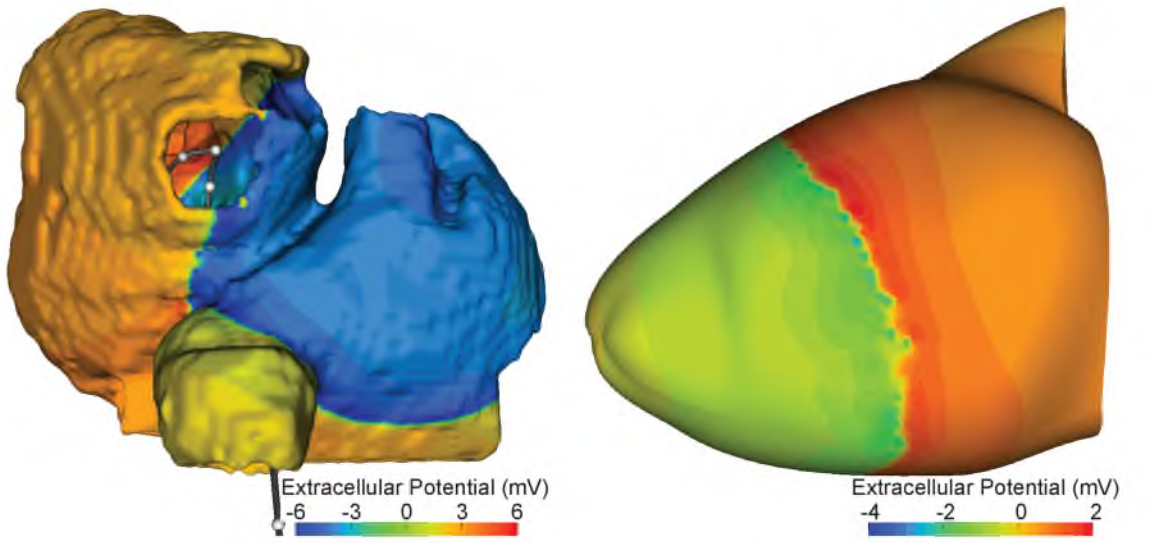

Fig. 1.2. Simulation of impulse propagation through anatomical models of cardiac tissue. The left panel shows an example of simulated propagation of excitation through a patient-specific model of human atria derived from MRIs. The gray shafts visible in the left atrium through the right inferior pulmonary vein ostia represent a catheter sampling intracardiac electrograms at two different orientations. The right panel contains a model of ventricular excitation in a rabbit heart when paced from the left ventricular apex.

manner, the bidomain formulation permits external stimuli to modulate the behavior of the ionic model and to set in motion a wave of cardiac excitation through the simulated cardiac medium. These models can incorporate many salient features of cardiac conduction, including anisotropy and regions of passive conductivity by altering conductivities or the properties of the membrane model.

To pursue the aims of this research, we have capitalized on the capabilities of the bidomain simulation to test substrate mapping systems and then validated the results through experimental and clinical mapping studies as outlined in Fig. 1.3. To conduct the simulation studies, we utilized the Cardiac Arrhythmia Research Package (CARP), a robust implementation of the bidomain model [20]. Using this powerful framework, we constructed virtual "test beds" in which existing approaches to substrate mapping were assessed for accuracy, and novel techniques for substrate characterization were explored. We recorded experimental and clinical electrograms and used them to validate our simulation studies. The investigators and facilities of the Cardiac Arrhythmia Research and Management (CARMA) Center and the Scientific Computing and Imaging (SCI) Institute of the University of Utah generously provided invaluable expertise and resources to carry this work to fruition.

1.1 Research Aims

This dissertation is comprised of three major projects that focused on the use of multi-scale computation models to evaluate electrophysiological mapping systems. The research aims address some of the clinically relevant challenges of EAM described above by assessing the performance of current clinical measures, suggesting new, or refined, approaches for cardiac substrate characterization. In limited cases, we also provided proof of concept for these novel techniques using animal and human experiments.

1.1.1 Aim 1: Characterize Voltage Mapping Performance

Voltage mapping is a valuable tool in the clinical electrophysiology laboratory for characterizing regions of diseased myocardium. Electrically active myocardium generates electric currents and fields that emanate throughout the surrounding tissue and media, generating measurable voltages [25]. The strength of these voltages is a function of the mass of depolarizing myocytes and proximity of the electrode(s) to moving wavefronts that separate depolarizing from still resting tissue. Consequently, regions of scar tissue that do not activate, or tissues in which conduction has been impaired, will generate lower extracellular voltages than healthy tissue, in the extreme insulating the electrode and producing no

discernible voltage. A voltage mapping study utilizes a catheter, often a dual purpose mapping and ablation catheter, to measure the electric potential difference, or voltage, between a probing electrode and a reference. Cardiac tissue that generates low currents during activation will appear as a region of low amplitude electric potentials in voltage mapping maps. The voltage recorded between the probe and reference will also depend on the positioning of the electrodes relative to the electric field (the gradient of extracellular voltage) generated by the propagation of activation impulses.

Bipolar EGMs are one type of extracellular voltage recorded from catheters in which the probing electrode and the reference are positioned a few millimeters apart (see Section 2.4.2). Such signals have high sensitivity for local tissue properties and are, consequently, most often used for clinical voltage mapping studies. The spatial proximity of the electrodes provides an advantageous feature known as "common mode rejection" in which the effect of any measured far field signal, i.e., electric fields generated by distant sources, is minimized in the bipolar EGM. Localized sensing permits improved discrimination between healthy and diseased tissue. During a modern clinical voltage mapping study, a navigation system tracks the location of the catheter in real time, permitting annotation of the local voltages throughout the heart for display and analysis. In this manner, regions of scarring following myocardial infarction and regions of atrial structural remodeling associated with atrial fibrillation have been detected [13, 15, 10]. However, the orientation of the electrodes with respect to the tissue and to the activation wavefront will affect the voltages measured in the bipolar EGMs. We hypothesized that the performance of clinical mapping and ablation catheters depends on the orientation of the recording electrodes with respect to activation wavefronts and the tissue and that the resulting errors will reduce sensitivity and specificity of such mapping studies.

The nature of percutaneous EAM studies, especially the inability to visualize directly the heart or mapping electrodes, precludes robust measurement of catheter orientation with respect to the cardiac anatomy. Estimation of the spatial orientation of a mapping catheter with respect to an excitation wavefront is even more limited due to the challenges associated with measuring and characterizing accurately an excitation wave. Specifically, robust determination of activation impulse direction requires either a high-resolution, multielectrode array for simultaneous acquisition during a single beat or sequential high-density activation mapping during a stable, repeated activation pattern. However, even with sufficiently high resolution, to determine the relative alignment of the catheter and activation wave, additional influences, such as errors in electrode localization, assignment of activation times,

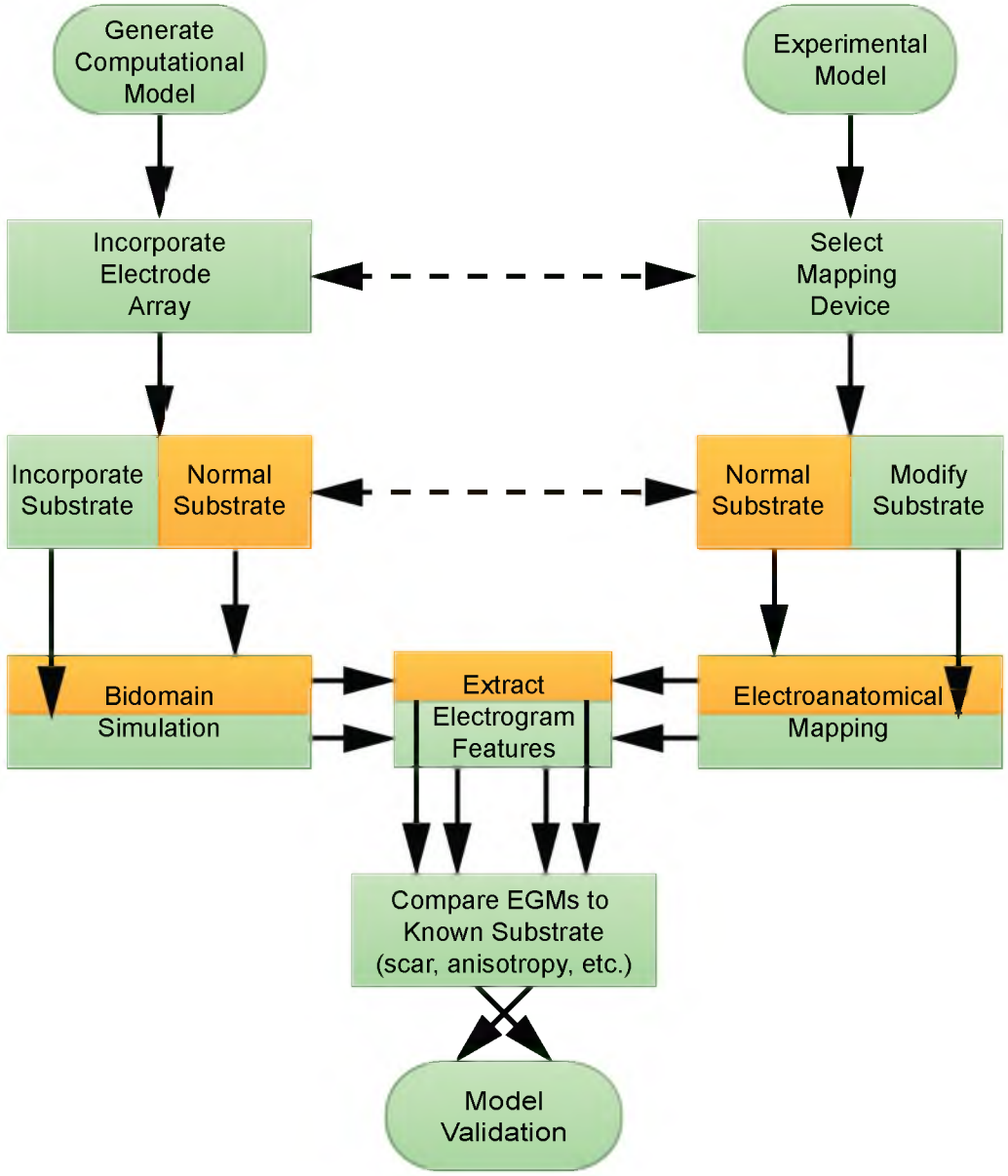

Fig. 1.3. Workflow for construction and validation of multiscale models of cardiac electrophysiology. The systems of cardiovascular disease in this research were explored using two parallel paths of investigation. To the extent possible, the computational models and experimental models implemented the same features of pathological myocardial substrate, i.e., lesion, or slowing of impulse propagation, and the same electrode geometries. Electrograms from each model were processed in the same manner for both paths, and features of the EGMs from both models were cross validated.

and interbeat variability, could obscure the spatial relationship between the catheter and activation impulse.

To access the necessary information, we constructed a computational model of cardiac excitation and simulated mapping and ablation catheters Computational models allow for explicit and virtually limitless control of variables of interest. In this case, we simulated an activation wavefront in a model of myocardial tissue and positioned the measurement electrodes of the catheter through an exhaustive sampling of possible orientations with respect to the parameters of interest. To the extent possible, we validated these computational models with the use of clinical mapping devices through in vivo experimentation with large mammals. The results of these studies helped us to parameterize the contribution of geometric factors to error in the ability of substrate mapping strategies to classify arrhythmogenic tissues.

1.1.2 Aim 2: Mapping of Multiple Activation Patterns

A further limitation of the majority of current techniques for clinical substrate mapping is that they capture electrical activity passively, with the measurement system as bystander. Specifically, whether EGMs are acquired in sinus rhythm or during arrhythmic activity, the activation sequence of the local tissue is an uncontrolled parameter. This point is especially pertinent given that ectopic beats or other forms of triggered activity, known to be critical factors in arrhythmogenesis, initiate activation patterns that differ from sinus rhythm activation (see Section 2.3.1) [26]. These aberrant activation patterns, initiated by the ectopy, may unmask proarrhythmic substrates that are innocuous during sinus conduction. For example, anatomical reentry, a common mechanism for the initiation of reentrant tachycardias, typically will not occur under conditions of sinus activation. This particular type of proarrhythmic substrate often requires the interplay of ectopy and unidirectional conduction block, due to refractory tissue, to precipitate an arrhythmia (see Section 2.3.2).

In this aim, we addressed this need for more revealing substrate mapping by developing and demonstrating the feasibility of a measurement and analysis approach based on controlled activation patterns stimulated and recorded from a trackable, multielectrode array, in this case what is known as a "lasso catheter". This approach is loosely related to a more coarse-grained application of pacing currently used to localize ectopic sources that are responsible for episodes of ventricular tachycardia (VT). In these "pace mapping" studies, a catheter is navigated to suspected sites of ectopy and interrogates each site through pacing. If the ECG waveform (12-lead electrocardiography) recorded during the pacing sufficiently

matches previously recorded, spontaneously ectopic ECGs, it is assumed the pacing location corresponds to the site of ectopy and the tissue can be ablated. However, in the pacing protocol we have developed, we analyzed not ECGs but rather electrograms EGMs recorded in proximity to each of a sequence of pacing sites to infer the properties and potential for arrhythmogenesis of the local tissue. Progressively pacing from each electrode on the array produces unique activation patterns through the local myocardium that can be recorded by the other electrodes on the array as the impulse passes. This process helps characterize the response of the tissue encompassed by the mapping array to excitation initiated across a range of activation patterns. In our studies, this examination of the tissue response to multiple activation patterns facilitated robust characterization of local tissue properties and revealed proarrhythmic substrates that were poorly discerned during sinus rhythm or arrhythmia-based substrate mapping. Identification of such proarrhythmic substrates will aid the development of next-generation therapies for diseases such as atrial fibrillation.

We evaluated conduction of activation in both longitudinal and transverse directions relative to the underlying fibers of the myocardial tissue as an initial effort towards robust characterization of proarrhythmic substrate with the multiple activation mapping technique. We used conduction velocity (CV) as a metric because it is a key factor in determining whether tissue may support reentry. More specifically, transverse CV has been shown to play an important role in wave break which, in turn, converts rapid but stable tachycardias into acutely life-threatening fibrillation (see Section 2.3.3) [27]. Previous studies have implemented pacing and recording strategies to assess conduction velocities or conduction times of cardiac tissue [28, 29]. However, these studies assessed CV at sites remote from the pacing sites with a mapping catheter, making it unclear if the velocities recorded represent longitudinal or transverse conduction, or some combination of the two. To date, no previous study has recovered transverse conduction velocities during clinical electroanatomical mapping.

A further factor that motivated our study and provides a feasible translational pathway is the appearance of a new generation of trackable multielectrode recording devices that has entered the market for clinical use, e.g., loop or basket catheters. Loop catheters, in particular, have achieved significant clinical adoption for evaluation of lesion patency surrounding the pulmonary veins in ablation of atrial fibrillation. The ubiquitous deployment, electrode tracking ability, and two-dimensional configuration of this devices make it an ideal candidate for attempting multiple activation pattern mapping in a clinical setting. In achieving this aim, we explored the feasibility of longitudinal and transverse CV measurement in

the multiple activation pattern mapping paradigm using both computational models and clinical testing. With this novel approach for extracting features of impulse propagation in the clinical setting, results from this study will help clarify the role of conduction anisotropy in the development of reentrant arrhythmias.

1.1.3 Aim 3: Simplified Conduction Velocity Measurement

The CV of cardiac excitation, and specifically its anisotropy, is a key indicator of myocardial viability, and yet it is underutilized for substrate mapping studies. To appreciate the value of clinical characterization of CV, it is critical to understand the vital role that rapid propagation of excitation plays in the prevention of arrhythmia-inducing reentry. Healthy myocardial tissue manifests two essential traits that impede the occurrence of reentry, namely refractoriness and rapid conduction of sinus activation. Refractoriness refers to the period following depolarization in which cardiac tissue is unable to fire another action potential until the transmembrane potential returns to rest and fully recovers. CV describes the rate at which an action potential propagates through the myocardium. Thus, the combination of the conduction velocity and the duration of the refractory period together determine the minimum path length, or wavelength, that a circuitous activation pattern must undergo in order for activation to perpetuate rather than block before completing a full cycle. Alterations in both parameters, i.e., shortening of the refractory period and slowing of conduction velocity, contribute to the clinical presentation of arrhythmias. We focused on a novel approach to measuring conduction velocity for this aim.

Cardiac CV is anisotropic and is influenced by numerous factors, including orientation and connectivity of myocytes. In healthy myocardium, extensive end-to-end coupling between adjoining myocytes permits rapid conduction of activation in the direction of the long axis of the cells that results in coordinated and efficient cardiac function. However, remodeling of the cardiac substrate due to aging, disease, or injury response can impact the connectivity of myocytes and alter the properties of conduction [30]. The longitudinal and transverse conduction velocities (along and across the fiber orientation, respectively) exhibit a differential response to substrate remodeling in a manner that is proarrhythmic [30, 31, 5].

Current techniques for measuring CV require an electrode configuration of known geometry and the assignment of activation times from acquired EGMs. With this information, it is possible to determine the time of wave propagation from one electrode to another over a known distance. However, the computation of activation times can be complicated by signal noise, such as multiple rapid deflections within the same QRS complex or EGM fractionation [32]. Additionally, the calculation of longitudinal and transverse CVs requires

the assessment of activation times from multiple channels, making it an error-prone and laborious process [33]. Recent progress by a collaborator, Dr. Anders Peter Larsen of the Nora Eccles Harrison Cardiovascular Research and Training Institute (CVRTI), has demonstrated a simplified means for measuring the longitudinal and transverse aspects of conduction velocity using what is known as a plaque electrode array, i.e., a dense array of electrodes with regular spacing of 1–5 mm. This method obviates the necessity of assigning activation times to electrograms from multiple electrodes by condensing properties of the spread of activation into a single signal, which Dr. Larsen termed the "mean Laplacian electrogram" (MLE), from which conduction velocities can be readily identified. The focus of this aim was to extend the preliminary efforts of Dr. Larsen into a model that could explain the behavior of the MLE, and to develop approaches for sampling MLE recordings with clinically feasible electrode arrays. Development of simplified strategies for measuring CV and for characterizing conduction anisotropy would assist the translation of critical experimental tools into clinical use. The MLE signal facilitates the measurement of direct indicators of substrate arrhythmic potential in a rapid and robust manner.

1.2 Organization of Dissertation

The following chapters in this dissertation are comprised of two background chapters on the basic aspects of cardiac electrophysiology relevant to these aims and of the primary arrhythmia of interest for substrate mapping approaches: atrial fibrillation. These chapters are followed by a previously published background chapter covering the use of clinical imaging modalities in the study and treatment of atrial fibrillation [34]. Following the background chapters are three chapters containing additional published work that resulted from each of the research aims detailed in the previous section. The final chapter summarizes the findings of this work and presents future directions that have emerged from the results to date.

CHAPTER 2

CARDIAC ANATOMY AND ELECTROPHYSIOLOGY

The heart contracts and pumps blood. The pressure generated by contraction causes blood to flow through vessels that permeate the body and transport nutrients to the body. Pump, pressure, flow, and transport are the fundamental aspects of circulatory and cardiovascular function. These mechanical phenomena, which are characteristic of the outward appearance of cardiac function, belie our modern conception of the heart as, first and foremost, an electrical organ. Electricity flows through its tissues, and regulates the mechanical function of the heart. Within the heart is an exquisite electrical apparatus with intricate mechanisms for timing, failure prevention, and intrinsic response to demand.

The rhythm of cardiac excitation is remarkably stable. Over the course of the average human life (approximately 75 years), the heart will excite around 3×10^9 times, often with no clinically relevant rhythm disturbance. However, the first rhythm disturbance that many people experience will also be their last. According to the Center for Disease Control, 2,596,993 people died in the United States in 2013 [35]. Of those deaths, nearly one in four was attributed to heart disease, of which half were caused by sudden cardiac death. In most cases of cardiac arrest (cessation of beating), a cardiomyopathy, e.g., ischemia, creates conditions within the heart that render it susceptible to arrhythmogenesis. Regardless of the contributing factors, it is clear that the electrical function of the heart is essential to health and well-being. In this chapter, we will review the basic aspects of cardiac electrical activity, the fundamentals of cardiac arrhythmias, and the biophysics of electric field generation and measurement.

2.1 Ions and the Generation of Excitability and Contractility

2.1.1 Membrane Potentials

The basis of electricity in the heart starts with the cell membrane. Cardiac myocytes are surrounded by a plasma membrane composed of a phospholipid bilayer that is selectively permeable to ions. The movement of ions across the membrane is regulated by ion channels, proteins embedded in the plasma membrane, that are generally specific to a particular ion species. These channels have mechanisms that close, open, or inactivate them from conducting ions in order to maintain homeostatic intracellular ion concentrations. At physiological pH, proteins and DNA that reside within the intracellular space carry an overall negative charge that attracts cations into the cell. K^+ has the highest conductivity through its channel proteins and consequently has a substantially higher intra- than extracellular concentration. However, the resulting concentration gradient of K^+ counteracts the ability of potassium to balance the negative electrical gradient caused by the negatively charged macromolecules by exerting an outward force on potassium ions. Consequently, the K^+ achieves what is known as Donnan equilibrium, in which the force generated by the transmembrane potential opposes and balances the force of diffusion generated by the concentration gradient (Fig. 2.1). Because K^+ has the highest membrane permeability, the transmembrane resting potential is closest to the equilibrium or "reversal" potential of potassium. Other ions also contribute to the resting membrane potential, including Na^+, Ca^{++}, and Cl^-, but their permeability is much lower that of K^+. A typical resting membrane potential for a cardiac myocyte is approximately -90 mV [36].

The Nernst equation can be used to determine the electric potential that will arise given the concentration gradient of a particular ion species. For example, if the intracellular and extracellular concentration of K^+ is known ($[K^+]_i$ and $[K^+]_o$, respectively), then the reversal potential E_{K^+} of potassium can be calculated as:

$$E_{K^+} = \frac{RT}{zF} ln \frac{[K^+]_o}{[K^+]_i}, \tag{2.1}$$

where R is the universal gas constant (8.314 $J/K\dot{m}ol$), T is the absolute temperature (K), z is the charge of the ion species (+1 for potassium), and F is the Faraday constant (96485 $J/V\dot{m}ol$). With the equilibrium potential (E_x) of a particular ion (X) and the membrane potential (V_m), it is possible to determine the driving force (V_{DF}) that will act to drive the ion to move into or out of a cell.

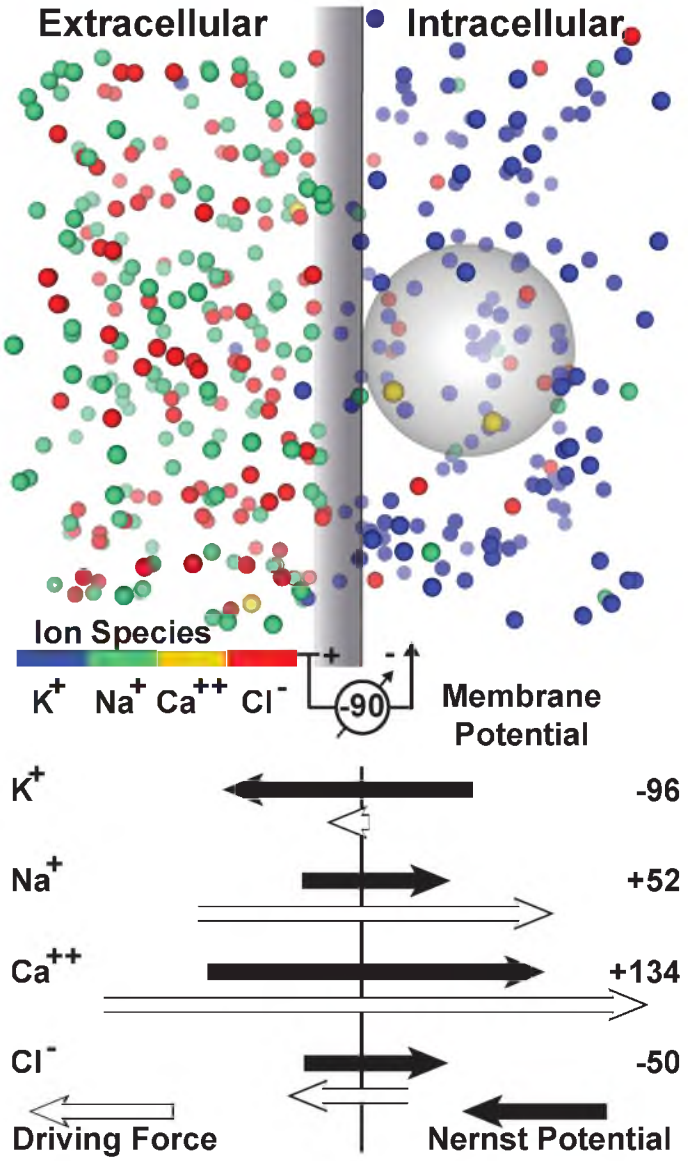

Fig. 2.1. Generation of cardiomyocyte membrane potential. The presence of membrane-impermeable macromolecules with net negative charge in the intracellular space draws cations to migrate into the cell. Selective membrane permeability dictates that potassium (K^+), with high membrane permeability, collects in the intracellular space at much greater concentrations than other cations (sodium (Na^+) or calcium (Ca^{++})). Ultimately, a Donnan equilibrium is established between the electric and concentration gradients, and cardiac myocytes rest at $\approx$ -90 mV. Top - Relative concentrations of ion species in the intra- and extracellular spaces. Intra- and extracellular Ca^{++} concentrations are roughly equivalent except that intracellular Ca^{++} is sequestered in the sarco-endoplasmic reticulum (gray sphere), functionally generating a large inward Ca^{++} concentration gradient. Bottom - Black arrows indicate the magnitude of the reversal potential for the existing concentration of each ion species in mV. Outlined arrows indicate the direction and magnitude of the driving force (Equation 2.2) acting on each ion species.

$$V_{DF} = V_m - E_x. \tag{2.2}$$

The Goldman-Hodgkin-Katz (GHK) equation describes the resting membrane potential in terms of the concentrations of ions and their relative permeability (P_{ion}):

$$E_m = \frac{RT}{F} ln \frac{P_K[K^+]_o + P_{Na}[Na^+]_o + P_{Cl}[Cl^-]_i}{P_K[K^+]_i + P_{Na}[Na^+]_i + P_{Cl}[Cl^-]_o}. \tag{2.3}$$

The GHK equation can be interpreted as the resting potential being the sum of the concentration gradients for each ion times the permeability of the respective ions. Ions for which the permeability is zero, or is negligibly small, i.e., calcium channels at resting membrane potential, do not significantly contribute to the transmembrane potential and drop out of the GHK equation. The GHK predicts how changes in the permeability of a particular ion, as seen during action potentials, will affect the membrane potential [36].

2.1.2 Action Potentials

2.1.2.1 Excitation

From its resting or fully recovered state, every myocyte in the heart is capable of firing an action potential. An action potential begins with the rapid depolarization of the membrane potential due to a sudden increase in the conductance of voltage-gated Na^+ channels in the cellular membrane (Fig. 2.2). This increase in conductance occurs when the membrane potential reaches a critical threshold and voltage-gated Na^+ channels open, allowing Na^+ to flow into the cell down the concentration and electrical gradients. Shortly after opening, the Na^+ channels begin to inactivate. This initial depolarization is known as phase 0 of the action potential. Phase 1 is characterized by an initial partial repolarization of the transmembrane potential due to the outward flow of K^+ down its concentration and newly formed electrical gradient through open K^+ channels. Phase 2 of the action potential is known as the plateau. During phase 0, depolarization of the myocyte voltage-dependent L-type Ca^{2+} channels begin to open and the resulting inward current of Ca^{2+} now counterbalances the outward flow of K^+. The plateau phase may last upwards of 200 ms but eventually ends as Ca^{2+} channels close in a time-dependent manner. The closure of the Ca^{2+} channels initiates the start of phase 3 in which the uncontested outward flow of K^+ causes a rapid repolarization of the transmembrane potential to -90 mV. Phase 4 starts when the cell has reached the resting membrane potential and the membrane starts a recovery phase, which must be complete before the next activation impulse can trigger excitation.

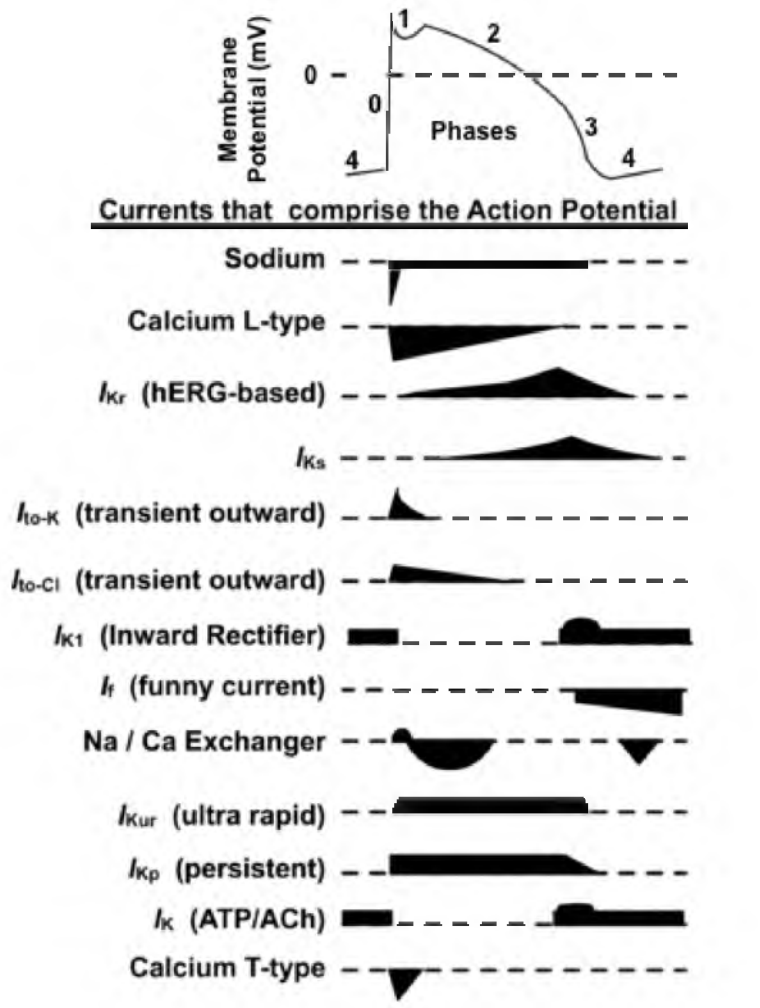

Fig. 2.2. Phases of the cardiac action potential and associated changes in ion channel permeabilities. Adapted with permission from Witchel et al. *Cardiovasc. Ther.* 2011 [38].

2.1.2.2 Excitation-Contraction Coupling

Action potentials signal the cardiac myocytes to contract through a process known as excitation-contraction (E-C) coupling. E-C coupling is primarily mediated through the cellular handling of Ca^{2+}. As previously mentioned, depolarization of cardiac myocytes initiates the opening of voltage-dependent L-type Ca^{2+} channels. These channels are co-localized with ryanodine receptors (RyR) that permeate the membrane of the sarcoplasmic reticulum (SR). The influx of calcium during excitation raises the local concentration of intracellular $[Ca^{2+}]$ that is detected by the RyRs, which then open to release even more Ca^{2+} from its storage in the SR. This positive feedback loop release system rapidly raises the intracellular Ca^{2+} concentration and triggers the actin-myosin contractile mechanism, causing cardiac contraction. Re-uptake of Ca^{2+} begins almost as soon as there is a rise in

intracellular Ca^{2+} and includes several pumps and exchangers located in the cell and SR membranes. The result is a restoration of intracellular Ca^{2+} and the SR loaded and ready for the next action potential [37].

The calcium handling of E-C coupling is critical to both cardiac mechanical and electrophysiological function. The processes involving Ca^{2+} signaling are relatively slow because they require diffusion of calcium to specific binding sites to initiate the myofibril contraction. As a result, muscular contraction begins over 50 ms after a myocyte depolarizes, whereas depolarization itself often requires only a few milliseconds. This slow step creates a vulnerability where the dynamics of calcium handing can become impaired, especially at very fast activation rates. In situations of rapid activation, the mechanisms that regulate Ca^{2+} concentration, such as the sodium-calcium exchange current and the uptake of calcium via the energy consuming SERCA2a pump, can fall behind. These excursions from normal physiological calcium homeostasis can significantly alter the properties of cardiac electrophysiology and lead to proarrhythmic, triggered activity (further detail provided in Section 2.3.1.)

2.1.2.3 Repolarization and Refractoriness

The return of the transmembrane potential to rest following activation (phase 3 of the action potential) is known as repolarization. One critical feature of myocyte excitability is that a myocyte cannot fire a new action potential until it has fully repolarized and a period of recovery has passed. This property, known as refractoriness, is a critical feature for maintaining organization of electrical activity in the heart. The refractory period, or the time from myocyte depolarization (phase 0) to completed repolarization (end of phase 3), ultimately regulates the frequency at which action potentials can be fired. The prolongation of the action potential caused by the inward calcium current during phase 2 contributes to an increase in the duration of the refractory period. At the whole organ scale, under normal conditions, the refractory period lasts longer than the time it takes for total activation of the ventricles, thus ensuring that only one activation sequence occurs in the heart at a time.

2.2 Cardiac Anatomy and Cardiac Conduction

2.2.1 Basic Cardiac Anatomy

The human heart is a four-chambered organ comprised of two atria and two ventricles. The atria, smaller and situated above the ventricles, receive blood flowing into the heart, and the ventricles pump the blood away from the heart. Another simple means of classifying the heart's structural components is based on whether the chambers are on the left or right

side. The right side receives systemic venous return and pumps deoxygenated blood to the lungs. The left side receives pulmonary venous return and pumps oxygen-rich blood into the systemic circulation. See Fig. 2.3 for a depiction of major anatomical features of the heart.

2.2.2 The Cardiac Syncytium

At a cellular level, the organization of myocytes in cardiac tissue has a profound impact on the spread of action potentials. Most cardiac myocytes are striated like typical muscle cells with sarcomeres comprised of contractile fibers. Cardiomyocytes tend to group in bundles or sheets in which the long axes of neighboring cells align in parallel to form an anisotropic media. The elongated cells connect end to end with each other, often including bifurcations leading to interactions with multiple other cells at regions known as intercalated

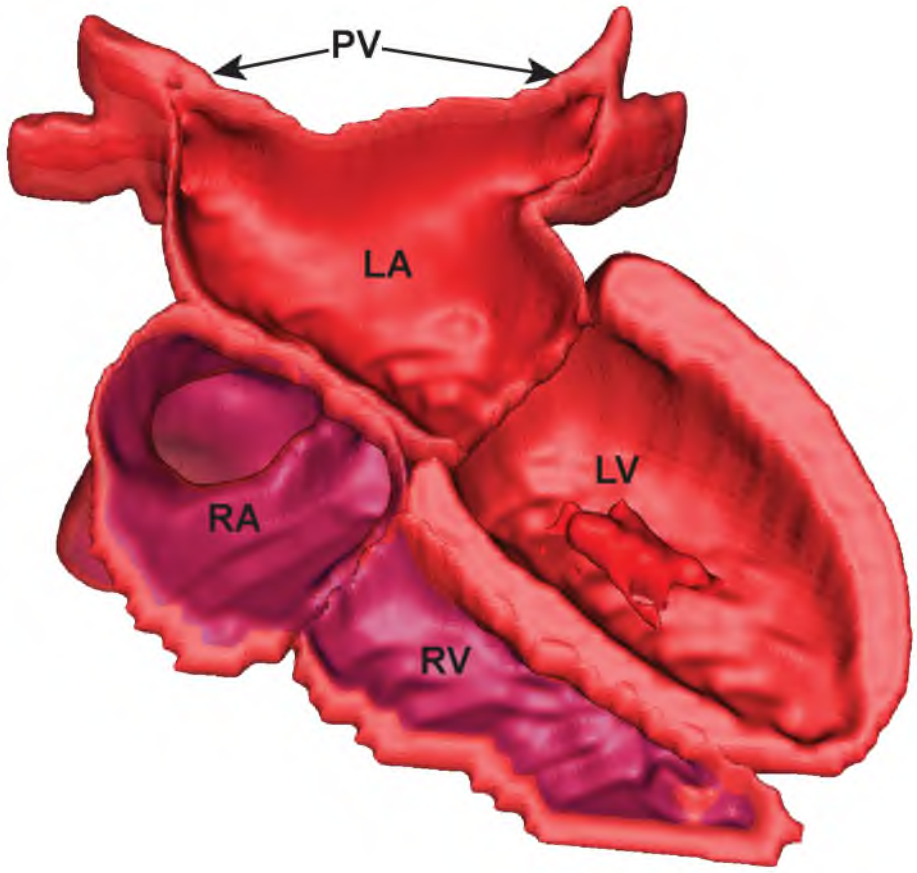

Fig. 2.3. Four-chamber view of the heart. A segmentation of a human heart derived from an MRI shows the four major chambers of the heart. RA = Right Atrium, RV = Right Ventricle, LA = Left Atrium, LV = Left Ventricle, PV = Pulmonary Veins.

disks. At the intercalated disk, channel proteins known as gap junctions form a patent connection from cell to cell through which ions can flow freely (Fig. 2.4). When an action potential is generated, it is communicated to surrounding cells through the gap junctions. Myocyte depolarization creates an electrical gradient between the activated cell and its unexcited neighbors. Positive cations will begin to move down this gradient through the gap junctions, and, if sufficient current is communicated, the unexcited neighbors will achieve their firing potentials and depolarize. The anisotropic organization of myocytes and the localization of the intercalated disks at the ends create lower resistance to the flow of ions along the long axis of the myocytes. Consequently, the spread of action potentials in cardiac tissue is also highly anisotropic [39, 40, 41].

Because the intracellular space of myocytes are linked by these connections, cardiac tissue is frequently referred to as a syncytium, meaning a single cytoplasmic mass. Each myocyte is eventually connected to every other myocyte so that a stimulus anywhere in the heart will result in the rest of the heart eventually responding.

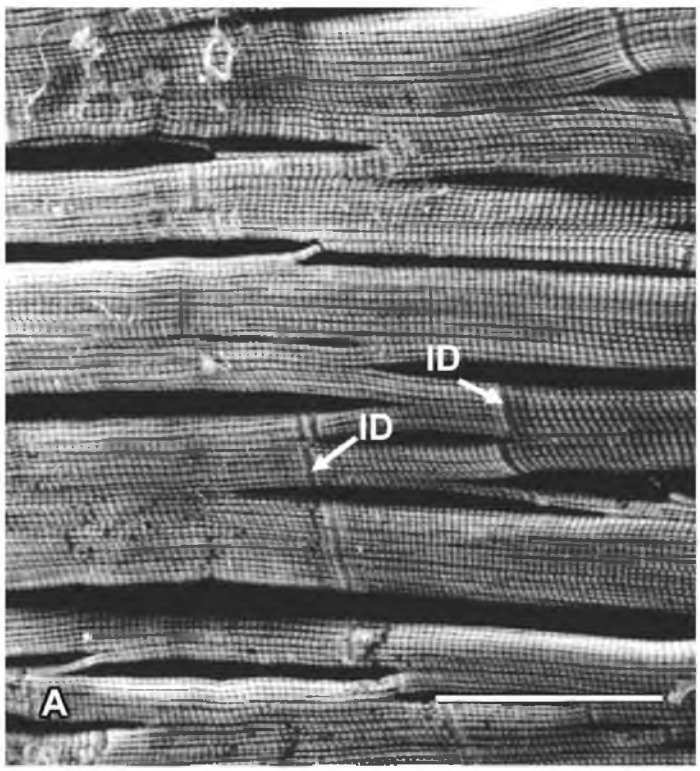

Fig. 2.4. Organization of human myocardial syncytium. The structure of cardiac tissue as seen under backscattered electron imaging of normal human left ventricular cardiomyocytes. A. Intercalated discs (arrows) define the boundaries between independent myocytes, and sarcomere striations throughout the myocytes define the contractile units. Bar=50 μm; magnification $\times$600. Modified with permission from Kanzaki et al. *Circ.* 2010. [42]

2.2.3 Conduction System

To function properly as a pump, the heart must autonomously generate action potentials and broadcast these impulses throughout the entire myocardium in order to coordinate contraction. All cardiac myocytes are capable of firing an action potential, but they require a stimulus for the voltage-dependent Na^+ channels to open and commence depolarization. Specialized myocytes and regions of myocytes within the heart, known as the cardiac conduction system, initiate excitation and conduct action potentials throughout the heart with timing that ensures efficiency of contraction (Fig. 2.5). The initial excitation of the heart occurs high in the right atrium in a region known as the sinoatrial (SA) node. The myocytes in this region of the heart have higher concentrations of a mixed Na^+–Ca^+ channel (I_f) that allows cation leakage into SA nodal cells during the resting phase, causing slow depolarization of the SA node until it reaches the critical threshold for voltage-dependent Na^+ channels to open and fire an action potential [43]. This leak, known as the funny current, can be directly modulated through neurohormonal mechanisms to increase or decrease the heart rate by changing the conductance of the funny channels. Specifically, catecholamines and acetylcholine act on the funny current to cause I_f channels to begin opening at earlier or later stages of repolarization, respectively [44, 45]. Early activation of the funny current decreases the diastolic interval and accelerates heart rate.

In a normal heart beat, action potentials begin in the SA node. Once an action potential is generated in the SA node, it is communicated to surrounding tissues in the atria, causing both upper chambers of the heart to depolarize. However, the activation impulse does not immediately pass to the ventricles. During atrial activation, a region of tissue known as the atrioventricular (AV) node, which serves as the gateway to the only conduction path to the ventricles, is stimulated. The AV node conducts action potentials slowly and momentarily delays the activation of the ventricles while the atria activate [47, 48, 49]. This delay allows the atria to fully contract for maximum precontraction filling of the ventricles. After passing through the AV node, an action potential impulse enters the His-Purkinje system, a network of myocytes specialized for rapid impulse conduction that interlaces the ventricles. The His-Purkinje system functions to rapidly distribute action potential impulses throughout the ventricles to synchronize contraction in order to generate efficient pumping. The morphology of the action potentials changes as impulses progress through the elements of the conduction system. The morphology of the transmembrane potential in a given region reveals characteristics of the activating tissue and its role in cardiac function (see Fig. 2.5). For example, the slow conduction of the AV nodal action potential impulses is predictable

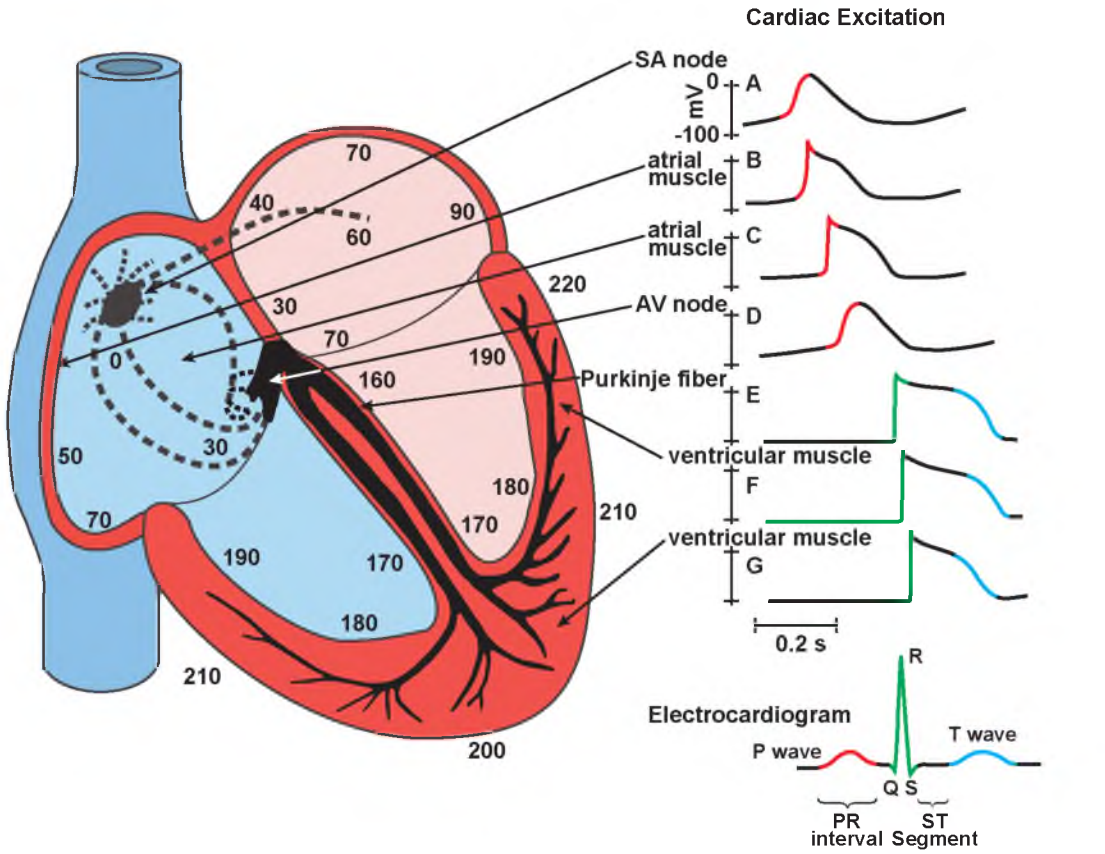

Fig. 2.5. Action potentials of the conduction system during cardiac excitation. The four-chamber view of the heart depicts the various elements of the cardiac conduction system and approximate activation times of regions throughout the heart (overlain numbers in milliseconds). The time signals on the right depict representative action potentials from the respective regions of cardiac conduction (A-G). The timing of these action potentials is referenced to the features observed on a body surface ECG (bottom right). Modified, with permission, from the Atlas of Human Cardiac Anatomy website: http://www.vhlab.umn.edu/atlas/. [46]

from the AV nodal action potential (Fig. 2.5D) in which the phase 0 upstroke of the action potential has a lower slope than working atrial myocytes [50]. As discussed in Section 2.2.4, the upstroke rate of the action potential is indicative of how fast downstream myocytes will be depolarized by the activation wave, and consequently determines how fast the wave will propagate.

2.2.4 Action Potential Propagation

The coupling and organization of the cardiac syncytium have a direct impact on the properties of action potential propagation. The elongated shape and size of cardiomyocytes, the localization and resistance of gap junctions, and the alignment of the myocytes, discussed in Section 2.2.2, all influence the spread of action potential impulses. These features influence such phenomena as the rate of depolarization and the resistance to the flow of ions from cell to cell. Variations of these properties will manifest as changes in the rate of action potential propagation through the cardiac tissue. For example, impulse propagation will progress faster down the long axis, or longitudinal direction, of the muscle fibers than it will perpendicular to the long axis, or transverse direction [39, 40, 41]. This property, known as conduction anisotropy, is critical to proper coordination of cardiac excitation and contraction. Conduction anisotropy is routinely characterized as the ratio of conduction velocity (CV) in the longitudinal direction to the transverse direction. Perturbation of the anisotropy or rate of action potential propagation through changes to the connectivity and organization of the myocardial syncytium can facilitate the development of life-threatening cardiac arrhythmias [30, 51, 14].

In principle, these characteristic features of myocardial tissue influence four properties that determine the rate of impulse propagation. The first property is the rate of excitatory depolarization or dV/dt of the transmembrane potential during excitation. This behavior is regulated by membrane channels that carry the inward depolarizing currents, including the current passing through gap junctions from proceeding myocyte depolarization and voltage-gated Na^+ (I_{Na}). The intracellular resistance to current flow is the second property. This resistance is an accumulation of the cytosolic and gap junction resistance in series. The third property is the capacitance of the membrane. Cation migration downstream from depolarized myocytes through gap junctions will displace charge to create a return current that completes the circuit; otherwise no current could flow. This outward displacement current is strongly influenced by the capacitive nature of the cell membrane, in which cations are forced away from the extracellular membrane by the positive charge accumulating in the intracellular space. The fourth property is the resistance of the extracellular space

to current flow. Numerous pathological processes can affect one or more of these tissue properties and alter the nature of action potential propagation. For example, phenomena such a edema or fibrosis can alter the nature of the extracellular space and the extracellular resistance. However, the nature of these changes may also affect the coupling of myocytes and consequently increase the intracellular resistance as well [52].

The rate at which action potential impulses propagate through the myocardium is a primary factor in determining whether a region of tissue is susceptible to the formation of arrhythmias (see Section 2.3.1) [53, 31]. Because of the relationship between CV and arrhythmogenesis, the measurement of CV has become a common experimental metric for characterizing proarrhythmic potential of influences ranging from common cardiomyopathies to investigational medications. Towards that end, a variety of experimental approaches have been developed to measure the longitudinal and transverse aspects of CV. Currently, two types of systems are most frequently used to characterize the rate of action potential propagation: electrode arrays and optical mapping.

Electrode arrays come in many shapes, forms, and sizes. Sock, plaque, loop, and needle-based electrode arrays have been used for the measurement of CV. However, a few key requirements determine whether an electrode array is suitable for the measurement of CV. First, the electrode array must have many, at the very least three, noncolinear electrodes that can record cardiac excitation remote from the site of activation. Measurement of CV is typically performed following the creation of an action potential impulse induced by pacing, or external electrical stimulation of the myocardium. The spread of activation away from a paced site will form an elliptical wavefront with the long axis of the ellipse lying along the direction of the myocytes, i.e., longitudinally. Recording electrodes surrounding the pacing site can then sense the local cardiac excitation. Second, the positioning of the electrodes relative to the pacing location must be known to calculate the velocity based on the distance traveled by the wave and the timing of its arrival (Fig. 2.6).

Optical mapping is another common technique used to measure the CV in which a voltage sensitive dye is introduced into the myocardium to reveal the action potential propagation. Voltage sensitive dyes are chemicals that exhibit shifts in spectral properties in response to changes in the local electric potential, i.e., the arrival of an action potential. These shifts in the spectral properties can be detected and recorded with digital camera technology at high temporal and spatial resolution. For an in-depth treatment of the capabilities of optical mapping, please refer to review articles by Herron et al. (2012) [55], and Boukens and Effimov (2014) [56].

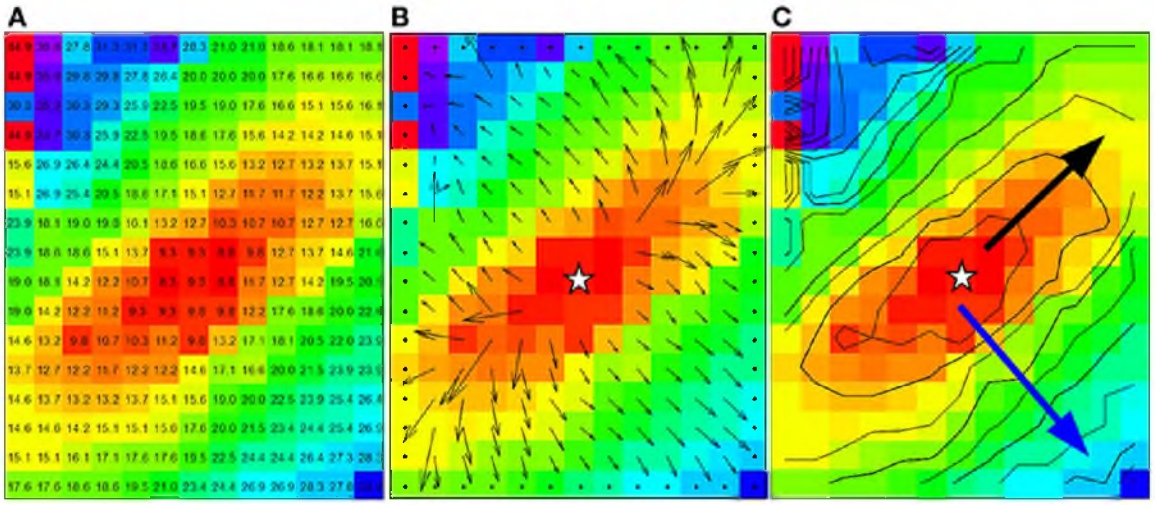

Fig. 2.6. Cardiac excitation recored from a dog heart with a 13 by 16 electrode plaque array (0.5 mm electrode spacing). A. Activation times computed for every electrode after excitation induced by pacing from an electrode at the center of the plaque. B. Vectors representing estimation of direction and velocity of conduction computed with a neighborhood least square fit on a 3 by 3 stencil over the array. C. Isochrones with 2 ms spacing indicating anisotropic action potential propagation. Black and blue arrows indicate direction longitudinal and transverse conduction, respectively. White stars on B and C indicate the pacing site. Image used with permission from Linnenbank et al. *Front. Physiol.* 2014 [54].

Regardless of the recording strategy, an essential element of measuring CV is the ability to detect the time of arrival of the action potential to the site of the recording element. In the analysis of unipolar electrograms (EGM), the activation time is traditionally annotated at the time of maximum negative slope during activation [57, 30]. The timing of this feature has been shown to correlate strongly with the upstroke of the transmembrane potential in the local myocytes. However, unipolar electrograms are prone to fractionation, the disruption of prototypical waveform morphology due to far field electric potentials or discontinuity in the activation wavefront [58]. In cases of fractionation, the change in EGM morphology will interfere with appropriate detection of activation time. Enhanced filtering and recording strategies have been developed to overcome challenges associated with detecting activation times from unipolar EGMs. One method that can be used on dense electrode arrays with small interelectrode spacing, as will be discussed in Section 2.4.2, utilizes the spatial rather than temporal derivative of electrograms over the array to determine activation times [59, 32].

2.2.5 Cardiac Rhythm

The rhythm of cardiac excitation is critical to proper function and the health of the heart. Regular cardiac activation stimulated by the SA node is known as sinus rhythm. During sinus rhythm, each myocyte will activate only once. Maintenance of regular cardiac activation allows for optimal cardiac pumping function through synchronized contraction of the myocytes. Irregular activation patterns or action potentials initiated from locations other than the SA node are known as arrhythmias. Many different forms of arrhythmias exist and may act to speed, slow, or completely disrupt excitation of the heart. Some arrhythmias are acutely life threatening and require immediate medical intervention. Others may go unnoticed and are of negligible clinical relevance. Regardless of their immediate implications, many common mechanisms are involved in the development of the various arrhythmias. Section 2.3 will cover commonly recognized mechanisms of arrhythmogenesis.

2.3 Mechanisms of Arrhythmogenesis

Cardiac arrhythmias are disruptions of the normal activation sequence of the heart. The disruptions include ectopy, when an action potential impulse originates somewhere other than the SA node; reentrant activity, repetitious circulation of activation; and fibrillation, complete disruption of excitation synchrony. Various risks attend different arrhythmias. For example, hemodynamically unstable ventricular tachycardia (VT) and ventricular fibrillation (VF) can cause sudden cardiac death through termination of systemic blood flow and the resulting cerebral anoxia. Atrial fibrillation creates an enhanced risk for ischemic strokes, ≈fivefold throughout all ages, when loss of functional contraction in the atria allows blood to pool and clot [60].

2.3.1 Triggers and Substrates

A mechanistic model of arrhythmogenesis relying on triggers that initiate irregular conduction pathways and a substrate in which the atypical conduction can perpetuate has been used to explain much of the arrhythmic behavior that is observed clinically. A trigger is electrical activity that originates from a location other than the SA node, which may come in the form of ectopy or afterdepolarization events [37]. Ectopic beats are classified either as premature atrial or ventricular contractions (PAC and PVC, respectively). Both PACs and PVCs occur commonly and in the absence of a proarrhythmic substrate are generally considered clinically insignificant. Afterdepolarizations also are autonomous depolarizations of the myocytes that induce nonsense conduction patterns. These depolarizations also come in two varieties, early and late. Early afterdepolarizations (EAD) occur during phase 2 or

phase 3 of the action potential with an augmented opening of calcium (possibly I_{Na} too), typically under conditions of prolonged action potential duration [61, 62]. If the membrane potentials of surrounding myocytes have sufficiently repolarized, the EAD may capture that tissue and induce an action potential impulse. Delayed afterdepolarizations (DAD) occur during phase 4 of the action potential immediately after the membrane potential has returned to rest. DADs occur when the sarcoplasmic reticulum becomes overloaded, due to increased cytosolic calcium concentration, and spontaneously release Ca^{2+}. This sudden increase in intracellular Ca^{2+} creates a depolarizing current through an ion channel known as the sodium potassium exchanger that can cause Na^{+} channels to open and depolarize the myocyte [63]. The nonsinus activation patterns initiated by ectopy or triggered activity will typically disrupt contraction for only one beat. After the triggered activity, sinus activation and normal cardiac function will resume. If this triggered activity becomes repetitious, it may lead to the induction of paroxysmal episodes of arrhythmias such as AF or VT. Under condition of continuous triggers, medication or treatment may be required to reduce the risk of more serious arrhythmias.

In the presence structural heart disease, i.e., a proarrhythmic substrate, triggered activity becomes much less benign as it can greatly increase the likelihood of reentrant arrhythmogenesis. There are numerous forms of arrhythmogenic substrates. Some arrhythmogenic substrates are purely anatomical. For example, in some hearts, a second conductive pathway, besides the AV node - His bundle pathway, exists between the atria and ventricles. With this second pathway, a loop of rapid electrical excitation, known as reentry, can occur when ventricular excitation conducts back up into the atria. Other arrhythmogenic substrates develop because of restructuring of the cardiac syncytium in a manner that disrupts conduction. Examples of this restructuring include scar formation that occurs following myocardial ischemia or fibrosis that is associated with aging and valvular dysfunction [64, 65, 66, 67, 30]. These regions of nonconductive tissue create a feature that electrical activity can circle to generate reentry.

2.3.2 Anatomical Reentry

With triggers and a substrate in place, the setting for reentrant arrhythmias is in place. However, as mentioned previously, the cardiac conduction apparatus is remarkably robust, and a particular set of circumstances is required for the development of reentry [53]. One essential feature of reentry initiation is known as unidirectional block. Block of an action potential impulse can occur for a number of reasons, including collision of two action waves; collision with inexcitable tissues, i.e., refractory or scarred; or if insufficient

depolarizing current is generated to depolarize downstream myocytes. Atrioventricular nodal reentrant tachycardia (AVNRT), an arrhythmia that produces an abnormally rapid heart rate, provides a classic example of how unidirectional block can lead to reentry [68, 69]. In the AV node, two pathways of conduction can develop due to a dissociation of conductive tissues. One of these pathways tends to conduct faster than the other (Fig. 2.7). When sinus activation captures the AV node, both pathways conduct the action potential impulse, but the fast pathway captures the His bundle whereas the slow pathway blocks when it reaches the His. However, because of the interplay among conduction velocity, rate of depolarization, and action potential duration, the slow conducting pathway has a shorter refractory period than the fast pathway. Consequently, if triggered activity causes an early action potential impulse to stimulate the AV node, it may find the fast pathway refractory, and conduct only down the slow pathway [70]. The activation in the slow pathway can then

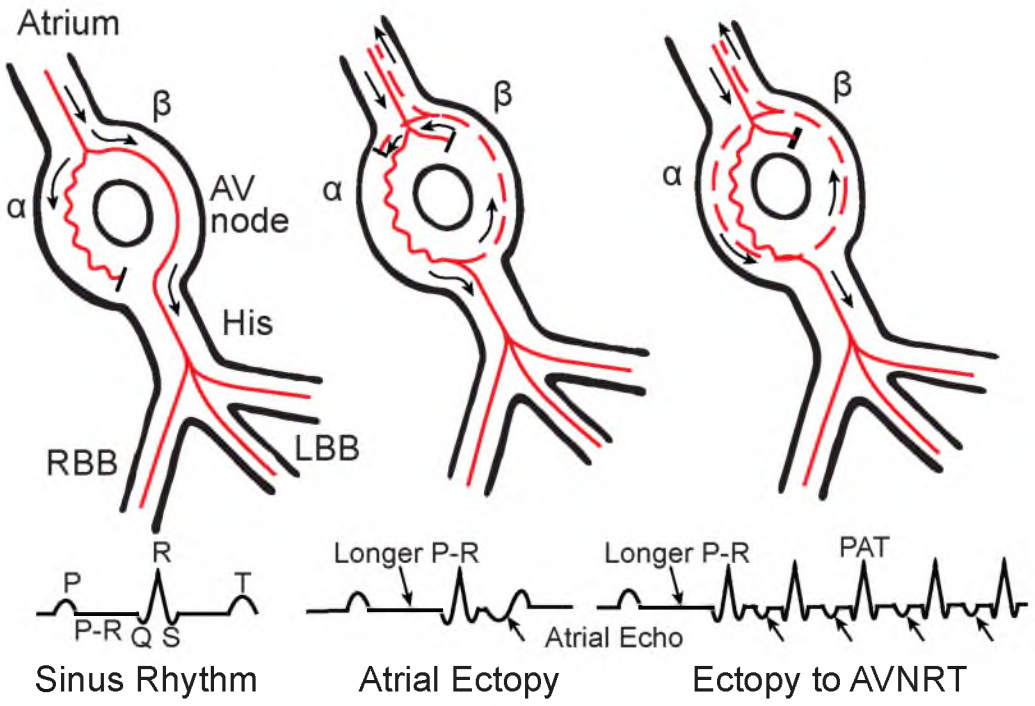

Fig. 2.7. Mechanism of A-V nodal reentrant tachycardia. Each part of the figure is shown as an atrium, A-V node (which is divided into an alpha (α) and beta (β) pathway), His bundle, and bundle branches. In the left panel, sinus rhythm is present, and the mechanism of the resulting QRS is shown. In the center, the response of the A-V node to a single atrial premature beat with a single atrial echo is depicted. In the right panel, the initiation of supraventricular tachycardia with an atrial premature beat is shown. See text for discussion of the interaction of trigger and substrate in arrhythmogenesis. PAT = paroxysmal atrial tachycardia; RBB = right bundle; LBB = left bundle branch. Reproduced with permission from Josephson and Kastor. Ann. Intern. Med. 1977 [69].

stimulate both the His and the tail end of the now excitable fast pathway. Because the fast pathway has regained excitability, it does not block in the retrograde direction, and activation can circle back to the slow pathway and form a reentrant circuit. In this manner, heterogeneity in the tissue refractoriness coupled with triggers can lead to reentry.

As displayed in the central image of Fig. 2.7, a circuitous pathway alone is insufficient for the initiation of reentry. It is possible that after the previously mentioned retrograde activation of the AV nodal fast pathway, the slow pathway will be refractory and unable to conduct the returning wave of excitation. Based on the conduction velocity (CV) of the action potential impulse and the effective refractory period (ERP) of the tissue, there is a minimum path length that can support the perpetuation of a reentrant circuit. Known as the wavelength (λ), this path length can be determined by the product of the circuit's CV and ERP [53, 31].

$$\lambda = CV \times ERP. \tag{2.4}$$

Consequently, if the wavelength of the dissociated AV nodal circuit is too short, conduction will block and sinus rhythm will resume.

2.3.3 Functional Reentry

The reentry discussed to this point has focused on circulating electrical activity that moves around anatomical features or through accessory pathways. Known as anatomical reentry, it is the primary driver of a class of arrhythmias known as macroreentrant tachycardias, e.g., atrial flutter, AVNRT, Wolf-Parkinson-White syndrome, and ventricular tachycardia. Another type of reentry, known as functional reentry, manifests in fibrillation arrhythmias, i.e., atrial and ventricular fibrillation, and relies on slightly different mechanism to produce circuitous activation patterns. Functional reentry is subject to the same conditions as anatomical reentry in that the reentry will terminate if it meets with refractory tissue. However, the functional reentry does not depend on a discrete conduction pathway or structural substrate to define its circuit. Instead, a refractory singularity is established around which a circulating wave can propagate [71, 72, 73, 74]. This type of conduction, often known as a rotor, can anchor its refractory core to features of the cardiac substrate, such as scar tissue, but it has also been observed to meander around the myocardium. A possible mechanism of initiation for functional reentry known as wave break has been suggested, but this and many other aspects of functional reentry remain topics of active research. The basis of wave break initiation of reentry relies on a fundamental property

of cardiac conduction: the reliance of action potential propagation on depolarizing current flowing downstream to activate resting tissues.

The next critical aspect of wave break is attributable to the dependence of downstream activation on the characteristics of upstream propagation. Specifically, the curvature of an action potential wavefront determines the speed with which it can propagate [75]. Independent of tissue anisotropy, wavefronts with high curvature can be accelerated or slowed depending on whether the wavefront is concave or convex relative to the downstream tissue (Fig. 2.8). As discussed in Section 2.2.2, depolarization of myocardium outside of the SA node is primarily dependent on upstream activation, in which positive ions from depolarized cells are communicated to resting myocytes through gap-junctions. Consequently, when multiple myocytes combine to depolarize a downstream myocyte, it will depolarize faster and speed propagation. This same effect can occur with a concave wavefront in which current is being injected into a small region from surrounding depolarized myocardium. The opposite, however, will occur with a convex wavefront. In this case, upstream myocytes must each facilitate the depolarization of multiple downstream myocytes. Each resting myocyte receives a relatively reduced amount of current, which delays depolarization and slows conduction velocity. In a condition known as current-source mismatch, if the curvature is too high and the depolarizing current too low, conduction will block. Current-source mismatch is an alternative mechanism for unidirectional conduction block as described in the previous section. In cases where complete block does not occur, the conduction velocity will slow.

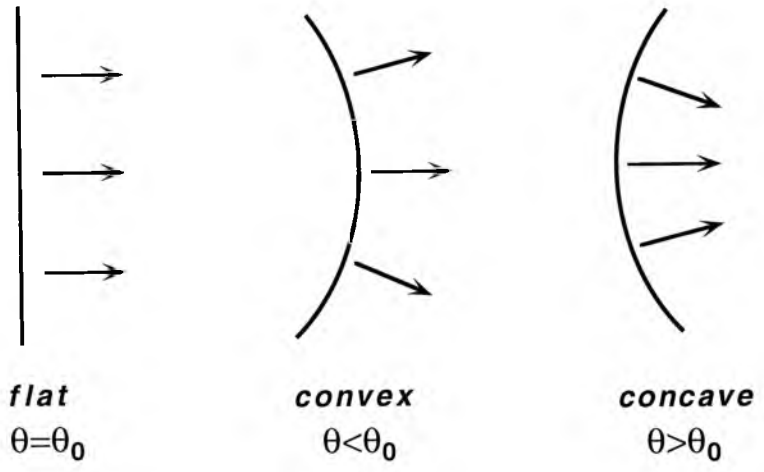

Fig. 2.8. Effect of wavefront geometry on propagation velocity θ. θ_0 denotes the steady-state velocity in a one-dimensional medium. Used with permission from Fast and Kléber. Cardiovasc Res. 1997 [27].

The consequences of wavefront curvature can combine to facilitate functional reentry by means of wavebreak. When a wavefront passes a sharp end of an obstacle to conduction, such as scar tissue (see Fig. 2.9) [27], the wave front can detach from the obstacle in a manner that the leeward tissue will not activate. The failure of the leeward tissue to activate can be explained by the high curvature the wavefront would need to negotiate in order for attached activation to propagate around the sharp edge of the obstacle. The high curvature causes activation to block in the leeward direction, leaving the activation front to spiral back in order to capture the unexcited tissue. At the leading edge of the pivoting spiral wave is a singular point at which resting, exciting, and refractory tissues intersect (annotated with a P in Fig. 2.9B). The radius of this spiral wave will reflect the ability of the wavefront to produce sufficient current to depolarize tissue both in the normal direction to the wavefront and laterally. This radius is known as the pivot radius (R_p). If R_p is larger than the wavelength of the local myocardium (Equation 2.4), the spiral wave may perpetuate around the singularity. Spiral waves, also commonly referred to as rotors, have been observed with a variety of recording strategies. In some cases, this functional reentry has been observed to anchor, possibly to some underlying substrate, in place, and other studies have described a meandering of the rotor position. Variations in the stability of rotors have also been observed. In some cases, an initial rotor has been observed to spawn new rotors and disappear. In other instances, a primary rotor spins off smaller spiral wavelets that are subsidiary to the central rotor. Regardless of the spatial and temporal stability of the functional reentry, the presence of rotors inevitably heralds the initiation of fibrillation in which virtually all rhythmic cardiac excitation has ceased.

2.4 Bioelectricity

As discussed to this point, gradients in the distribution of charged atoms and molecules in biological tissues generate electric potentials. Resistive elements, or channels, in the cell membrane allow these charges to migrate in a manner that generates current. The changes in resistance, i.e., permeability, that occur during an action potential cause changes in the local electric field that can be measured. The measurement of cardiac bioelectric potentials generated by cardiac excitation was started by Einthoven and continues as a critical aspect of clinical cardiology and medicine in general to this day [76, 77]. The study of potentials that arise from the heart is known as electrophysiology. This section will provide a brief background to the physics, techniques for measurement, and basic strategies for analyzing features of bioelectric potentials.

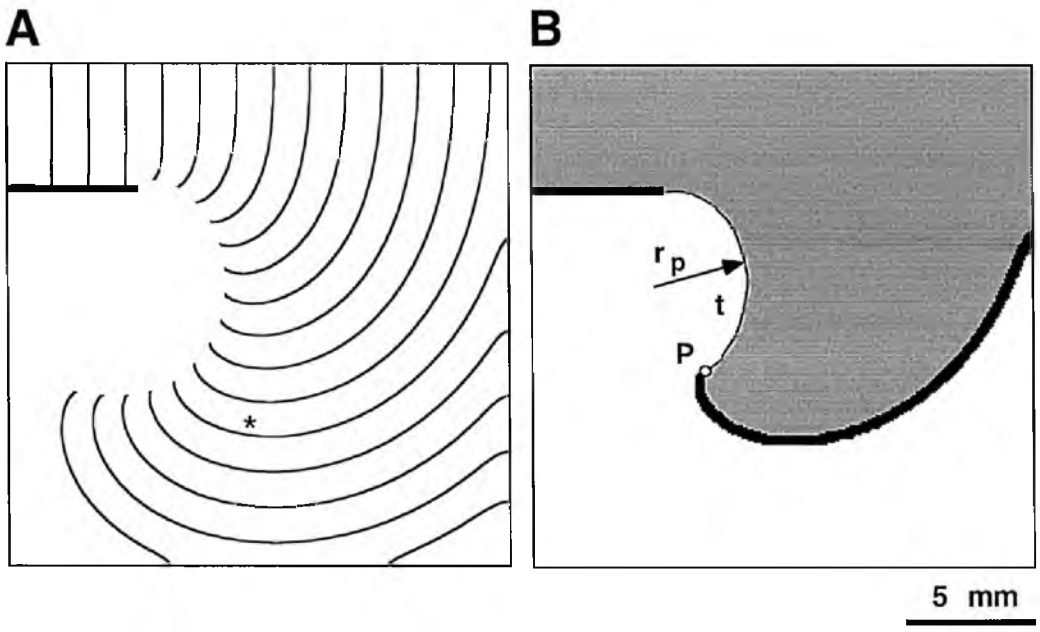

Fig. 2.9. Detachment of an excitation wave from the sharp edge of an unexcitable obstacle. Used with permission from Fast and Kléber. Cardiovasc Res. 1997 [27].

2.4.1 Electric Fields and Potentials

Ions in the biological media carry a charge that generates an electric field, which is a force that attracts or repels other charges depending on polarity. The electric field ($\vec{E}$) at any given point (r) is a function of the density of charged particles (q_i) whose electric fields superimpose on that point from their respective locations (r_i).

$$\vec{E}(r) = \sum_{i=1}^{N} \vec{E}_i(r) = \frac{1}{4\pi\epsilon_0} \sum_{i=1}^{N} q_i \frac{r - r_i}{|r - r_i|^3} \tag{2.5}$$

where ϵ_0 is the permittivity of the medium. Under these conditions, the force (F) exerted on a charged particle at position r is simply the product of the charge of that particle and the electric field:

$$F = q\vec{E}. \tag{2.6}$$

A consequence of the superposition of electric fields is the possible scenario in which charges surround a point in space such that the sum of all the forces, repellant or attractive, is zero. In this scenario, there is no electric field at that point. Similarly, when charged particles are uniformly distributed through a conductive medium, such as the intra- or extracellular spaces, and there is no difference in the potential energy of a charge particle

across that domain, the force of the electric field is zero. However, differences in ionic concentrations that exist across cell membranes generate an electric field. This transmembrane gradient in potential energy of a charged particle is known electric potential (ϕ).

$$\vec{E} = -\nabla\phi. \tag{2.7}$$

An inherent property of conductive medium is that charges will move when acted upon by an electric field to create a current. The magnitude of the current density (J) will be inversely proportional to the resistance to the movement of that charge as described by Ohm's law,

$$J = \sigma\vec{E} = -\sigma\nabla\phi. \tag{2.8}$$

In Equation 2.8, σ is the conductivity (inverse of resistance) of the medium in which the charge is moving. When myocytes are at rest and the forces acting on ions in the heart have either equilibrated or the resistance to flow is very high, current flowing across the membrane is minimal (with the obvious exception of depolarizing currents in the conduction system). However, when an action potential is triggered by an abrupt change in the permeability of the membrane to Na^+, the current responds proportionately. This injection of current into the myocyte reverses the transmembrane potential and gives rise to intra- and extracellular electric fields where the gradient electric potential at rest is zero. The gradients in electric potential that arise during cardiac excitation between depolarized and resting myocardium produce the electric signals that are measured in electrophysiology. The difference in the extracellular potential (ϕ_e) measured between two points on the body will depend on their relative positioning with respect to the excited and resting portions of the myocardium and the direction in which the depolarizing wave is moving.

2.4.2 Electrograms

Electrograms (EGM) are measurements of the temporal change in electric potential between two electrodes. In clinical electrophysiology, electrograms are acquired from various locations, including the surface of the skin and the surface of the heart. Regardless of electrode location, EGMs can be classified into two basic varieties: unipolar and bipolar. All electrograms are a measurement of the electric potential between two electrodes, i.e., bipolar. However, in the case of unipolar EGMs, the anodal electrode is either placed or computed in a manner so as to minimize the amount of common electric field sensing between itself and the exploratory electrode. The assumption of this practice is that the

unipolar EGMs will better represent the potential generated by the local current sources. This type of local sensing was first achieved by placing one electrode in proximity to heart, the probe, and the reference electrode as far away from the heart as possible, e.g., on the leg/foot. Later, a common reference was computed by averaging multiple leads in an attempt to remove dependence on the position of the reference. An early example of a common reference is Wilson's central terminal (WCT), which was developed by Frank Wilson in 1934 and is frequently used to this day [78]. With an indifferent reference, unipolar electrograms are well suited to assess whether an electrode is near a current source and when cardiac activation arrives at a given location. Unipolar EGMs also display largely predictable morphology from point to point as they are not affected by the direction of the activation wavefront relative to the probe [79, 80, 81]. However, the large distance between the probe and the reference electrodes makes unipolar EGMs susceptible to detection of large electric potentials that arise from distant locations, i.e., far-field signals. Because electric fields decay rapidly over distance, the local potentials will typically appear more prominently in the unipolar EGMs. Under certain circumstances, however, the far-field signal can obscure the local potentials of interest or simply generate unwanted noise in the EGM, e.g., sensing ventricular activation when recording potentials in the atria.

With bipolar EGMs, neither electrode is specifically a reference. Rather, these EGMs represent the potential difference along the vector that connects the locations of both electrodes. Bipolar electrocardiograms (ECGs) are the basis of the limb leads that were first acquired by Einthoven, and also represent the primary EGM used in clinical characterization of cardiac surface potentials. The primary advantage of bipolar EGMs, and the reason for their wide adoption in clinical electrophysiology, is their insensitivity to far-field potentials. Electrophysiological catheters frequently contain numerous small electrodes that are spaced at small intervals (2–5 mm). It is between these close electrodes that intracardiac bipolar EGMs are acquired. With this geometric configuration, the distance between the electrodes is very close compared to far-field sources. Returning to the previous example of atrial EGM acquisition, when a bipolar EGM is acquired in the atria, the distance between electrodes is much smaller than the distance of the pair to the ventricular working myocardium. Consequently, even though unipolar EGMs from those same electrodes might sense a very strong ventricular potential, the ventricular components of the signal would appear nearly identical. In the bipolar EGM, which is measuring the potential difference between the two electrodes, the ventricular components would then negate each other in a phenomenon known as common mode rejection. Due to the common mode rejection, the bipolar EGM

is sensitive only to potentials that are produced in proximity to the electrode pair and may provide a better characterization of local tissue properties. However, a number of limitations arise due to the proximity of the recording electrodes. First, bipolar EGMs have a high degree of variability in morphology due to their orientation with respect to the activation wavefront (Fig. 2.10) [82]. Depending on which electrode the wavefront arrives at the first, the polarity of the bipolar EGM can switch. Additionally, that speed of the wavefront relative to the spacing of the electrodes can cause a variable number of deflections from the isopotential line. Finally, if the wavefront passes both electrodes at the same time, i.e., when the axis of the electrode pair is aligned perpendicular to the direction of a planar wavefront, there may be little to no potential difference between the electrodes. In this scenario, the bipolar EGM may incorrectly lead an operator to believe a region of myocardium is scarred [83, 79]. In this work, the question of bipolar EGM performance in characterizing tissue properties features prominently and is the primary subject of Chapter 4.

Plaque electrodes and intracardiac multielectrode mapping arrays, with known electrode geometries, can extend the sampling of electrograms to the examination of spatial properties of cardiac electrophysiology. EGMs generally measure temporal signals but

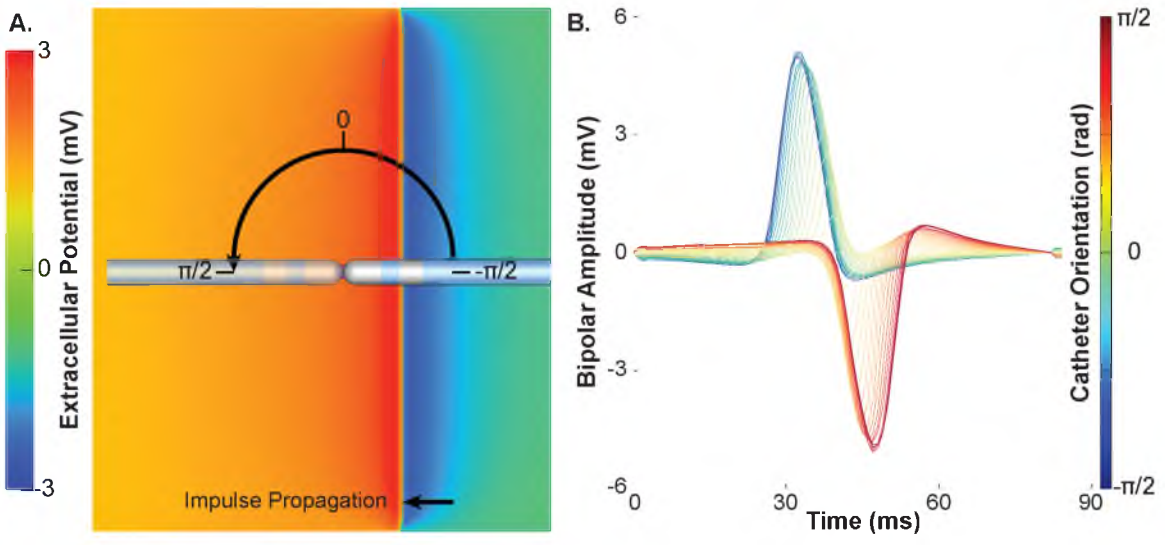

Fig. 2.10. Change in bipolar electrogram morphology caused by rotation of bipolar electrodes around the distal electrode at a fixed point. A. Slab model of cardiac excitation in which a planar activation wave, moving from right to left, is sensed by a clinical mapping catheter at orientations with respect to the wavefront ranging from $-\pi/2$ to $\pi/2$ rads. B. Bipolar electrograms (n=33) acquired with both electrodes in contact with the tissue at increments of approximately 0.05 rads.

may be assessed as spatial phenomena with many of the same sampling considerations, i.e., sampling frequency. For certain applications, such as detection of activation times, applications that take into account the dynamics of electrophysiological phenomena over the spatial domain have demonstrated greater robustness to noise than purely temporal domain strategies. One approach that capitalizes on the spatial information provided by dense electrode arrays is known as Laplacian electrograms [84]. The Laplacian is a spatial derivative of the electrograms over the array geometry. With sufficient sampling, the Laplacian EGM also provides an approximation of current sources and sinks. This technique provides useful signal conditioning that can improve the detection of activation times and reduce sensitivity to noise [59, 32]. In this work, we will present a novel adaption of Laplacian EGMs for rapid and simplified measurement of longitudinal and transverse conduction velocities (see Chapter 7).

2.4.2.1 Body Surface EGMs

The electric potentials that arise from cardiac excitation can be noninvasively measured from the surface of the body. Electrocardiograms (ECG), as depicted in Fig. 2.5, provide extensive information about the electrical function and health of the heart. The P-wave and QRS complex are indicative of atrial and ventricular activation, respectively. The T-wave is generated by ventricular repolarization. Atrial repolarization is masked by the QRS complex. Analysis of ECGs is useful for the detection of many cardiac illnesses, and various aspects of the ECG are employed for diagnosis. ECG features of interest include the timing, morphology of the various waves, and even the presence of a potential where no signal would otherwise be expected. Heart block is an example in which the timing of ECG features can be used to detect an abnormality in the cardiac conduction system. In normal cardiac conduction, the time between the P-wave and the R-wave of the QRS complex, i.e., the PR interval, is 120 to 200 ms. A PR interval greater than 200 ms is considered to be heart block [85, 86]. Moderate to severe cases of heart block require placement of a pacemaker.

Pathologies that change the pattern of cardiac activation will likely change the morphology of features observed in the ECG. For example, ectopic beats in the ventricles, known as premature ventricular contractions (PVC), are common in healthy hearts. PVCs are readily detectable in an ECG. Because excitation originates in the ventricles, there is typically no apparent P-wave. Additionally, the amplitude and width of the QRS complex both increase. The increased width of the ventricular activation signal is attributable to the inefficient capture of the Purkinje systems that rapidly distributes activation across

the ventricles during sinus rhythm. PVCs in the absence of structural heart disease are generally considered benign and are of clinical significance only if they occur in extended runs [87].

A final example of ECG utility for diagnosing cardiac disease is the detection of myocardial ischemia. Ischemia arises in the heart when the arterial blood supply reaching a portion of the myocardium is insufficient. This most often occurs in conjunction with coronary artery disease when one of the coronary arteries, which supply oxygen-rich blood to the myocardium, becomes obstructed. In an ECG, ischemia can be detected as the presence of a body surface potential when the heart should otherwise be isoelectric. Specifically, the action potential of ischemic tissue is much shorter and has a lower amplitude than that of healthy myocardium. As the ischemic tissue repolarizes, a large potential gradient arises between the healthy and ischemic tissues that causes current to flow [88]. In the ECG, this ischemic current appears as an elevation or depression in the potential during the ST segment [89, 90]. Rapid detection of ischemia can be critical to the prevention of myocardial infarction, in which myocytes begin to die, as well as the prevention of sudden cardiac death due to arrhythmias that can arise with the advent of myocardial ischemia [91].

These examples illustrate the broad utility of ECGs for monitoring cardiac health. Additionally, these examples illustrate how various factors can influence the appearance of electrograms. In later chapters, this work will focus on the use of cardiac surface electrograms to characterize the properties of the myocardium. As has been shown for features of the ECGs, indicators such as the timing and morphology of electrical signals are powerful metrics of the health and function of cardiac tissue.

2.4.2.2 Cardiac Surface EGMs

During clinical electrophysiological studies, catheter-based electrodes are used to measure EGMs from various locations on the endo- or epicardial surface of the heart. Though inherently more invasive than ECG recordings, cardiac surface electrograms generally have a high sensitivity to local tissue properties. Intracardiac EGMs, obtained through catheter introduction into peripheral vasculature, are more commonly utilized than epicardial recordings, though the latter have recently been utilized with increasing frequency. In this setting, both unipolar and bipolar EGMs are utilized depending on the application and preference of the operator.

2.4.3 Potential Mapping

Potential mapping in electrophysiology describes the analysis of EGMs in which particular attention is paid to the location from which the signals are acquired. Subsequent analysis for EGM morphological features then allows assignment of specific properties to an anatomical location. This approach is employed for both body surface EGMs and cardiac surface potentials, i.e., body surface potential mapping (BSPM) and electroanatomical mapping (EAM), respectively [92, 93, 94]. For example, a commonly used application for intracardiac potential mapping is known as activation mapping [58, 95]. In activation mapping, the local activation time (LAT) for a given electrode location is estimated from features in the electrogram. With LATs measured at multiple locations, it is possible to generate a visual representation, or map, of the cardiac activation sequence (see Fig. 2.6). Activation maps are particularly useful for localizing sites of ectopy or establishing the path of an anatomical reentrant arrhythmia. Another application of mapping is the measurement of potentials at relevant times in the cardiac cycle. On the body surface, this technique is employed to detect myocardial ischemia in which potentials during the ST segment become elevated. For intracardiac electroanatomical mapping, the peak-to-peak amplitude of the EGM during activation is frequently assessed to identify scarred or otherwise diseased tissue in a process known as voltage mapping [13, 15]. Voltage mapping is a type of potential mapping known as substrate mapping, which will be addressed in greater detail in the following section. Briefly, substrate mapping is the use of EGMs acquired from the surface of the heart to infer the functionality, health, or proarrhythmic potential of that region of tissue. Substrate mapping is commonly employed to guide the application of therapy in the treatment of arrhythmias and is a major focus for this work.

One critical aspect of potential mapping is the necessity to record the location of electrodes when EGMs are acquired. For BSPM, this necessity can largely be addressed through the use of digitizers, photography, or three-dimensional imaging systems. However, tracking the location of catheter-based electrodes that are introduced into the heart via venous access presents a unique challenge. Multiple imaging and catheter tracking systems have been developed, primarily with the objective of delivering therapy for arrhythmias, that can assist with the construction of electroanatomical maps. These systems, and their relative capabilities as they relate to the treatment of AF, are further addressed in Chapter 4 [96, 97].

2.4.4 Substrate Mapping

The electrophysiological properties of myocardium are intimately linked to the tissue-, cellular-, and molecular-level composition and structure of the tissue. Consequently, in one form or another, all cardiomyopathies will impact action potential impulse propagation. Due to the relative robustness of the cardiac conduction system, many of these effects will be insufficient to provoke disruption of sinus rhythm. Furthermore, even moderate disruption, in the absence of an appropriate trigger, will often fail to produce arrhythmogenesis (see Section 2.3.1 - Triggers and Substrates). However, cardiomyopathies do frequently facilitate arrhythmogenesis and necessitate the characterization of the diseased tissue. Identification and treatment of proarrhythmic substrates have generated significant interest over the last 15 years. Magnetic resonance imaging (MRI) and other imaging modalities have recently shown promise for the characterization of cardiomyopathies including infarction and other gross scarring and fibrosis. These promising advances are discussed in detail in Chapter 4. In the electrophysiological mapping domain, advances have also been made in identifying the effect of cardiomyopathies on cardiac surface EGMs. The utility of these EGMs differs from more classic electrophysiological mapping studies in which the relative timing of signals from a given location is of primary interest. In substrate mapping, the EGMs are analyzed for indications that the underlaying tissue is proarrhythmic. As mentioned previously, this application of electroanatomical mapping was initiated by Marchlinski et al. who used the peak-to-peak voltage of EGMs to differentiate between infarct related scar and healthy tissue in patients with infarct-related VT [13]. Depicted in Fig. 2.11, this differentiation of substrate allowed this group to develop ablation strategies targeted at the slow conduction pathways in the infarcted region in order to terminate this anatomical reentrant arrhythmia. Soon after, the same concept was applied to the assessment of cardiomyopathy associated with atrial fibrillation. In this case, Verma et al. were able to show that patients with extensive AF remodeling also had large regions of low voltage EGMs before ablation [15]. Oakes et al. followed this study with a comparison of preablation voltage maps to atrial enhancement seen in preablation LGE-MRI images, which indicate regions of structural remodeling of the cardiac tissue [10]. The findings of this study suggest that low voltage regions correlate with proarrhythmic structural changes that occur during the entrenchment of AF.

These studies and others that followed demonstrated the potential utility of substrate mapping for identifying proarrhythmic substrates and the development of new treatment strategies based on the mechanisms of arrhythmogenesis. Given this impetus, other signal

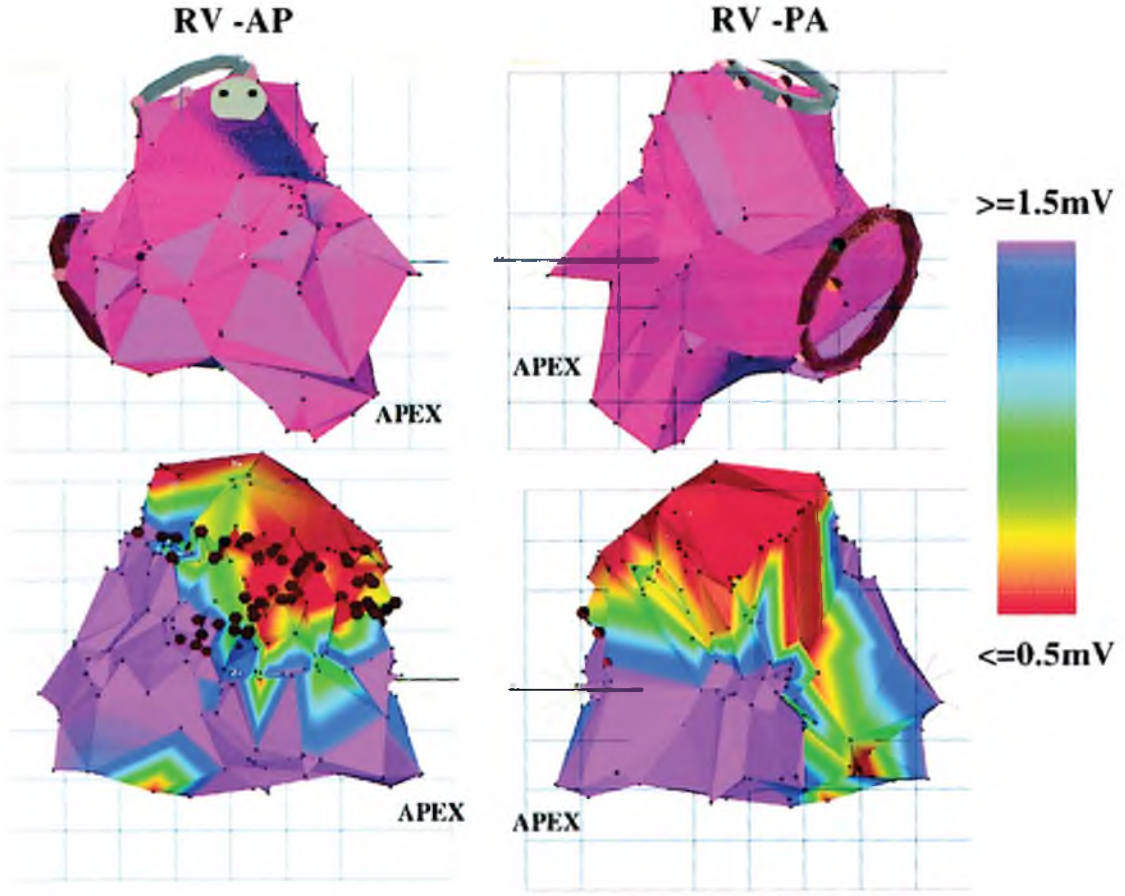

Fig. 2.11. Characterization of myocardial infarct with voltage mapping of the ventricles. Bipolar amplitudes recorded from a mapping and ablation catheter on the endocardial surface of the left ventricle assist in the identification of scarred versus viable myocardium. Based on comparison to voltage mapping performed in structurally normal hearts, Marchlinski et al.[13] classified tissue with a bipolar amplitude of >1.5 mV as normal tissue, and <0.5 mV as dense scar. Used with permission from Marchlinski et al. Circ. 2000.

features that appear in intracardiac EGMs were assessed for association with diseased cardiac tissues. One such feature that sparked interest was fractionated EGMs. Frequently referred to as CFAEs ("cafes"), or complex fractionated electrograms, these EGMs contain multiple spikes indicative of activation in a relatively small time span. The EGMs are often associated with fibrillatory conduction and disruption of the electrophysiological substrate in a manner that allows multiple activation waves to pass in proximity through uncoupled pathways. EGMs acquired during mapping of AF are assessed for the complexity of the CFAEs and are used to guide ablation therapy. By targeting areas with highly complex CFAEs, Nademanee et al. were able to report a high rate of success for terminating AF [98]. These findings have proven difficult to reproduce in other centers but remain an active area

of research.

Dominant frequency (DF) mapping is another substrate mapping strategy used for and acquired during AF. DF mapping analyzes the frequency content of EGMs by identifying the dominant frequency in the EGM's power spectra. Sites with high DF are thought to represent drivers of arrhythmic activity either by micro reentry or rotors [17, 99]. These sites have been targeted with ablation therapy in order to remove the substrates that are responsible for the maintenance of AF. These approaches have also met with mixed success and are a major focus of current research.

In later chapters, this work explores the performance of substrate mapping for detecting diseased tissue using computer simulations. Additionally, other simulations are used to explore the feasibility of other markers as indicators of proarrhythmic tissue for substrate mapping. In this case, the primary features of interest are conduction velocity and conduction anisotropy. Though these parameters are frequently measured in experimental settings, they are rarely used in the clinical environment. As previously mentioned in the discussion of reentry, these factors are direct contributors to the arrhythmic potential of cardiac tissue. Through this work, we will demonstrate novel mapping strategies and analysis techniques that will facilitate the acquisition of these important metrics of substrate viability in the clinical setting.

2.5 Computer Models of Cardiac EP

The measurement of electric fields that are generated from within a living organism presents challenges to efforts aimed at characterizing the behavior and properties of those sources. The heart in particular, with constant movement, vital life-sustaining function, and encapsulation in the thoracic cavity, is difficult to assess. Numerous experimental and clinical techniques have been successfully developed for recording cardiac electric potentials. However, these studies can be very expensive, and ultimately, some variables are effectively uncontrollable in clinical and experimental settings. For these reasons, there is a rich history of mathematical modeling and simulation being used in the study of cardiac electrophysiology. This section will briefly touch on facets of cardiac electrophysiology models relevant to this work. For a more comprehensive treatment of this topic, please refer to reviews by Rudy et al. [100], Vigmond et al. [101], or Winslow et al. [102].

Most modern computational models of cardiac electrophysiology are based on representations of the underlying currents that generate action potentials in cardiac tissue. Due to the variation in action potential morphology that occurs in different regions of the heart (see Fig. 2.5), these representation, or membrane models, strive to reproduce

these characteristic action potentials based on their respective compositions of ion channels (Fig. 2.12). For example, the Luo-Rudy model of a ventricular myocyte describes a cardiac action potential based on the activity of the constituent ionic currents [103]. This model has been revised over time to incorporate newly discovered channels or mechanisms that inform the generation of action potentials in the ventricular myocardium [104, 105]. Membrane models are based on the formalism of Hodgkin and Huxley in which the cell membrane is treated as an ideal capacitor in parallel with ion channels that are resistors to the flow of current across the membrane [106]. The transmembrane voltage (V_m) follows the equation describing the current and voltage with capacitance:

$$\frac{dV_m}{dt} = -\frac{1}{C_m}\left(\sum_j I_j + I_{stim}\right), \tag{2.9}$$

where t is time, Cm is the capacitance of the membrane, I_j represents ionic current j, and I_{stim} is an applied stimulus current [101, 107]. Such models are able to capture the characteristic features of cardiac action potentials and have been invaluable for the understanding of individual myocyte behavior. However, because of the computational overhead required to simulate these models, is it currently infeasible to construct whole heart models in which a transmembrane potential is computed for every myocyte.

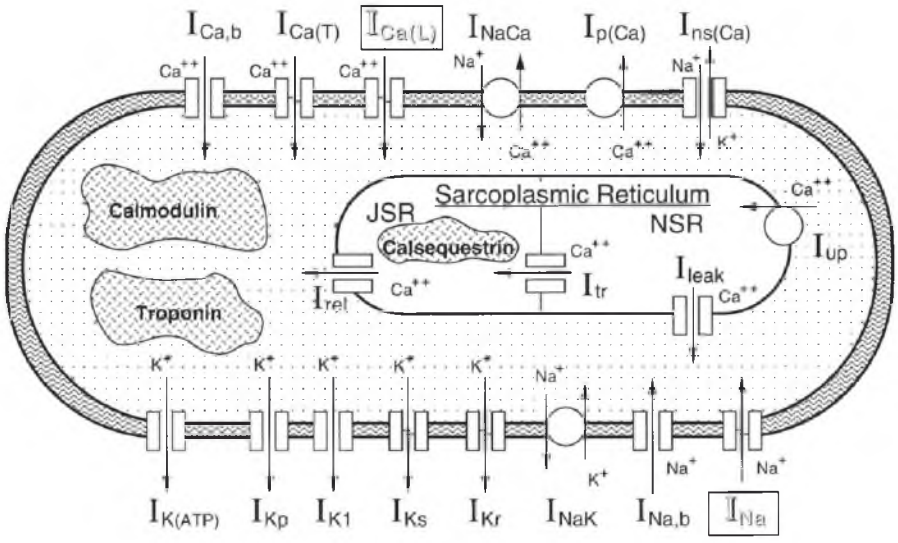

Fig. 2.12. Depiction of ionic currents incorporated into a ventricular myocyte membrane model. Each channel is modeled as a resistor to the flow of ionic currents in parallel with the capacitance of the membrane. The conductance of each channel is determined by its molecular structure including gating and inactivating mechanisms. Used with permission from Shaw et al. Circulation Research. 1997 [105].

The bidomain equations facilitate simulation of cardiac excitation by homogenizing the cardiac tissue into a syncytium, rather than solving a membrane model for every coupled myocyte [108]. Bidomain models discretize the cardiac tissue into a collection of points that average the electrical properties over small regions, e.g., gap junction conductivity and tissue anisotropy, and solve for a transmembrane potential at each point (Fig. 2.13). Throughout the model, the bidomain equations relate the intracellular potential (ϕ_i) to the extracellular potential (ϕ_i) through the transmembrane current density, (I_m):

$$\nabla \cdot \sigma_i \nabla \phi_i = \beta I_m, \tag{2.10}$$

$$\nabla \cdot \sigma_e \nabla \phi_e = -\beta I_m - I_{stim}, \tag{2.11}$$

where σ_i and σ_e are the intra- and extracellular conductivity tensors, respectively, β is the surface to volume ratio of the cardiac cells, and I_m is the transmembrane current [108, 101].

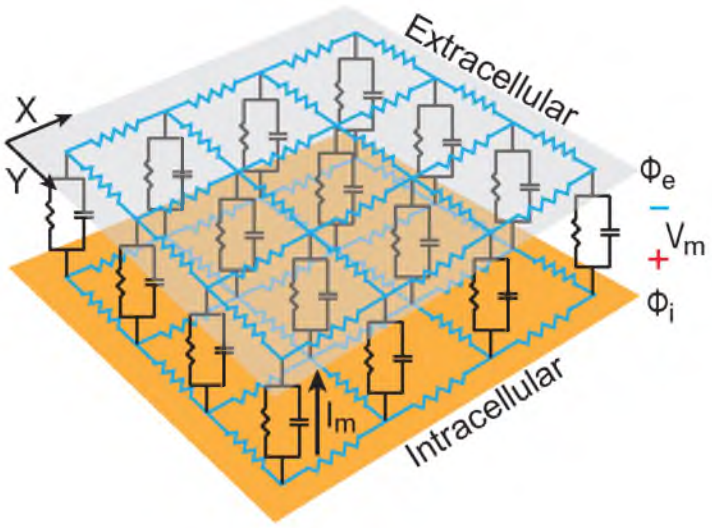

Fig. 2.13. Two-dimensional bidomain representation of myocardium. The intra- and extracellular domains (orange and transparent gray planes, respectively) are discretized into small regions with anisotropic resistances in each direction as depicted by the blue network of resistors in both domains. At each point, or region, the intra- and extracellular domains are coupled by the capacitance of the membrane and the cumulative resistance of ion channels to the flow of ion current across the membrane (I_m). This current–voltage relationship can be described in terms of the transmembrane potential (V_m), i.e., the difference in intra- and extracellular potential at each point (ϕ_i, ϕ_e, respectively). Modified with permission from Vigmond et al. Prog Biophys Mol Bio. 2008 [101].

With this formulation, the membrane models can be solved at each point in the model to provide values for the transmembrane potential. Next, the intracellular potential can be removed from Equations 2.10 and 2.12 with the relationship:

$$\phi_i = V_m + \phi_e. \tag{2.12}$$

Finally, with addition and some recombination, a description of the extracellular potential (ϕ_e) in terms of the transmembrane potential (V_m) can be obtained [109].

$$\nabla \cdot (\sigma_i + \sigma_e)\nabla\phi_e = -\nabla \cdot \sigma_i \nabla V_m. \tag{2.13}$$

The bidomain formalism provides a powerful tool for exploring electric fields generated by excitable membranes. Bidomain models allow for reconstruction of electrograms that result from cardiac excitation. With the bidomain, it is possible to adjust cell models and conductivity tensors to mimic a variety of cardiomyopathies that arise in the clinical setting. Bidomain simulations have been particularly useful in the study of arrhythmogenic mechanisms [110, 111, 112]. One downside of bidomain simulations is the requirement of significant computational resources to simulate realistic models. However, in recent years, great progress has been made towards improving the efficiency and time required to run these simulations. Much of this progress is based on distribution of the model for solving on multiple cores or graphical processing units (GPU) [113]. This dissertation utilized the Cardiac Arrhythmia Research Package (CARP) to solve bidomain simulations of cardiac electrophysiological mapping studies [20].

CHAPTER 3

ATRIAL FIBRILLATION

In the previous chapter, a model of arrhythmogenesis was proposed in which triggered electrical activity interacts with disrupted myocardial substrates to produce arrhythmic activity. Various examples of arrhythmic activity, e.g., AVNRT, heart block, etc., were also discussed to illustrate these mechanisms and how they are detected using ECG. In this chapter, we will delve further in one particular arrhythmia, atrial fibrillation (AF), using the context of the triggers and substrate to guide the exploration of contributing factors to AF.

3.1 Background and Significance of AF

AF is the most common clinically relevant cardiac arrhythmia causing complete disruption of atrial electrical activation and, by association, collapse of atrial mechanical function. The clinical significance of AF is primarily attributable to the cessation of coordinated contraction in which blood pools and coagulates in the left atrial appendage. These coagula can then break free, embolize in the cerebral vasculature, and precipitate an ischemic stroke. According to the CDC, AF increases the risk of stroke by $\approx$ fivefold for all ages, with 15% of all ischemic strokes traceable to AF [60, 114]. This alarming risk is compounded by the sheer number of people experiencing AF. In the United States alone, the prevalence of AF in 2010 was estimated to range from 2.7 to 6.1 million and is expected to rise to 5.6 to 12 million in 2050 [115]. Estimates put the cost of AF treatment in the United States in excess of $6 billion per year [116]. Based on these figures, it is clear that AF is a significant detriment to human health. However, the pathogenesis of AF is complex, with multiple comorbidities, e.g., valvular disease, coronary artery disease, hypertension, diabetes, heart failure, advancing age, etc., increasing the likelihood of AF occurrence [117]. In fact, the occurrence of lone AF, or AF without any attendant comorbidities, is estimated to be around 10% [118, 119, 120]. Cast in this light, AF appears more as a debilitating symptom of atrial cardiomyopathy induced by the aforementioned comorbidities [121]. The remainder

of this chapter will largely focus on this particular point, that is, AF is primarily a reflection of pathological alterations to the electrical and structural substrate of the atrium.

3.2 Detection of AF

Symptoms of AF may include racing of the heart, irregular or weak pulse, rapid fatigue, lightheadedness, shortness of breath, and chest pain. However, some people with AF have no symptoms and may go undiagnosed. Additionally, the duration of AF in patients can vary across a broad spectrum, with some patients experiencing episodes that last less than a minute whereas others are in constant AF. Along this spectrum, AF is typically divided into three categories: paroxysmal, persistent, and permanent (or long-standing persistent). Paroxysmal AF describes AF in which episodes self-terminate within 7 days of initiation. Persistent AF is characterized by episodes of AF that do not autonomously resolve within 7 days and require termination through electrical or chemical cardioversion. Permanent or long-standing persistent AF is defined as continuous AF of greater than 12 months duration [7]. Permanent AF typically does not respond well to cardioversion, often reinitiating after only a few sinus beats. The severity of AF as based on these classifications is important in guiding treatment options for patients afflicted with this arrhythmia.

In addition to the presence of the symptoms mentioned above, standardized diagnosis of AF is accomplished by ECG. Classic features that indicate the presence of AF include absence of a P-wave, rapid heart rate, and irregular R-R intervals (Fig. 3.1) [122, 7]. In sinus rhythm, the P-wave is produced by the synchronized activation of the entire atria. The absence of a clear P-wave in AF is attributable to the uncoordinated and incessant activation of the atrial tissue. In some cases, this may appear as baseline noise in the ECG. In AF, the portions of the atria may be activating at rates of upward of 300 beats per minute. This high rate of activation will cause a rapid ventricular response, and the heart will race even when the patient is at rest. However, the high rate of atrial activation exceeds the maximum refractory rate of the AV node, and only a portion of the impulses that stimulate the AV node will actually transmit to the ventricles. The irregular activation patterns of the atria and the block of some impulses combine to cause increased variability of ventricular activation. This increased variability can be quantified by measuring the time between QRS signals from beat to beat (R-R interval). Occasionally, AF can produce ECG findings similar to those of atrial flutter, leading to misdiagnosis [123].

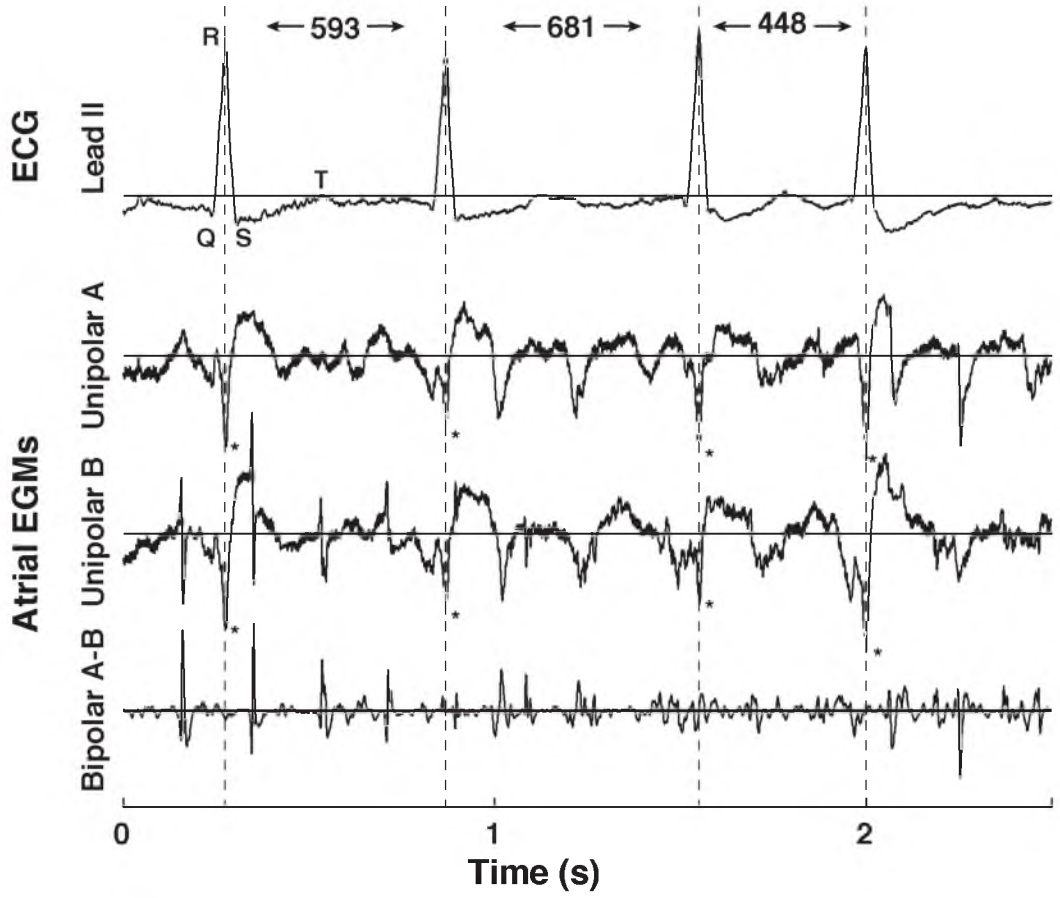

Fig. 3.1. ECG and EGMs acquired from patient in AF. The ECG from lead II shows classic AF presentation including variable R-R interval, absence of P-wave, and rapid ventricular response. The atrial EGMs were acquired from two neighboring electrodes on a loop mapping catheter in the left atrium. The unipolar EGMs demonstrate the rapid and chaotic atrial electrical activity but also sense far-field ventricular activation (*). The ventricular signal is conspicuously absent in the bipolar EGM due to effective common mode rejection of far-field signal.

3.3 Initiation of AF

Initiation of AF is typically attributed to the classic reentry mechanisms introduced in Chapter 1. In 1998, Hassaguerre et al. demonstrated that the triggered activity necessary for reentry is primarily associated with ectopic foci located in the pulmonary veins [26]. In this work, the earliest site of activation was mapped with an endocardial catheter via percutaneous access. Subsequent ablation of these sites of ectopy with radio-frequency (RF energy) prevented a recurrence of AF in 62 % of patients at 8 months. This landmark finding helped to clarify the source of the trigged activity necessary to initiate reentry. Over 15 years later, the prevention of ectopic impulse propagation from the pulmonary veins remains a cornerstone of AF treatment and general mechanistic understanding [124, 125, 126, 127, 7].

However, as previously discussed, triggers alone are insufficient to provoke sustained reentry and must interact with a proarrhythmic substrate, e.g., slow conduction pathways. Over the same 15 years, extensive research has focused on the nature of the substrate that is responsible for AF initiation and the mechanism of reentry that allows it to persist.

3.4 Entrenchment of AF

In the study of the AF substrate, it has been established that multiple cardiac tissue properties are altered in patients with AF. Importantly, findings from Wijffels et al. in 1995 showed that alteration of these cardiac tissue properties progresses as AF persists to further entrench the arrhythmia [128]. This process, summarized as "AF begets AF," encapsulates remodeling of both electrical and structural tissue properties that promote the initiation and maintenance of AF. However, as previously mentioned, multiple pathways can lead to AF, and no one AF substrate is quite like another. Consequently, it is difficult to attribute any one factor as the cause of AF, and the whole spectrum of factors must be considered. Regardless of the proarrhythmic features that may manifest in a given patient, sustained AF requires a trigger and a substrate, whatever that substrate may be. Sections 3.4.1 and 3.4.2 will cover the electrical and structural properties that promote AF initiation and further remodel to facilitate the entrenchment of AF.

3.4.1 Electrical Remodeling

Through aggressive stimulation protocols, AF is inducible in any heart, albeit for short episodes in some cases [129]. This arrhythmic potential can be enhanced through continuous rapid activation of the atrial tissue. In 1995, two groups, Morillo et al. [130], and Wijffels et al. [128], reported on changes in the electrophysiological properties of the atria when pacing was used to maintain rapid activation rate (150 ms cycle length) in canines or perpetuate AF in goats, respectively. Both studies were able to demonstrate a significant shortening of the atrial effective refractory period (ERP) following periods of rapid atrial excitation (Fig. 3.2). Furthermore, in the goat model, it was shown that within a week of stimulated maintenance of AF, episodes became sustained, i.e., lasted over 24 hours, whereas the duration of control episodes was less than 10 seconds (Fig. 3.3). These findings led to the oft-repeated phrase coined in the Wijffels et al. paper that "AF begets AF." The basis of this theory is that the arrhythmic conditions that present in AF induce adaptation of the electrophysiological substrate in a manner that entrenches atrial fibrillation. This adaptation is now commonly referred to as AF-induced electrical remodeling [131, 132].

Electrical remodeling can be traced primarily to alterations in ionic current and cellular

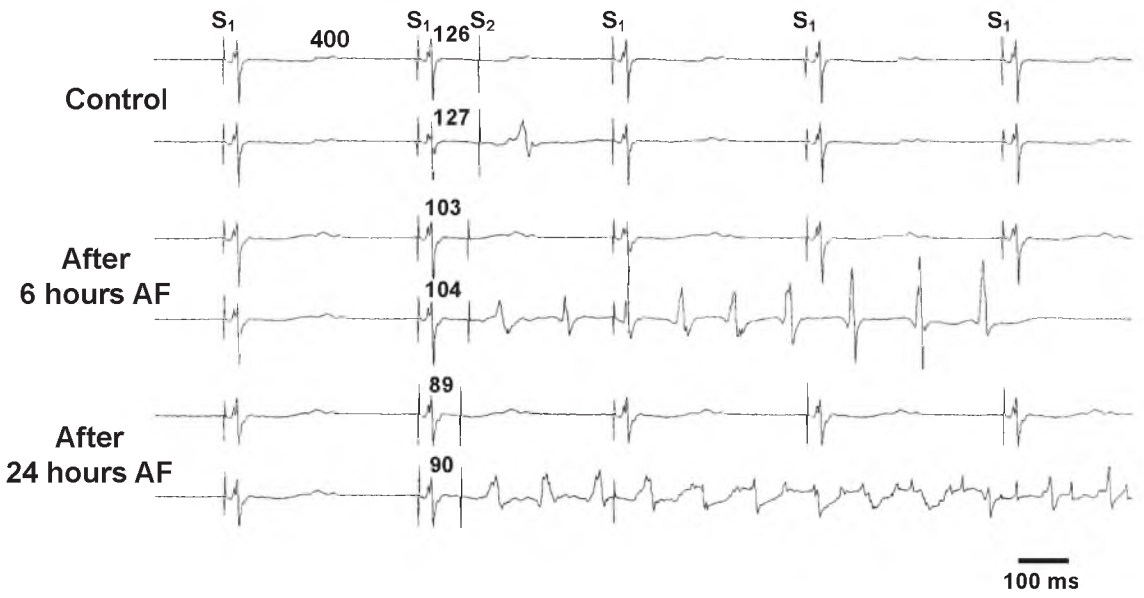

Fig. 3.2. Illustration of the shortening of the atrial refractory period during the first 24 hours of electrically maintained atrial fibrillation. Two electrograms (EGM) are shown for each state, i.e., control, 6 hours, 24 hours, in which the atrial effective refractory period (ERP) was evaluated. The top EGM for each state illustrates the coupling interval (S_2) at which pacing capture failed due to the ERP when a train of 400 ms cycle length S_1 beats was followed by the indicated S_2 stimuli. The lower EGM demonstrates successful capture when the coupling interval exceeds the ERP. The ERP progressively shortens over the 24 hours of AF maintenance with 50 mHz burst pacing. Used with permission from Wijffels et al. Circ. 1995. [128]

excitability. In acute settings of rapid heart rate, as might occur with physical exertion, the shortening of action potential duration, known as restitution, is an essential physiological control that allows the heart to accommodate increased demand. Such restitution may play a role in the initiation of AF, but electrical remodeling is generally regarded as additional changes that occur over days and weeks of exposure to rapid activation rates. Yue et al. demonstrated progressive down-regulation of the transient outward K^+ current (I_{TO}) and the L-Type Ca^{++} current over 6 weeks of rapid atrial pacing that accounted for shortening of the atrial action potential duration and consequently the refractory period [133]. Through shortening of the refractory period, AF decreases the wavelength necessary for reentry to occur, facilitating both AF initiation and perpetuation.

In addition to changes in action potential generating currents, the response of the intramyocyte coupling connexin proteins to AF has also been studied. Multiple studies of right atrial tissue extracted from patients with AF have asserted that changes occur in the

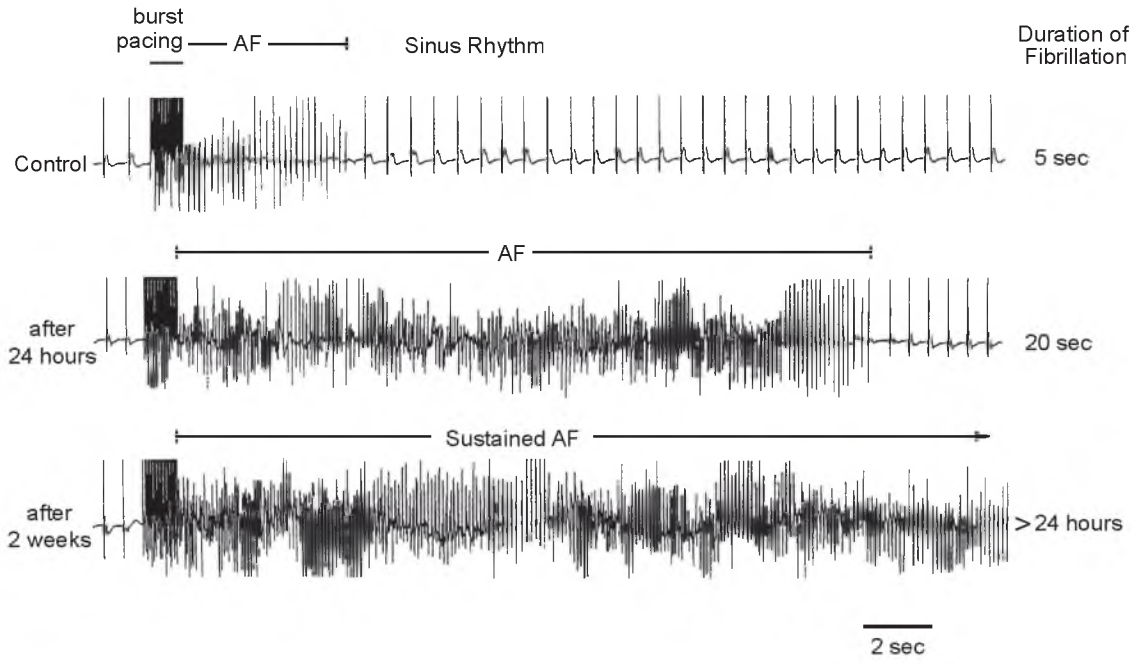

Fig. 3.3. Prolongation of the duration of episodes of electrically induced atrial fibrillation maintaining AF for 24 hours and 2 weeks, respectively. Burst pacing (50 mHz) stimulation of the atrial tissue provoked stimulation of AF in chronically instrumented goats. AF was continuously reinduced following AF resolution to sinus rhythm in order to maintain fibrillation. Over the course of 2 weeks of this stimulus protocol, the duration of provoked AF episodes increased from seconds to hours to persistence, indicating that the AF induces changes in the electrophysiological substrate that entrench the arrhythmic behavior. Used with permission from Wijffels et al. Circulation. 1995. [128]

distribution and expression of atrial specific connexin 40 (CX 40) gap junctions. However, the results of these studies were inconsistent, with one study showing increased CX 40 expression and movement of the protein position to the lateral membrane of the myocytes [134]. Other studies in persistent and longstanding AF indicated that CX 40 expression was decreased [135, 136]. This lack of consensus is not wholly surprising given the many different factors that can lead to AF, and may simply be a product of differing patient populations. Regardless, connexins play an important role in distributing depolarizing impulses to resting myocytes. Changes in the amount of current and directional flow of depolarizing current could contribute to reentry through multiple mechanisms, including the slowing of conduction velocity.

3.4.2 Structural Remodeling

Atrial fibrillation is strongly associated with structural disruptions of the myocardial substrate that create proarrhythmic conduction abnormalities [1, 137, 2, 121]. These disruptions may manifest as atrial fibrosis, dilatation, or dissociation of myofibrils [135]. It is clear that the extent of the substrate disruption, or structural remodeling, directly impacts the entrenchment of AF. Structural remodeling contributes to the entrenchment of atrial fibrillation both through disruption of action potential propagation and by increasing the maximum potential wavelength of a reentrant circuit [29]. Many factors including mitral valve regurgitation, hypertension, and congestive heart failure are known to induce remodeling of the structural substrate and promote AF. Conversely, the rapid ventricular activation rate caused by AF can initiate or exacerbate heart failure and further promote structural remodeling. In many cases, it is unclear what is cause and what is effect. Current understanding indicates that structural disruption of the atria promotes AF and, in a classic positive feedback loop, AF induces increased structural remodeling.

Dilation of the atria is a key aspect of structural remodeling mediated promotion of AF [138, 139, 140, 141]. In the absence of a tortuous path for reentry, a small atrium provides few and short paths for reentry to develop. In the wavelength model of the arrhythmic potential of a cardiac substrate, as introduced in Section 2.3.2, the CV and ERP were cited as the primary factors (Equation 2.4) in determining whether the wavelength of a given circuit would be sufficient to sustain reentry. Atrial expansion, however, demonstrates the inverse of this model. By simply increasing the atrial size, dilatation broadens the possible path length available for a reentrant circuit, irrespective of changes to CV or ERP. Patients with AF have frequently been observed to have left atrial volumes in excess of 150 mL, or nearly three times the normal size (<50 mL) of an atrium [142, 143], and occasionally even larger (Fig. 3.4) [144, 145]. Such extreme dilatation provides ample path length and pathways for the initiation and perpetuation of AF inducing reentry.

Extreme cases of atrial dilatation are most commonly attributed to valvular dysfunction, e.g., mitral valve regurgitation, hypertension, and congestive heart failure. Compromised function of the mitral valve permits reversed flow of blood into the left atrium during ventricular systole. This flow reversal is believed to create a hemodynamic burden on that atrial tissue that ultimately results in atrial dilatation [139]. This expansion of atrial size provides a clear path to increased wavelength and entrenchment of atrial fibrillation. However, as has been previously discussed, with atrial fibrillation cause and effect are frequently interchangeable. In 1990, Sanfilippo et al. reported on echocardiography findings

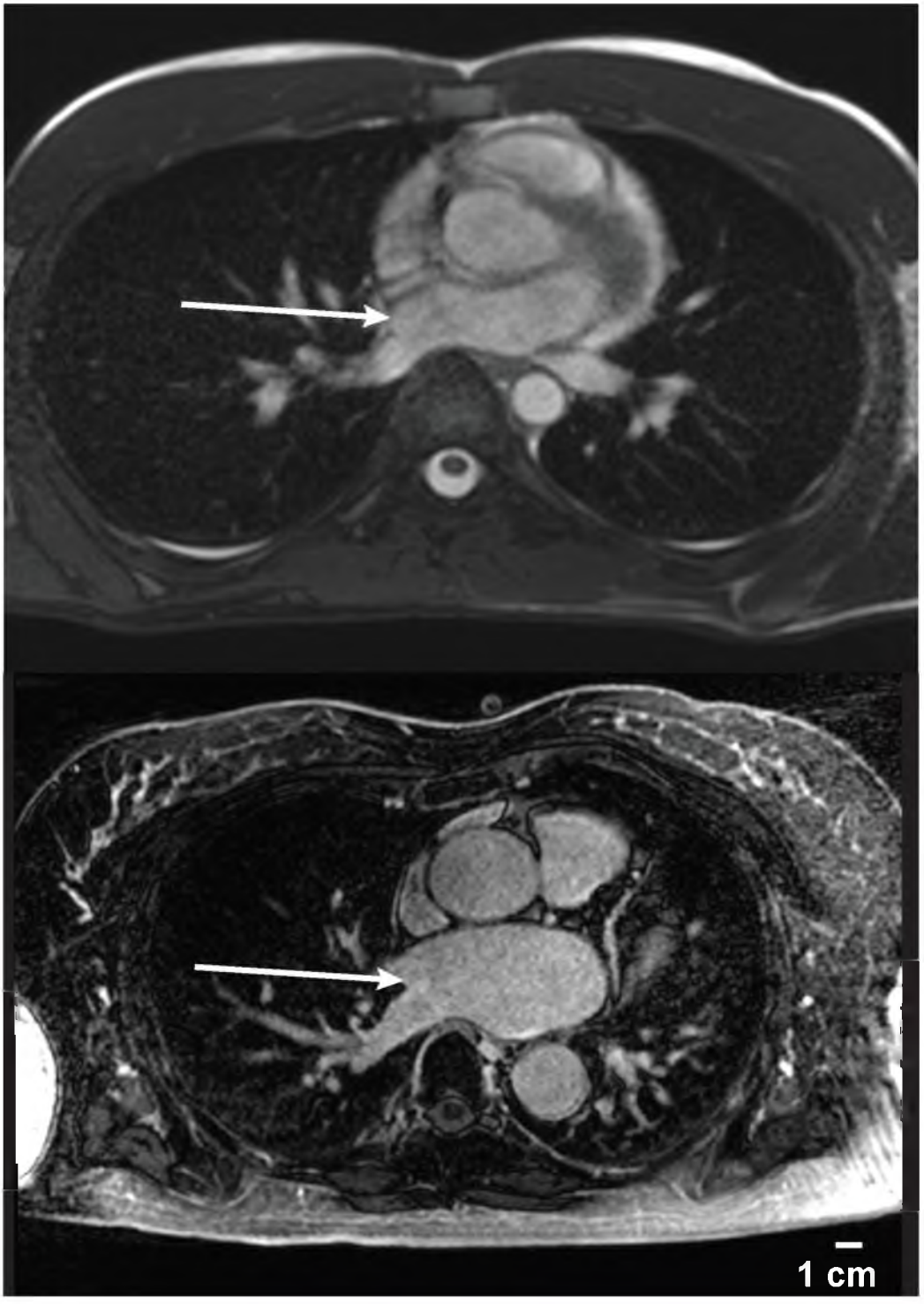

Fig. 3.4. MRI of structurally normal and dilated left atria (LA). The top image depicts my, I hope, structurally normal LA. The bottom image shows an approximately slice matched dilated LA of a patient with AF. The AF patient's LA is nearly 40 mL larger in volume than my own, in spite of my being 0.22 m taller and 18 kg heavier.

from a cohort of patients recruited for a study on anticoagulation in AF [142]. As part of the enrollment for this study, patients received an echocardiographic assessment of both right and left atrial chamber volumes. Capitalizing on these data, this group examined the cohort of 246 patients for cases in which normal atrial volumes and no valvular or structural heart disease that might independently result in dilatation were observed. Of the original cohort, 15 patients met the inclusion criteria and consented to receive a follow-up echocardiographic examination. The average time between the initial and secondary examination was on average 20.6 months (range, 12-28 months). In this small cohort, all patients experienced an increase in left and right atrial volume. The increase in volume for both the left and right atria was highly significant (45.2 mL to 64.1 mL and 49.2 mL to 66.2 mL, respectively). This increase in volume, in the absence of structural or valvular heart disease, was an early indication that AF itself had a deleterious effect upon the structural substrate of the heart.

Fibrosis, or the excesses deposition of extracellular matrix, is also strongly associated with AF entrenchment, and provides another strong indication that AF induces structural remodeling of cardiac tissue [67, 146, 137, 147]. Cardiomyocytes are surrounded by a matrix of proteins, e.g., collagen, that provides structural support to the tissue. The amount and organization of this extracellular substrate can strongly affect the cell-to-cell communication and mechanical function. Fibrosis can occur in most tissues and is usually in response to a physiological inflammatory response mechanism. Consequently, fibrosis is often seen in the context of wound healing, accumulation of oxidative injury that occurs with age, or in mechanical overload. On a microscopic level, cardiac fibrosis predominantly accumulates along the lateral aspect of myocytes, causing side-to-side uncoupling or dissociation of myofibrils. The presence of fibrosis disrupts cardiac impulse propagation by slowing conduction and altering conduction anisotropy by attenuating the close coupling of myocytes [30, 5, 148]. As with atrial dilation, fibrosis frequently manifests in the presence of valvular heart disease, hypertension, and heart failure and promotes the entrenchment of AF from paroxysmal to persistent. Once again, however, this pathway also appears to work in reverse with AF itself, causing enhanced fibrosis.

Structural remodeling is a key feature of AF domestication. Whereas the physiological adaptations associated with electrical remodeling appear to rapidly accommodate AF entrenchment following initiation (within minutes to days), they also seem to return to normal status soon after the resumption of sinus rhythm. However, the substrate associated with AF structural remodeling develops more slowly (weeks to years) and is less amenable to reverse remodeling [149]. Features of structural remodeling including

dilatation and fibrosis may take years to develop and may not completely dissipate upon the resumption of sinus rhythm [150, 151]. Recent studies using MRI to characterize the structural substrate in patients with AF have demonstrated the importance of structural remodeling on the entrenchment of AF. Oakes et al. [10], Mcgann et al. [11], and Marrouche et al. [152] were able to show that patients with extensive structural remodeling had a much higher likelihood of failing treatment of AF with catheter ablation (Fig. 3.5). More information about imaging techniques employed in the treatment of AF is available in Chapter 4. These findings support early and aggressive treatment on atrial fibrillation and the concomitant stressor that elicit structural remodeling of the atrial electrophysiological substrate [153, 154].

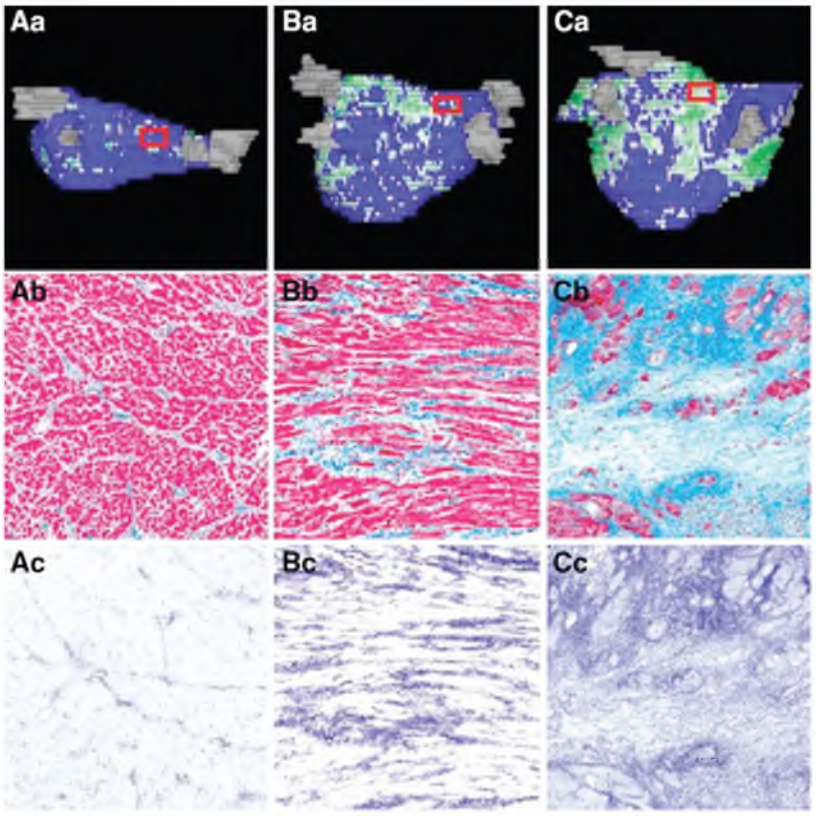

Fig. 3.5. Left atrial (LA) wall structural remodeling (SRM) on late gadolinium enhancement MRI (LGE-MRI) correlates with surgical biopsy specimens. Examples from three surgical patients who underwent both three-dimensional (3D) LGE-MRI scanning and biopsy of the LA wall. Control patient without atrial fibrillation (AF) shown in left (AaAc), AF patient with moderate amount of SRM in middle (BaBc), and AF patient with advanced SRM on right (CaCc). Three-dimensional LGE-MRI renderings show fibrosis/SRM in green with normal tissue in blue (top). Masson trichrome stains collagen blue and LA myocytes red (middle, standard staining; bottom, subtraction images). Red box shows biopsy location. Used with permission from Mcgann et al. Circ. Arrhythmia Electrophysiol. 2014. [11]

3.5 Mechanisms of AF

The mechanisms behind AF initiation and perpetuation have been the source of interest and debate for over a century. As mentioned in Section 3.3, the mechanism of AF initiation was largely settled with the work of Hassaguerre et al., when ectopic beats were demonstrated to trigger fibrillation in humans [26]. However, the nature of fibrillatory conduction that drives AF to persist remains a controversial topic. Two candidate sustaining mechanisms are: 1) spatially localized sources, e.g., rotors (spiral waves) that drive fibrillation or, 2) nonlocalized spatially meandering mechanisms, e.g., multiwavelet reentry (Fig. 3.6) [155, 117].

Support for stable sources of functional reentry, in the form of rotors or spiral waves, as a sustaining mechanism for AF has come from various sources [156]. Optical mapping studies of AF in sheep have shown stable rotors to drive AF [157]. However, until recently, scant evidence existed to support this type of AF driver in humans. Specialized signal processing of basket catheter recordings by Narayan et al. purports to show proof of stable rotors in patients with AF [99]. Furthermore, targeted ablation of these rotor sites was reported to have a beneficial effect in preventing AF recurrences. These findings have sparked considerable interest in mapping techniques geared towards the detection of rotor

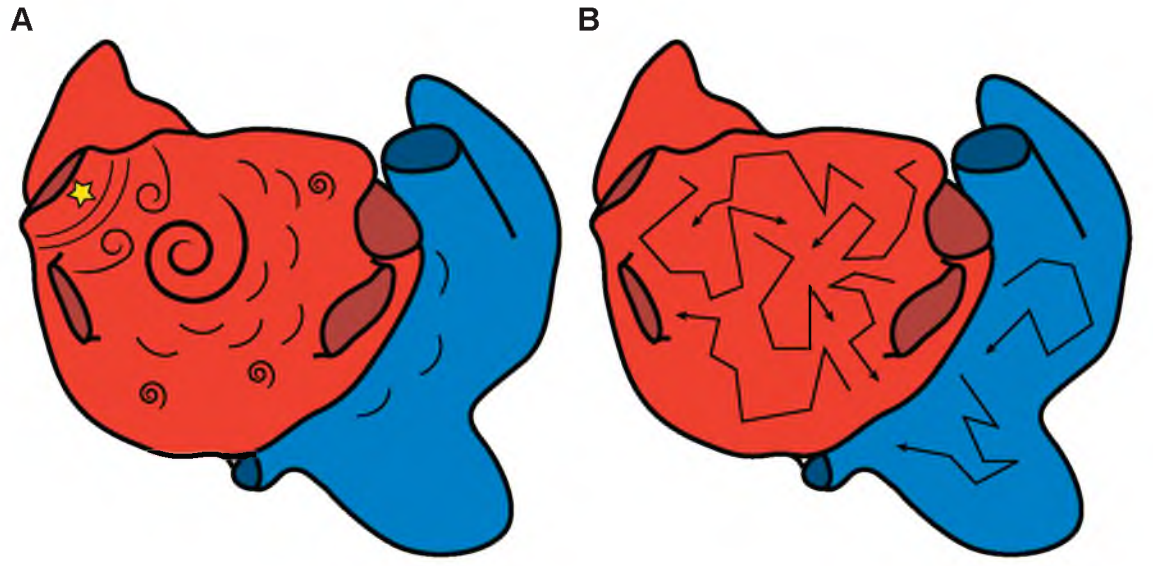

Fig. 3.6. Proposed AF sustaining mechanism. A – Posterior view of left (red) and right (blue) atria depicting AF as driven by a stable mother rotor, triggered by pulmonary vein ectopy (yellow star), that spawns other spiral waves. B – Depiction of multiwavelet reentry where numerous wavefronts simultaneously capture dissociated regions of myocardium.

activity, e.g., dominant frequency mapping. The limited resolution of current clinical basket catheters and the challenge of interpreting EGMs acquired during AF suggest the need for further exploration of the role of stable reentry as a sustaining mechanism of AF.

Multiwavelet reentry is predicated on the utter disruption and fragmentation of action potential impulses such that at any given time, multiple dissociated wavefronts exist and are able to capture new reentry pathways and spawn new wavelets at a faster rate than other wavelets annihilate due to conduction block. This mechanism of sustaining AF was first proposed by Moe and Abildskov [158] and has more recently been championed in the work of Allessie et al. [159, 5], Konings et al. [160], and de Groot et al. [4]. This model of AF perpetuation requires the electrical activity of the atria to become so fragmented and chaotic that waves of activation may literally pass one another across microscopic dissociations of muscle fibers and the endo- and epicardial layers of the atrial. This transmural dissociation becomes so complete that interlayer communication of wavelets appears at only a few preserved intramural connections and manifests as epicardial breakthrough when recorded from the surface of the heart. These findings are based on recordings from the epicardial surface of human hearts using high-resolution plaque electrodes. Unlike the basket electrodes, these plaques have small interelectrode spacing, but have much less overall coverage of the atria. Much like the rotor mapping, the analysis of the fibrillatory EGMs requires extensive signal processing with notable dependence on heuristic interpretation of what signal constitutes local tissue excitation.

At this stage, evidence for both sustaining mechanisms of AF has been reported and may indicate that different types of AF may occur in different populations with different comorbidities. It is also possible that some as yet unrealized process is at work. Ongoing work into the characterization of the sustaining mechanisms is a very active and developing field of research.

3.6 Management of Atrial Fibrillation

A thorough review of the treatment options in the management of atrial fibrillation is well beyond the scope of this document. For detailed coverage of this topic, the reader may refer to published consensus statements and review articles [7]. In this work, a very brief introduction will be provided on some of the medical and treatment options currently available for the treatment of AF.

3.6.1 Anticoagulation

Ischemic stroke is the primary concern for patients with newly diagnosed AF. During AF, the left atrial appendage does not efficiently contract, causing blood to pool and potentially coagulate. If this coagulum embolizes, it can travel to the brain, block vital arterioles, and cause downstream cell death through ischemia. In response to this heightened risk, patients with AF are placed on anticoagulation therapy. In the past, such therapy typically meant warfarin (coumadin), which can be difficult to titrate and may lead to episodes of internal hemorrhage. Recently, a number of new anticoagulants have entered the market and have compared favorably to warfarin, e.g., rivaroxaban, apixaban, or dabigatran. For further information on aspects of anticoagulation in AF, please refer to a review article by Lip et al. [161].

3.6.2 Rhythm Versus Rate Control

Antiarrhythmic medications known as rhythm control drugs have been developed to prevent or terminate cardiac arrhythmogenesis. Rhythm control medications come in different classes depending on what ion channel they augment. For example, amiodarone is a class III antiarrhythmic agent that acts on K_+ channels to prolong phase 3 of the action potential. Extending the action potential prevents arrhythmogenesis by extending the refractory period. Amiodarone is a potent antiarrhythmic drug, but, like most rhythm control agents, can have potent side effects, e.g., pulmonary fibrosis, thyroid dysfunction, etc. Interestingly, one paradoxical yet established effect of antiarrhythmic medications is proarrhythmia [162, 163, 164]. Prolongation of the action potential clearly inhibits reentry through the extension of the refractory period, but may render the heart susceptible to arrhythmia, such as life-threatening torsades de pointes (also known as polymorphic ventricular tachycardia) that can occur in conditions of long QT intervals and dispersion of QT intervals. These considerable risks associated with rhythm control therapy necessitate careful selection of drugs based on the unique presentation of each patient. Ultimately, many AF patients, especially the old and persistently fibrillating, have little to gain with rate control therapy [165, 166].

AF can induce a rapid ventricular response that can induce palpitations and if allowed to persist may trigger the onset of heart failure. For patients in which rhythm control fails, or is contraindicated, it is still desirable to mitigate the tachycardic ventricular response to AF. Rate control therapy uses pharmaceutical agents that target neurohormonal mechanisms that dictate cardiac rate under normal physiological conditions. For example, agents known as "beta-blockers" modulate the sensitivity or function of beta-adrenergic receptors that are

the primary signaling target for rate accelerating factors such as epinephrine. Coupled with effective anticoagulation therapy, rate control strategies can mitigate the effect of AF on the rest of the heart. However, it is generally conceded that this approach leaves the atria susceptible to the chronic effects of AF-induced remodeling (see Section 3.4) [165, 166].

3.6.3 Intervention

Before the advent of minimally invasive percutaneous cardiac catheterization, surgical techniques were developed for treating AF. First performed in 1987, the Cox maze procedure gained access to the atrium through medial sternotomy and cardiac bypass in order to create permanent lines of block that could prevent fibrillatory conduction through compartmentalization of the heart [167]. These lines of block were created by literally cutting through the atrial wall and and then stitching the cut back together. This approach for AF management was refined and culminated in the Cox max III procedure, which has reported a success rate of over 90% [168]. This high rate of success made the Cox maze III a natural choice for cases in which open-heart surgery was already indicated, e.g., mitral valve repair. However, such invasive surgical procedures come with considerable risk to the patient. Nevertheless, the Cox maze III procedure remains the gold standard for interventional abolition of AF. Regardless of this efficacy, the focus of AF intervention has shifted to the percutaneous catheter ablation due to the reduced invasiveness of these approaches.

In Section 3.3, the work of Hassaguerre et al. was introduced as a defining study for current understanding of the mechanism of AF initiation [26]. In addition to the identification of ectopic triggers as the source of AF initiation, this work was able to demonstrate that targeted destruction of trigger sources with radio frequency ablation (RFA) could potentially cure AF. This finding has informed the basis of interventional treatment of AF since the turn of the century. However, due to the risk of pulmonary stenosis that can arise with ablation of ectopic sources in the pulmonary veins (PV) [169], ablation strategies have shifted from one of source targeting to one of source isolation. Specifically, Pappone et al. and others pioneered a strategy of PV isolation that would create ablation lesions surrounding, but not in, the PVs that would block ectopic activation attempting to enter the atria at large [124, 125, 126]. This anatomical rather than functional approach to rhythm management represented a significant departure from traditional electrophysiological procedures that exert great effort to identify proarrhythmic accessory pathways or ectopic sources. However, this approach has shown reasonable success at terminating paroxysmal AF. At present, pulmonary vein isolation remains fixed as the cornerstone of AF intervention, and numerous technologies and systems have emerged in an attempt to simplify and optimize the task.

However, high rates of AF recidivism following PV isolation, particularly in patients with persistent AF, have led the electrophysiological community to return to the concept of compartmentalization previously associated with the Cox maze procedure.

Numerous compartmentalization or substrate modification strategies have been proposed in an attempt to improve the success of ablation procedures in patients with persistent AF. An in-depth description of these strategies and their relative merits is beyond the scope of this document. However, given that substrate mapping strategies are germane to this topic, it is worth mentioning that ablation strategies based on substrate mapping (see Section 2.4.4) primarily fit in this category, i.e., adjunctive ablation based on the identification of substrates that either support initiation of AF or assist its perpetuation. These adjunctive ablation strategies may be purely anatomically driven as with PV isolation where connecting lines of ablation lesion are made between the PV encirclement lines, between other nonconductive barriers, e.g., valves, or debulking strategies that seek to reduce that amount of tissue that can harbor fibrillatory conduction in areas known to be problematic, i.e., the LA posterior wall (Fig. 3.7). Other approaches use electrophysiological recording from the cardiac surface, or substrate mapping, to identify tissue characteristics that are believed to reflect the proarrhythmic potential of local tissues.

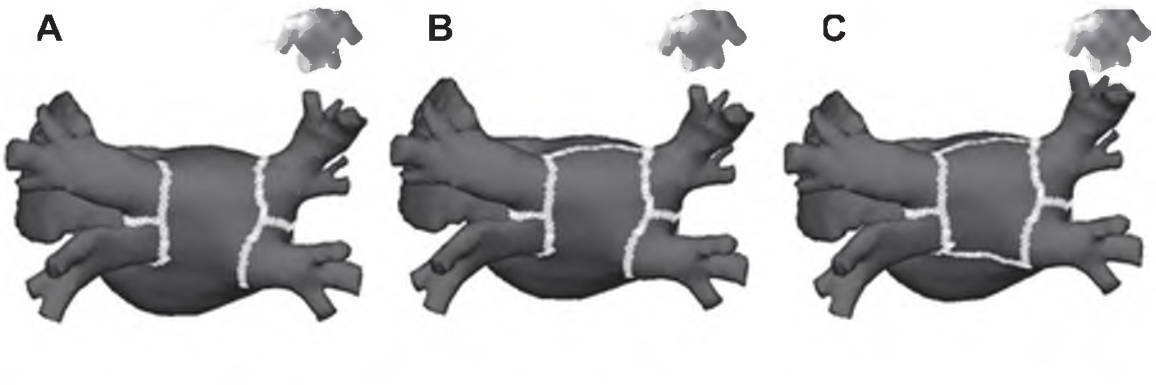

Fig. 3.7. Left atrial lesion sets used for radio frequency ablation (RFA) of atrial fibrillation. A – Lesion set depicting standard pulmonary vein isolation (white lines). B and C – Stepwise strategy of RFA in which a roof line (B) and additional lines of ablation are used to compartmentalize the atria. Used with permission from Mun et al. Heart. 2012 [170].

CHAPTER 4

MULTIMODAL IMAGING IN ATRIAL FIBRILLATION

Modern clinical electrophysiology is inextricably linked with radiology. Fluoroscopy, ultrasound, MRI, and CT all play significant roles in the treatment of patients with cardiac arrhythmias, and in particular atrial fibrillation. The following chapter appeared in the collection *Multimodal Cardiovascular Imaging: Principles and Clinical Applications* and covers the use of medical imaging in the treatment of AF [34]. It appears here in the published format with the permission of McGraw-Hill, the publisher.

CHAPTER 25
ATRIAL FIBRILLATION

Rob MacLeod and J. J. E. Blauer

INTRODUCTION

Atrial fibrillation (AF) is the most common form of cardiac arrhythmia, so a review of the role imaging in AF is a natural topic to include in this book. Further motivation comes from the fact that the treatment of AF probably includes more different forms of imaging, often merged or combined in a variety of ways, than perhaps any other clinical intervention. A typical clinical electrophysiology lab for the treatment of AF usually contains no less than six and often more than eight individual monitors, each rendering some form of image-based information about the patient undergoing therapy. There is naturally great motivation to merge different images and different imaging modalities in the setting of AF, but this is also very challenging as a result of a host of factors, including the small size, extremely thin walls, large natural variation in atrial shape, and the fact that fibrillation is occurring so atrial shape is changing rapidly and irregularly. Thus, the use of multimodal imaging has recently become a very active and challenging area of image processing and analysis research and development, driven by an enormous clinical need to understand and treat a disease that affects approximately five million Americans alone, a number that is predicted to increase to almost 16 million by 2050.[1]

In this chapter, we attempt to provide an overview of the large variety of imaging modalities and their uses in the management and understanding of AF, with special emphasis on the most novel applications of magnetic resonance imaging (MRI) technology. To provide clinical and biomedical motivation, we outline the basics of the disease together with some contemporary hypotheses about its etiology and management. We then describe briefly the imaging modalities in common use in the management and research of AF, and then focus on the use of MRI for all phases of the management of patients with AF and indicate some of the major engineering challenges that can motivate further progress.

CLINICAL PROFILE OF AF

AF is a growing problem in modern societies, with an enormous impact on both short-term quality of life and long-term survival.[2] Approximately 0.5% of people age 50 to 59 years have AF, and 9% of people age 80 to 89 years have AF, and these prevalence are increasing.[1,3] Although many people with the condition go untreated, AF is associated with an almost twofold increase in the risk of mortality. AF patients experience a dramatically increased rate of stroke (from 1.5% for those age 50 to 59 years to 23.5% for those between age 80 and 89),[4] a risk that, by contrast, decreases with age in the normal population. Treatment of AF represents a significant health care burden, with the annual costs estimated at approximately seven billion US dollars.[5]

Restoring and maintaining normal sinus rhythm remains one of the major goals in treating patients with AF. One treatment modality is a combination of cardioversion and antiarrhythmic drugs[6]; however, only 40% to 60% of the AF population is maintained in regular rhythm 1 year after such treatment. The treatment itself may also have serious adverse effects[7-9] and must usually continue for the lifetime of the patient. By contrast, maintaining sinus rhythm without the use of antiarrhythmic drugs seems to be associated with increased survival.[10] The inadequacies of drug-based treatments for AF have long been the major motivation for finding a truly curative approach to maintain sinus rhythm and suppress AF.

MECHANISMS OF AF

The mechanisms underlying AF have been the topic of extensive research over many years, and there is consensus that the disease, like most cardiac arrhythmias, has two components, the tissue substrate and some initiating electrical events or triggers. Perhaps the most complete description of the substrate of AF comes from Wijffels et al, who first postulated that the longer the atria spend in the state of fibrillation, the more difficult it becomes to reverse the condition (ie, "Atrial fibrillation begets atrial fibrillation").[11] Their conclusions were based largely on animal studies in which rapid pacing of the heart induced AF through a continuous process of electrical and then structural remodeling, a transition that is initially reversible but then becomes essentially permanent. Rapid pacing of the heart does not, of course, occur spontaneously, and the etiology of the disease in humans is thought to be closely linked to the gradual and inevitable elevation of fibrosis in the atria that comes with age[12,13] and that predisposes a heart to AF whether

or not associated conditions such as heart failure are present.[14] In animals subjected to the rapid pacing protocols developed to induce AF, treatment with a drug that suppresses the formation of fibrosis reduced the likelihood of developing AF compared with control animals,[15] hence the clear link between fibrosis and the AF substrate. As we will discuss later, one application of imaging, especially MRI, is directed at identifying and quantifying the extent of fibrosis in the left atrium and thus identifying the progression of the disease substrate.

The role of triggers in AF is also motivation for novel imaging approaches. With electrical and electroanatomic mapping (ie, recording electrical activity from a number of known sites on a surface the heart), it is possible to identify the sites of triggers and thus also localize causes of induction of AF. Leaders in mapping triggers of AF are Haissaguerre and coworkers,[16-19] who identified trigger sites both in the atria and especially within the pulmonary veins of the left atrium. Once identified and localized, it is possible to electrically isolate these triggers, which was the unknown consequence of an earlier surgical technique for AF management, known as the Cox maze procedure, first performed in 1988.[20] This operation isolates not only the pulmonary veins but also different regions of the atria by creating a "maze," a tortuous path for electrical conduction in the atria, reducing the ability of triggers to interact with a substrate that could sustain arrhythmias. Modern, catheter-based *ablation* approaches seek to achieve similar goals by applying very focused energy to the endocardial surface of the atria to isolate the triggers known to exist in the pulmonary veins[17] and create the same maze of broken conduction in the left atrium.[16,21,22] The electroanatomic mapping approaches necessary to guide such interventions are, however, invasive and often time consuming, so there remains a pressing need to develop noninvasive imaging approaches to localize trigger sites. Current research in AF management seeks to develop imaging based on MRI,[23-25] ultrasound,[26] and computed x-ray tomography[27] to visualize the ablation lesions and thus direct the intervention.

IMAGING AND AF

We outline in subsequent sections the use of a broad range of imaging modalities in AF management and then focus on a comprehensive approach to the management of AF using MRI for all phases of evaluation and intervention. The most novel approaches to imaging in AF are in the areas of merging multiple modalities and in the rapid expansion of the use of MRI. The rationale for this growth is that, unlike other modalities, MRI is naturally suited to detect changes in soft tissue characteristics and hence capable of revealing the progress of substrate in AF and in visualizing the creation of lesions during ablation. These capabilities, combined with the ability to reveal atrial anatomy at high resolutions, make MRI the natural adjunct to all phases of management of AF patients.

OVERVIEW OF CURRENT IMAGING MODALITIES

The use of imaging is ubiquitous in clinical electrophysiology, especially in interventions that require remote access to the heart by means of catheters. One the one hand, imaging is required to guide the catheter, and on the other hand, the catheter itself often captures and conveys functional and diagnostic information that must be integrated into the procedure. Figure 25–1 summarizes the most common modes of displaying information in a typical electrophysiology study, and we describe here briefly these modalities. The focus of subsequent, more detailed discussion will be MRI, the modality that is now the topic of extensive research and development.

FLUOROSCOPY

Fluoroscopy is an x-ray–based modality that has been a mainstay of cardiac catheterization procedures from their inception. Like all x-ray–based imaging, fluoroscopy can reveal dense materials like bone and metallic objects (eg, electrodes, devices, catheters) but, without contrast agents, is not capable of visualizing soft tissue or blood. In catheter ablation, fluoroscopy serves primarily to guide catheter navigation and to direct the transseptal puncture of the atrial septum that is necessary to access the left atrium. With contrast agent injection, it is also possible to visualize vessels and cardiac chambers using fluoroscopy. Significant

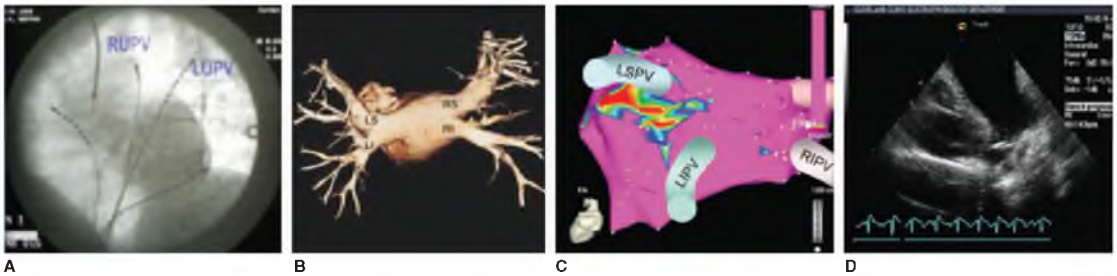

FIGURE 25–1. Overview of imaging modalities in common use for atrial fibrillation evaluation and ablation. The figure shows examples of fluoroscopy (**A**), computed tomography (**B**), electroanatomic mapping (**C**), and intracardiac echocardiography (**D**) as they are used for guiding ablation of atrial arrhythmias. LI, left inferior; LIPV, left inferior pulmonary vein; LS, left superior; LSPV, left superior pulmonary vein; LUPV, left upper pulmonary vein; RI, right inferior; RIPV, right inferior pulmonary vein; RS, right superior; RUPV, right upper pulmonary vein.

strengths of fluoroscopy include the ability to perform real-time imaging at frame rates of tens per second, the simplicity provided by very evolved technology, and ready availability. Acknowledged weaknesses include the poor soft tissue contrast and the cumulative exposure to ionizing radiation. More fundamentally, fluoroscopy is generally considered to be a two-dimensional modality so that revealing three-dimensional cardiac shape is difficult.

Modern fluoroscopy systems seek to address these limitations by providing multiple, orthogonally oriented cameras (biplaner fluoroscopy) and rotational angiography systems for full, three-dimensional reconstructions of venous and cardiac shape during catheterization procedures,[28,29] all at the lowest possible field strengths. The anatomic models obtained by rotational angiography systems approach the resolution and accuracy of computed tomography (CT) and MRI images. Furthermore, because imaging occurs intraprocedurally, the resulting models can be better aligned to the coordinate system in which the procedure occurs and are less vulnerable to intravascular volume changes and shifts in body position and shape that may limit the accuracy of remotely acquired MRI and CT images.[30,31] Acquisition of geometric information in the same reference frame and at the same time of procedures significantly aids the integration of imaging modalities by obviating the need for registration.[32]

ELECTROANATOMIC MAPPING AND IMAGING

Electroanatomic mapping (EAM) is an essential component of cardiac ablation procedures that has been used widely since the mid-1990s.[33-38] All such systems produce a patient-specific geometric model of the endocardium together with electrograms at numerous sites on that surface. There are two competing EAM technologies, CARTO from Biosense Webster (Diamond Bar, CA)[39] and EnSite from St Jude Medical (St. Paul, MN),[33] which differ in the manner by which they generate the electrical signals on the endocardium. CARTO measures potentials directly by touching a manually steered catheter sequentially to the heart surface and can thus be used on both the endocardial and epicardial surfaces. Its major weakness is the time required to sample enough points to create true maps of electrical activity, which can present challenges when the underlying arrhythmias are unstable and poorly tolerated by the patient. The EnSite technology differs in that it is based on simultaneously recording from an inflatable catheter containing 80 electrodes that is placed inside the chamber of interest. The system solves the resulting bioelectric field inverse problem in terms of endocardial potentials from a single heartbeat, reducing the burden on patients with unstable arrhythmias.

More recently, clinicians have adopted EAM for evaluation and guidance during ablation of AF,[34-36] but here, the goal is often simpler—to measure only the amplitude of electrical activity in the posterior wall of the left atrium and thus evaluate the success of ablation. EAM is just as essential in the context of MRI-guided AF ablation, and such systems have been developed for this application.[24]

ECHOCARDIOGRAPHY/ULTRASOUND

Various modalities of ultrasound-based echocardiography are used in the management of AF. Transthoracic echocardiography (TTE), transesophageal echocardiography (TEE), and intracardiac echocardiography (ICE) are routinely used before, during, and after catheter ablation of AF, always with the goal of providing detailed and fine-scale anatomic information. We will briefly describe the context in which each of these modalities is commonly used.

Transthoracic Echocardiography

TTE is routinely used for screening and evaluation purposes in the management of AF, typically to screen for underlying heart disease, including heart failure, valvular heart disease, and left ventricular hypertrophy.[40] Additionally, TTE can be used to assess left atrium size and anatomy.[41] Postablation TTE can be used to detect pericardial effusion and to evaluate left atrial function and size.[42] Although other imaging modalities outperform TTE in these tasks, TTE remains an effective, readily available, noninvasive, and relatively inexpensive modality.

Transesophageal Echocardiography

TEE has shown high sensitivity and specificity for the detection of left atrial thrombus before ablation treatment.[43] It is also useful for assessment of the location and number of pulmonary veins when CT and MRI are not feasible. Due to patient discomfort (the probe must be placed in the esophagus at the left of the heart) and need for airway management, TEE has not traditionally been used intraprocedurally.[42]

Intracardiac Echocardiography

ICE has become a standard imaging utility in most modern electrophysiology laboratories because of its high spatial and temporal resolution, achieved in part from the immediate proximity of the sensor and the heart. ICE is capable of visualizing the anatomy of the left atrium, including the pulmonary veins and appendage, as well as other local anatomy including the aorta, mitral valve, and esophagus. In AF ablation procedures, the ultrasound catheter is navigated intravenously to the right atrium and is used to guide transseptal punctures, navigate ablation catheters, confirm electrode-tissue contact, and titrate energy delivery.[44-47] Additionally, ICE plays a critical role in the prevention and detection of complications by monitoring the formation of thrombus or coagulum, pericardial effusion and tamponade, and flow acceleration indicative of pulmonary vein stenosis.[48-51] Limitations of ICE include the requirement for additional intravenous access and confinement to two-dimensional imaging.

ANATOMIC MRI/MULTISLICE CT

Multislice CT (MSCT) and MRI-based angiography are routinely performed before ablation to define left atrial and pulmonary vein anatomy and size. Models of the relevant cardiac anatomy, generated from these images, are created to help guide

intraprocedural navigation and tissue targeting.[52-54] Trade-offs exist between the selection of MSCT or MRI for angiography. MSCT-based angiography is faster and has higher spatial resolution, whereas MRI does not require exposure to ionizing radiation. Most patients with pacemakers or implantable cardiac defibrillators are also ineligible for MRI. High-fidelity representations of the anatomy can be generated from both modalities, and consequently, both are considered acceptable for this purpose. Both modalities are also used after ablation to identify complications such as pulmonary vein stenosis, atrioesophageal fistula, and reverse remodeling (ie, decrease in atrial volume).[42,55-59] MRI and MSCT have also been successfully used to identify surrounding structures that may be at risk of collateral injury during AF ablation, including coronary vessels and the esophagus.[60-62]

MERGING OF MODALITIES

Clearly, no imaging modality is a panacea for all of the requirements inherent in the assessment and treatment of a disease with such diverse and complex imaging needs as AF. Often a merging of modalities is necessary or at least desirable to achieve the necessary coverage of anatomic and functional information to manage the disease. The challenges presented by merging imaging modalities include the need to align or register images acquired in different coordinate systems and different resolutions and then to present them to the operator in a way that is flexible and intuitive enough to be useful.

The centerpiece of contemporary integrated image merging systems tends to be the EAM system, which includes the necessary merging, registration, and visualization hardware and software. The goal of such systems is almost always to use a previously acquired angiography (by MRI or MSCT) to provide a geometric substrate for the subsequent EAM of the heart.[63-69] This registration step usually relies on operator identification of landmarks common to both the angiography and the EAM to rigidly align them in the coordinate system of the EAM system. Further refinements of the alignment are then updated as more points are sampled for the EAM. Much of the mismatch that remains can be attributed to the differences in the MSCT and MRI data acquired sometimes days before the procedure. Other sources of error in the match of MRI and MSCT models to intraprocedure anatomy include respiration, patient movement, and changes in cardiac rhythm.[70,71] Real-time integration of ICE imaging with the EAM system has recently emerged as a means to allow intraprocedural generation and updating of anatomic models, further improving navigational accuracy.[72,73]

MRI-BASED EVALUATION OF ATRIAL TISSUE

Cardiac MRI has become the gold standard for imaging and analysis of numerous cardiac conditions. Generally, MRI is limited by comparatively slow image acquisition and reconstruction times, low resolution, susceptibility to noise, and magnetic field incompatibility of some patients. However, the two primary benefits of MRI are soft tissue contrast and absence of ionizing radiation. These two strengths come to bear significantly in the arena of AF management. First, AF is known to influence cardiac structural properties in a process known as remodeling. Second, the stated goal of AF ablation is to modify, isolate, or abolish arrhythmogenic tissues. In both cases, the soft tissue contrast available in MRI provides insight for physicians into the entrenchment of AF and success of scar formation, respectively. Finally, modern ablation procedures still rely heavily on fluoroscopy for procedural guidance. The introduction of AF ablation procedures into the MRI environment opens the door for the departure of ionizing radiation from the management of AF.

Late gadolinium-enhanced (LGE) MRI is used to evaluate alterations in tissue structure associated with numerous cardiomyopathies.[74,75] To acquire LGE images, a dose of chelated gadolinium contrast agent is administered intravenously as would be done for standard magnetic resonance angiography. Following the injection, the gadolinium is allowed time to wash clear of normal myocardium, and an inversion-recovery prepared gradient echo pulse is acquired to detect regions of tissue where the contrast agent remains sequestered. Any region in which perfusion has decreased or extracellular space has increased will appear bright in LGE images due to enhanced concentrations of gadolinium relative to surrounding tissues.[76]

EVALUATION OF POSTABLATION SCAR FORMATION

The first reported use of LGE-MRI of atrial tissue to assess ablation lesions came from Peters et al.[77] In this prospective study, contrast enhancement was found in the left atrium and pulmonary vein ostia of all patients who had previously undergone radiofrequency (RF) ablation of AF 1 to 3 months previously. These findings were supported by McGann et al,[78] who quantified the extent of enhancement observed in the left atrial wall 3 months after ablation using the methods outlined in Fig. 25–2 and compared extent of scar to procedural outcomes. In this study, patients who experienced a recurrence of AF were found to have less enhancement (12.4 ± 5.7%) compared with patients who did not experience recurrence (19.3 ± 6.7%, $P = .004$).[78] Subsequent studies have expanded on these initial findings to show that lesion remodeling stabilizes by 3 months after ablation and that the extent and continuity of lesions encompassing the pulmonary veins play an important role in preventing recurrences.[79-81]

The ability to noninvasively assess the lesion sets created in AF ablation procedures can provide valuable feedback to electrophysiologists searching for the optimal ablation strategy. Although freedom from AF after a single intervention will remain the goal for procedural success, LGE-MRI can help explain how and why a particular lesion set succeeds or fails at terminating AF and provide direction in subsequent ablation procedures.

EVALUATION OF AF SUBSTRATE

As previously noted, AF is associated with structural remodeling of the left atrium. Motivated by the success of LGE-MRI in

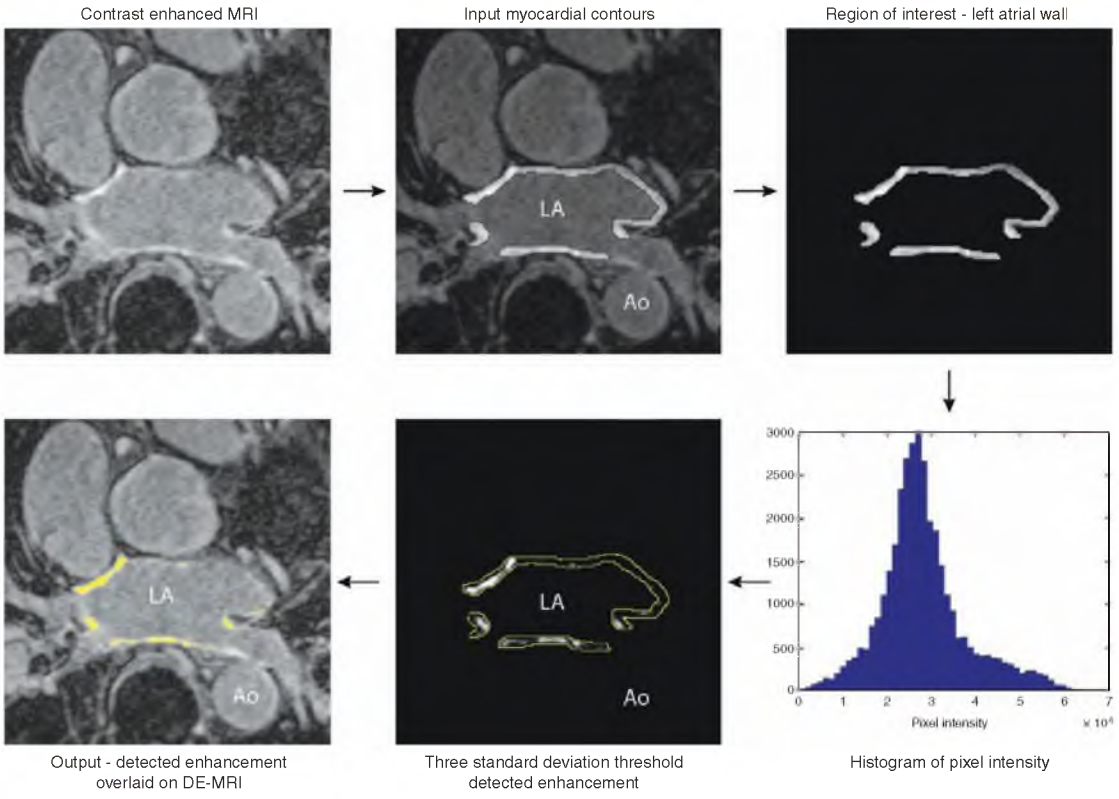

FIGURE 25–2. Algorithm for quantification of postablation scar burden in the left atrium (LA). The wall of the LA in late gadolinium-enhanced magnetic resonance imaging scans (top left) is segmented on a slice-by-slice basis (top center). Once isolated (top right), a histogram of the LA wall pixel intensities is generated (bottom right), and the rising phase of the primary mode is used to predict normal tissue pixel intensities. Pixel intensities three standard deviations above the mean of normal tissue is marked as scar (bottom center). Overlays of pixels marked as scar onto original images shows good correlation with hyperenhancement. Ao, aorta; DE-MRI, delayed-enhanced magnetic resonance imaging.

identifying structural heart disease and, in particular, fibrosis, Oakes et al[82] analyzed LGE-MRI scans from a cohort of 81 AF patients and six normal volunteers to explore the relationship between contrast enhancement and AF structural remodeling. This study revealed a positive correlation between low-voltage tissue regions in EAMs (bipolar voltage amplitude ≤0.5 mV) and left atrial wall enhancement ($r^2 = 0.61$, $P < .05$). Furthermore, patients with mild (<15%, n = 43), moderate (15%-35%, n = 30), and extensive (>35%, n = 8) amounts of left atrial wall enhancement were found to have significantly different rates of AF recurrence at a mean follow-up of 9.6 months (14%, 43%, and 75%, respectively). These findings suggest that the degree of left atrial wall enhancement, which is assumed to reflect extent of fibrosis in the atrial tissue, is a predictor of failure for ablation. Based in part on these results, a staging system for determining the amount of enhancement has been proposed. Figure 25–3 shows the Utah staging system, with examples of LGE-MRI scans from each of the four stages. Under this system, patients with Utah stage III or IV enhancement are not considered to be ideal candidates for ablation therapy.

The utility of the Utah AF stage s is currently under extensive evaluation, both at our institution and through a multicenter clinical study involving major AF centers from around the world.

REAL-TIME MRI FOR ABLATION OF AF

As outlined in the Introduction, catheter-based ablation of the left atrium represents the most common intervention to cure or at least suppress the symptoms of AF. To carry out ablation requires considerable imaging support in order to identify anatomy, evaluate substrate, and determine success of the intervention. Conventional approaches to AF ablation make use of fluoroscopy, CT, intracardiac ultrasound, and EAM. Not only is MRI used as a preprocedural method to generate anatomic images, but also its broader use represents the leading edge of research in real-time imaging to support the guidance

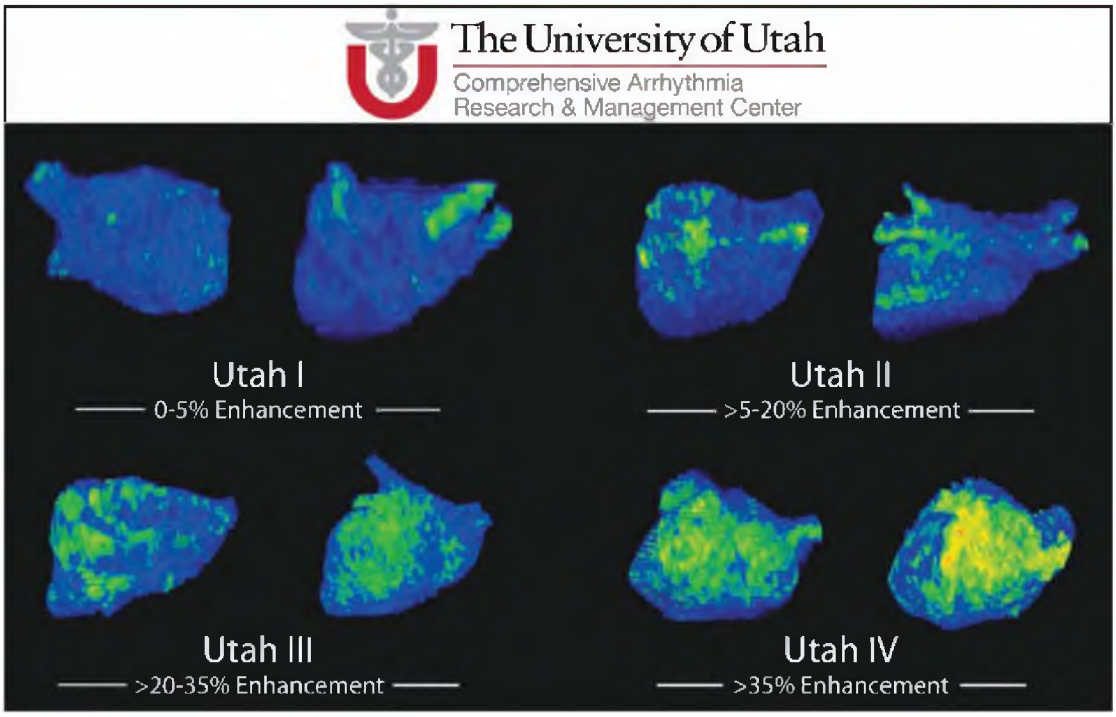

FIGURE 25–3. Utah staging system for stratifying the amount of preablation enhancement of the left atrial wall. Images in each of the four panels show examples of late gadolinium-enhanced magnetic resonance images, with enhanced regions color coded in green and normal tissues colored in blue.

of catheters and the evaluation of lesion formation in a three-dimensional form. The need to combine anatomic and functional information continues to drive the development of novel merging and registration approaches.[34]

CATHETER ABLATION OF AF

The past decades have seen significant progress in understanding the underlying mechanisms of AF that sustain its persistence,[11,17] and this knowledge has led to the treatment paradigm of AF ablation, which is the targeted destruction of tissue predominantly in the left atrium in order to isolate electrical triggers and reduce the ability of the atrium to sustain rapid activation. AF ablation, typically based on RF energy delivery through a venous catheter, has already produced encouraging results and is the topic of innumerable research reports, but it has yet to reach its full potential. Despite the fact that ablation, when successful, allows the patient to discontinue the use of antiarrhythmics anticoagulants, the success rate of ablation in maintaining regular sinus rhythm without the use of such medications is still only 60% to 80%.[83] Moreover, the penetration of ablation, although difficult to measure with accuracy, appears to lie well below the need; there are fewer ablations carried out each year than there are new cases of AF. In an effort to increase the penetration of this potentially curative approach, there have been many modifications to the ablation procedure aimed at improving outcome and hence promoting the adoption of the ablation approach.[16,34,72,84-89] Despite such progress, daunting technical challenges to carrying out successful ablation remain, and many of these are related to imaging.

Currently, AF ablation is performed using catheters that can be visualized under fluoroscopy and/or projected onto a three-dimensional virtual shell acquired through EAM during the procedure.[34] There are multiple challenges associated with these approaches. First, it is impossible for the operator to visualize the catheter tip/tissue interface; hence, delivery of RF energy is based on guidance from the morphology of local electrogram or by using the virtual shell from EAM to assure that the catheter tip is in contact with the atrial wall. However, both of these approaches have known errors that can exceed 1 cm,[90] leading to frequent delivery of inappropriate lesions that may only partially damage the atrial tissue, promoting tissue recovery and hence reoccurrence of the arrhythmia. Moreover, this lack of visualization of the catheter tip can result in localized heating of blood, thus leading to char formation, a major cause of embolic stroke during the ablation procedure.[91] Defining a technology or a system that would allow accurate visualization of the catheter tip/tissue interface would overcome this major problem for the

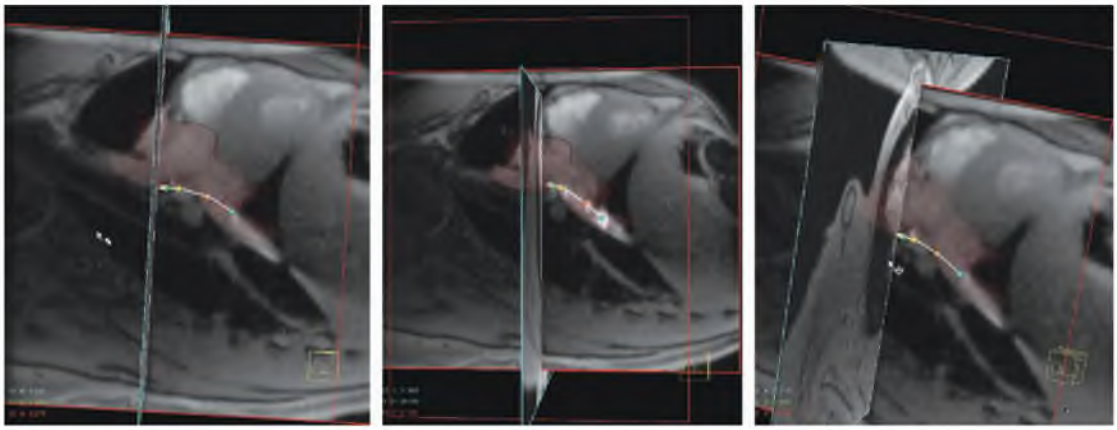

FIGURE 25–4. Visualization of catheter during real-time magnetic resonance imaging (MRI). Each panel shows a slightly different view of the MRI-compatible catheter superimposed on the local MRI image together with a rendered mesh of the right atrium and superior and inferior vena cava from this animal.

operator. Another major challenge of the ablation procedure is the lack of an imaging modality that allows immediate assessment of tissue damage as the RF energy is applied. MRI is the most obvious and perhaps only imaging system that could overcome this problem.

Although MRI has the inherent capability of visualizing soft tissue and thus providing both anatomic and functional guidance for RF ablation of AF, there are challenges to creating a viable MRI-based approach. First, it is necessary to develop an MRI-compatible catheter and associated software that allows visualization of the catheter during navigation and energy delivery within the atrial chamber. This catheter and software must be part of a system that tightly integrates the diverse instrumentation required to complete a clinical atrial ablation procedure. The system must exploit the benefits of soft tissue contrast unique to MRI (near real-time visualization of myocardial interfaces and ablation lesions) while providing a smooth workflow for the physician and technicians. Recent reports showing progress toward these ends by our and other groups[23-25] suggest that a full AF ablation procedure in humans, although still very challenging, is likely.

MRI-COMPATIBLE CATHETERS

The development of an MRI-guided system for AF ablation is completely novel in terms of the devices and support systems that are required to create a working system. MRI-compatible catheters have just begun to appear in the literature[23,33,52,92] but are still prototypes and have not been used in any human ablation studies. Similarly, the real-time MRI guidance systems required to place the catheters in the appropriate locations are in their infancy, with only sparse reports of placing an MRI-compatible catheter in the human heart under MRI guidance.[52] Most of the other elements of the contemporary AF ablation instruments—the lasso catheter, the coronary sinus catheter, and the needle required to carry out transseptal punctures—are also only just under initial development and have yet to receive approval for use in humans.

We have participated in the development of catheters that are MRI compatible, steerable in a way similar to standard clinical catheters, and capable of both delivering RF energy and recording endocardial electrograms.[25] It is possible to track the location of the catheters and to display their position superimposed on the real-time MRI images and with a geometric shell model of the atria and great vessels that we create from volumetric MRI scans recorded in the early phases of the procedure. Figure 25–4 shows an example of MRI images recorded during a real-time ablation procedure in which the catheter is visible superimposed on the orthogonal MRI images. Also visible in the image is a polygonal surface or shell of the right atrium and inferior and superior vena cava, created by segmenting a previously acquired high-resolution scan of the animal's atrial anatomy.

VISUALIZATION OF IMAGING RESULTS

Scientific visualization is an essential step in using imaging data, and the unique and challenging needs of AF ablation continue to drive new approaches. For example, EAM requires the integration of spatial information describing the shape of the endocardial surface with time signals, electrograms recorded from that surface, and parameters extracted from them. In addition, there is volumetric information from MRI and CT that can be visualized as s sequence of two-dimensional images but is much richer when rendered in a three-dimensional form. Naturally, there is a need to merge these two (and other) forms of anatomic and functional information, and novel visualization technology continues to improve such merging in a setting of interactive manipulation and rendering.[34]

We have developed techniques that combine not only visualization of volume- and surface-based approaches but also

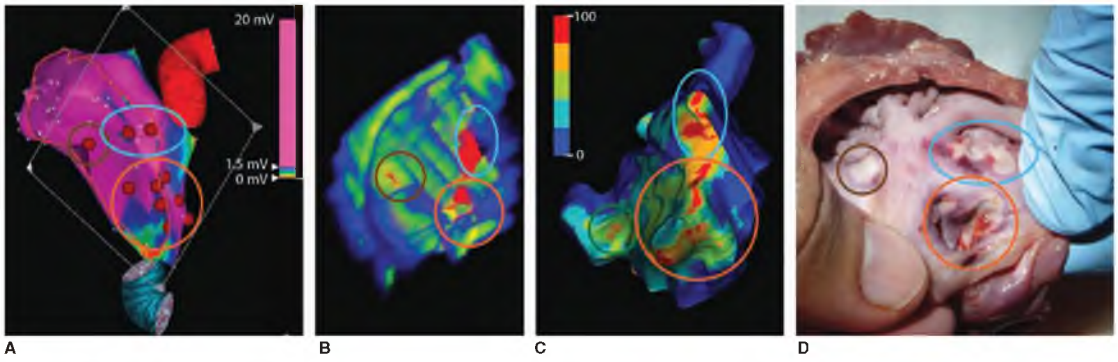

FIGURE 25–5. Multimodal visualization of ablation lesions from an experiment using magnetic resonance imaging (MRI) during and after lesion formation. The images show the results of electroanatomic mapping (**A**), late gadolinium-enhanced MRI (**B** and **C**), and gross dissection of the right atrium from an animal experiment (**D**).

projection of the information from the volume to the surface. Figure 25–5 shows an example of such a visualization in which Fig. 25–5A shows an EAM from an animal experiment showing three clusters of lesions performed under fluoroscopy guidance; the red dots in panel A show the lesion sites. Figure 25–5B shows the LGE rendering of the same heart, performed in the MRI scanner directly after the ablation procedure. We then used segmentation of the volume images to define the endocardial surface and projected the information from the MRI scan onto that surface, shown in Fig. 25–5C. Confirmation of the actual lesion locations is evident from dissection documented in Fig. 25–5D.

The motivation of such projection approaches is to present information from multiple modalities (in this case, EAM of electrogram amplitude and MRI tissue changes) in a common reference frame (in this case, the endocardial surface). Such merging of information provides for quantitative analysis and comparisons and also a means of conveying information in a form that is familiar to the clinicians (in this case, electrophysiologists who are highly conversant in the conventions of endocardial and epicardial mapping).

REAL-TIME DETECTION OF LESION FORMATION

The most significant advantage of MRI-guided ablation is its potential to obtain rapid feedback on tissue changes during the ablation procedure—to watch the lesions form. There is no viable modality at this time that can determine the effectiveness of ablation; even electrical mapping approaches only measure depressed electrical activity in the endocardium that may return within weeks of the ablation and cause a recurrence of AF. MRI, on the other hand, has the potential to visualize changes in tissue structure related to permanent cell damage following the application of energy and thus establish the presence and depth in the atrial wall of terminally destructive lesions. Visualization of lesion formation and extent would improve the effectiveness and the safety of RF ablation procedures.

To visualize lesion formation with MRI requires acquisition of high-quality images in rapid sequence in order to achieve adequate spatial and temporal resolution. As with all imaging modalities, there is a trade-off in MRI between the time needed to acquire the image and the quality of that image. Furthermore, real-time imaging of the heart is driven both by the need to capture information rapidly enough to avoid blurring due to cardiac and respiratory motion and the desire to optimize image quality to see small changes within structures that are only a few millimeters thick. Another challenge specific to ablation is the need to see changes quickly enough to allow the operator to control the time and the energy dose in order to create lesions that are deep enough, but not so deep as to degrade the structural integrity of the heart wall.

In animal studies within our group, we have achieved image refresh rates of up to 5.5 frames per second based on customized MRI scan sequences and have been able to visualize lesion formation within 10 to 15 seconds of onset of RF energy.[25,92] Figure 25–6 shows just one example of such a case, in which catheter placement is documented in Fig. 25–6A, followed by a sequence of images (using a different MRI scan sequence) that reveal the formation of the lesion in Fig. 25–6B to 25–6F. Figure 25–6G shows a postmortem image in the same plane, and Fig. 25–6H contains a photographic record of the lesion seen immediately after the experiment. To our knowledge, this is the first report of visualizing lesion formation as it occurs in any tissues of the heart. We have also compared lesion sizes measured from MRI imaging with those determined through postmortem dissection and shown excellent agreement.[25]

SUMMARY

Imaging has always been an essential component of the management of all forms of cardiac arrhythmias, and its use will continue to expand in pace with improvements in the imaging acquisition technology, the image processing and analysis, and the integrating software that can efficiently support the clinical workflow. In the setting of AF, the use of MRI is making particular advances as its utility in all phases of the disease becomes

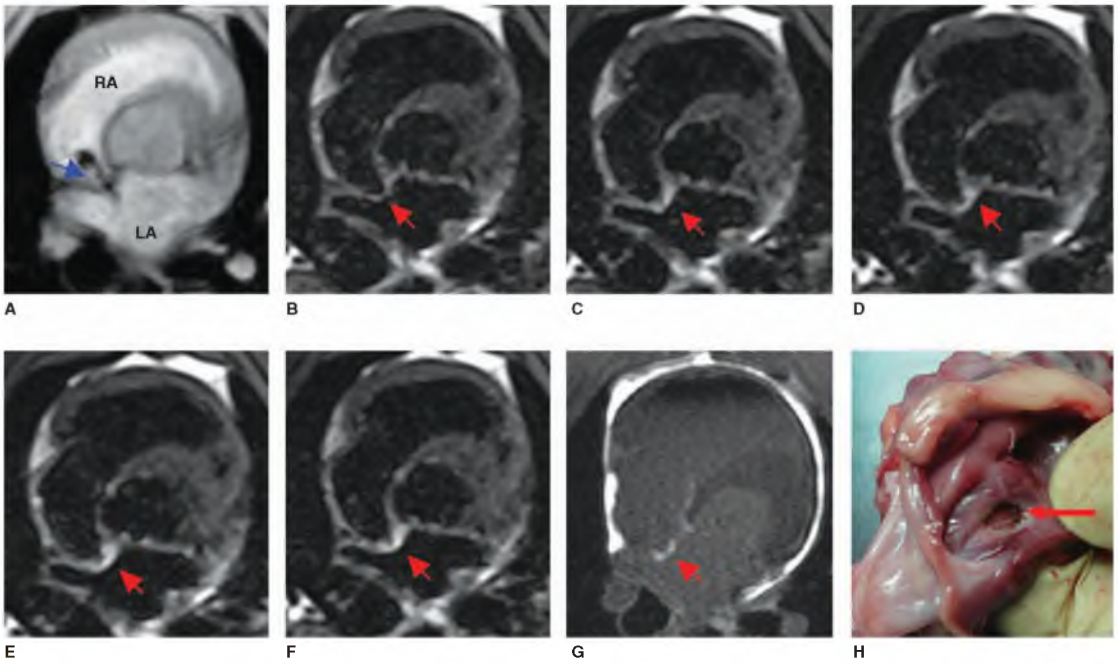

FIGURE 25–6. Detection of acute atrial lesion. **A.** Image from a three-dimensional scan to locate the catheter tip. **B-F.** T2-weighted dark blood images acquired before ablation (**B**) and after ablation at 20 seconds (**C**), 50 seconds (**D**), 2.5 minutes (**E**), and 8 minutes (**F**). **G.** Postmortem, high-resolution, delayed-enhancement magnetic resonance image. **H.** Photo of excised heart. Blue arrow indicates the position of the catheter tip at septal wall. Red arrows indicate the location where the lesion was created using a 30-second ablation with 30 W. LA, left atrium; RA, right atrium.

evident. Preablation imaging provides a means to stage patients and determine their best treatment options; the emergence of the Utah AF staging system suggests a very specific means by which image analysis and quantification can indicate disease status and risk. Similar techniques provide a means of noninvasively determining the outcome of AF ablation by mapping the formation of scar to both evaluate interventional success and to guide subsequent interventions, should they be necessary. The Comprehensive Arrhythmia Research and Management Center has carried out over 600 scans on over 250 patients to date and is now collaborating with similar laboratories around the world in multicenter trials of these MRI-based approaches. The results of these studies could completely transform the way that AF is treated when it arises and even enable preventative measures that are simply impossible without a means of tracking the tissue changes that preface the onset of electrical symptoms

The potential for imaging and especially MRI in the treatment of patients with AF is equally exciting and bright. We have now carried out over 30 animals studies to date in developing the prototype MRI-guided navigation system and are focused on developing and testing such a system for use in humans. We have created lesions both under fluoroscopy and real-time MRI guidance in the atria and ventricles of anesthetized dogs and swine and then carried out detailed imaging both of the entire animal thorax and of the excised preserved heart. In the process, we have made advances in MRI-compatible catheter design, exploitation of novel sensing coils, incorporation of tracking coils into catheter housings, improvement in pulse sequence design for rapid acquisition, integrated interactive display of images and devices, and image processing and analysis tools for postprocedure evaluation of results. Other groups have made similar progress, and there is little doubt that the first human studies

A major initial goal of these studies was to ensure that it is indeed possible to visualize lesions soon after ablation, despite the thin atrial walls and small extent of RF lesions. Figure ?? shows an example of such a result in which we sampled from the same slice before, during, and repeatedly after application of the RF energy.[93]

ACKNOWLEDGMENTS

The authors are deeply indebted to the contributions of the other members of Comprehensive Arrhythmia Research and MAnagement (CARMA) Center at the University of Utah for this material (www.carmacenter.org). The mission of CARMA is to provide worldwide pioneering leadership in advancing clinical treatments and research for cardiac arrhythmias,

especially atrial fibrillation. We also thank the Cardiovascular Research and Training Institute (CVRTI) for their support in experiments of MRI guided ablation.

Support for this research comes from the NIH NCRR Center for Integrative Biomedical Computing (www.sci.utah.edu/cibc), NIH NCRR Grant No. 5P41-RR012553-10 at the Scientific Computing and Imaging (SCI) Institute and from research grants from Surgivision Inc. and Siemens Healthcare.

REFERENCES

1. Miyasaka Y, Barnes ME, Gersh BJ, et al. Secular trends in incidence of atrial fibrillation in Olmsted County, Minnesota, 1980 to 2000, and implications on the projections for future prevalence. *Circulation*. 2006;114:119-125.
2. Calkins H, Brugada J, Packer DL, et al. HRS/EHRA/ECAS expert consensus statement on catheter and surgical ablation of atrial fibrillation: recommendations for personnel, policy, procedures and follow-up. *Europace*. 2007;9:335-379.
3. Benzinger GR, Kyle JW, Blumenthal KM, Hanck DA. A specific interaction between the cardiac sodium channel and site-3 toxin anthopleurin B. *J Biol Chem*. 1998;273:80-84.
4. Kannel WB, Wolf PA, Benjamin EJ, Levy D. Prevalence, incidence, prognosis, and predisposing conditions for atrial fibrillation: population-based estimates. *Am J Cardiol*. 1998;82(8A):2N-9N.
5. Coyne KS, Paramore C, Grandy S, Mercader M, Reynolds M, Zimetbaum P. Assessing the direct costs of treating nonvalvular atrial fibrillation in the United States. *Value Health*. 2006;9:348-356.
6. Falk RH. Atrial fibrillation. *N Engl J Med*. 2001;344:1067-1078.
7. Brodsky MA, Allen BJ 3rd, Walker CJ, Casey TP, Luckett CR, Henry WL. Amiodarone for maintenance of sinus rhythm after conversion of atrial fibrillation in the setting of a dilated left atrium. *Am J Cardiol*. 1987;60:572-575.
8. Crijns HJ, Van Gelder IC, Van der Woude HJ, et al. Efficacy of serial electrical cardioversion therapy in patients with chronic atrial fibrillation after valve replacement and implications for surgery to cure atrial fibrillation. *Am J Cardiol*. 1996;78:1140–1144.
9. Van Gelder IC, Crijns HJ, Tieleman RG, et al. Chronic atrial fibrillation. Success of serial cardioversion therapy and safety of oral anticoagulation. *Arch Intern Med*. 1996;156:2585-2592.
10. Corley SD, Epstein AE, DiMarco JP, et al. Relationships between sinus rhythm, treatment, and survival in the Atrial fibrillation Follow-Up Investigation of Rhythm Management (AFFIRM) study. *Circulation*. 2004;109:1509-1513.
11. Wijffels MC, Kirchhof CJ, Dorland R, Allessie MA. Atrial fibrillation begets atrial fibrillation. A study in awake chronically instrumented goats. *Circulation*. 1995;92:1954-1968.
12. Boldt A, Wetzel U, Lauschke J, et al. Fibrosis in left atrial tissue of patients with atrial fibrillation with and without underlying mitral valve disease. *Heart*. 2004;90:400-405.
13. Nattel S, Shiroshita-Takeshita A, Cardin S, Pelletier P. Mechanisms of atrial remodeling and clinical relevance. *Curr Opin Cardiol*. 2005;20:21-25.
14. Cha TJ, Ehrlich JR, Zhang L, et al. Dissociation between ionic remodeling and ability to sustain atrial fibrillation during recovery from experimental congestive heart failure. *Circulation*. 2004;109:412-418.
15. Lee KW, Everett TH, Rahmutula D, et al. Pirfenidone prevents the development of a vulnerable substrate for atrial fibrillation in a canine model of heart failure. *Circulation*. 2006;114:1703-1712.
16. Haissaguerre M, Jais P, Shah DC, et al. Electrophysiological end point for catheter ablation of atrial fibrillation initiated from multiple pulmonary venous foci. *Circulation*. 2000;101:1409-1417.
17. Haissaguerre M, Jais P, Shah DC, et al. Spontaneous initiation of atrial fibrillation by ectopic beats originating in the pulmonary veins. *N Engl J Med*. 1998;339:659-666.
18. Takahashi Y, Hocini M, O'Neill MD, et al. Sites of focal atrial activity characterized by endocardial mapping during atrial fibrillation. *J Am Coll Cardiol*. 2006;47:2005-2012.
19. Takahashi Y, Sanders P, Jais P, et al. Organization of frequency spectra of atrial fibrillation: relevance to radiofrequency catheter ablation. *J Cardiovasc Electrophysiol*. 2006;17:382-388.
20. Cox JL, Schuessler RB Jr, D'Agostino HJ, et al. The surgical treatment of atrial fibrillation. III. Development of a definitive surgical procedure. *J Thorac Cardiovasc Surg*. 1991;101:569-583.
21. Jais P, Haissaguerre M, Shah D, et al. Staged approach for paroxysmal atrial fibrillation ablation. *PACE*. 1996;19:I-265.
22. Marrouche NF, Dresing T, Cole C, et al. Circular mapping and ablation of the pulmonary vein for treatment of atrial fibrillation: impact of different catheter technologies. *J Am Coll Cardiol*. 2002;40:464-474.
23. Dukkipati SR, Mallozzi R, Schmidt EJ, et al. Electroanatomic mapping of the left ventricle in a porcine model of chronic myocardial infarction with magnetic resonance-based catheter tracking. *Circulation*. 2008;118:853-862.
24. Schmidt EJ, Mallozzi RP, Thiagalingam A, et al. Electroanatomic mapping and radiofrequency ablation of porcine left atria and atrioventricular nodes using magnetic resonance catheter tracking. *Circ Arrhythm Electrophysiol*. 2009;2:695-704.
25. Vergara GR, Vijayakumar S, Kholmovski EG, et al. Real time MRI guided radiofrequency ablation and visualization of lesion formation at 3 tesla. Poster session presented at Heart Rhythm Society Scientific Sessions 2010, Denver.
26. Wright M, Harks E, Deladi S, et al. Catheter assessment of lesion quality using a novel ultrasound radiofrequency ablation catheter. *Heart Rhythm Soc*. 2010;(Suppl):S86.
27. Girard-Hughes E, Fahrig R, Moore T, Boese J, Lauritsch G, Al-Ahmad A. Visualization of radiofrequency ablation lesions with iodine contrast-enhanced cardiac dynact. *Heart Rhythm Soc*. 2010;(Suppl):S85.
28. Kriatselis C, Tang M, Roser M, Fleck E, Gerds-Li H. A new approach for contrast-enhanced x-ray imaging of the left atrium and pulmonary veins for atrial fibrillation ablation: rotational angiography during adenosine-induced asystole. *Europace*. 2009;11:35-41.
29. Li JH, Haim M, Movassaghi B, et al. Segmentation and registration of three-dimensional rotational angiogram on live fluoroscopy to guide atrial fibrillation ablation: a new online imaging tool. *Heart Rhythm*. 2009;6:231-237.
30. Nolker G, Gutleben KJ, Marschang H, et al. Three-dimensional left atrial and esophagus reconstruction using cardiac C-arm computed tomography with image integration into fluoroscopic views for ablation of atrial fibrillation: accuracy of a novel modality in comparison with multislice computed tomography. *Heart Rhythm*. 2008;5:1651-1657.
31. Thiagalingam A, Manzke R, d'Avila A, et al. Intraprocedural volume imaging of the left atrium and pulmonary veins with rotational x-ray angiography: implications for catheter ablation of atrial fibrillation. *J Cardiovasc Electrophysiol*. 2008;19:293-300.
32. Burkhardt JD, Natale A. New technologies in atrial fibrillation ablation. *Circulation*. 2009;120:1533-1541.
33. Beatty GE, Remole SC, Johnston MK, Holte JE, Benditt DG. Non-contact electrical extrapolation technique to reconstruct endocardial potentials. *PACE*. 1994;17:765.
34. Dong J, Dickfeld T, Dalal D, et al. Initial experience in the use of integrated electroanatomic mapping with three-dimensional MR/CT images to guide catheter ablation of atrial fibrillation. *J Cardiovasc Electrophysiol*. 2006;17:459-466.
35. Marrouche NF, Verma A, Wazni O, et al. Mode of initiation and ablation of ventricular fibrillation storms in patients with ischemic cardiomyopathy. *J Am Coll Cardiol*. 2004;43:1715-1720.
36. Paul T, Windhagen-Mahnert B, Kriebel T, et al. Atrial reentrant tachycardia after surgery for congenital heart disease: endocardial mapping and radiofrequency catheter ablation using a novel, noncontact mapping system. *Circulation*. 2001;103:2266-2271.
37. Smeets J, Haim SB, Rodriguez L, Timmermans C, Wellens H. New method for nonfluoroscopic endocardial mapping in humans. *Circulation*. 1998;97:2426-2432.
38. Thiagalingam A, Wallace EM, Boyd AC, et al. Noncontact mapping of the left ventricle: insights from validation with transmural contact mapping. *Pacing Clin Electrophysiol*. 2004;27:570-578.
39. Callans DJ, Ren JF, Michele J, Marchlinski FE, Dillon SM. Electroanatomic left ventricular mapping in the porcine model of healed anterior myocardial infarction. Correlation with intracardiac echocardiography and pathological analysis. *Circulation*. 1999;100:1744-1750.
40. Nieuwlaat R, Capucci A, Camm AJ, et al. Atrial fibrillation management: a prospective survey in ESC member countries: the Euro Heart Survey on Atrial fibrillation. *Eur Heart J*. 2005;26:2422-2434.

41. Lang RM, Bierig M, Devereux RB, et al. Recommendations for chamber quantification: a report from the American Society of Echocardiography's Guidelines and Standards Committee and the Chamber Quantification Writing Group, developed in conjunction with the European Association of Echocardiography, a branch of the European Society of Cardiology. *J Am Soc Echocardiogr*. 2005;18:1440-1463.
42. Calkins H, Brugada J, Packer DL, et al. HRS/EHRA/ECAS expert consensus statement on catheter and surgical ablation of atrial fibrillation: recommendations for personnel, policy, procedures and follow-up. A report of the Heart Rhythm Society (HRS) task force on catheter and surgical ablation of atrial fibrillation. *Heart Rhythm*. 2007;4:816-861.
43. Pearson AC, Labovitz AJ, Tatineni S, Gomez CR. Superiority of transesophageal echocardiography in detecting cardiac source of embolism in patients with cerebral ischemia of uncertain etiology. *J Am Coll Cardiol*. 1991;17:66-72.
44. Epstein LM, Smith T, TenHoff H. Nonfluoroscopic transseptal catheterization: safety and efficacy of intracardiac echocardiographic guidance. *J Cardiovasc Electrophysiol*. 1998;9:625-630.
45. Marrouche NF, Martin DO, Wazni O, et al. Phased-array intracardiac echocardiography monitoring during pulmonary vein isolation in patients with atrial fibrillation: impact on outcome and complications. *Circulation*. 2003;107:2710-2716.
46. Mitchel JF, Gillam LD, Sanzobrino BW, Hirst JA, McKay RG. Intracardiac ultrasound imaging during transseptal catheterization. *Chest*. 1995;108:104-108.
47. Verma A, Marrouche NF, Natale A. Pulmonary vein antrum isolation: intracardiac echocardiography-guided technique. *J Cardiovasc Electrophysiol*. 2004;15:1335-1340.
48. Jongbloed MRM, Bax JJ, van der Wall EE, Schalij MJ. Thrombus in the left atrial appendage detected by intracardiac echocardiography. *Int J Cardiovasc Imaging*. 2004;20:113-116.
49. Ren J-F, Marchlinski FE, Callans DJ. Left atrial thrombus associated with ablation for atrial fibrillation: identification with intracardiac echocardiography. *J Am Coll Cardiol*. 2004;43:1861-1867.
50. Ren J-F, Marchlinski FE, Callans DJ, Zado ES. Intracardiac Doppler echocardiographic quantification of pulmonary vein flow velocity: an effective technique for monitoring pulmonary vein ostia narrowing during focal atrial fibrillation ablation. *J Cardiovasc Electrophysiol*. 2002;13:1076-1081.
51. Saad EB, Cole CR, Marrouche NF, et al. Use of intracardiac echocardiography for prediction of chronic pulmonary vein stenosis after ablation of atrial fibrillation. *J Cardiovasc Electrophysiol*. 2002;13:986-989.
52. Mansour M, Holmvang G, Sosnovik D, et al. Assessment of pulmonary vein anatomic variability by magnetic resonance imaging: implications for catheter ablation techniques for atrial fibrillation. *J Cardiovasc Electrophysiol*. 2004;15:387-393.
53. Marom EM, Herndon JE, Kim YH, McAdams HP. Variations in pulmonary venous drainage to the left atrium: implications for radiofrequency ablation. *Radiology*. 2004;230:824-829.
54. Scharf C, Sneider M, Case I, et al. Anatomy of the pulmonary veins in patients with atrial fibrillation and effects of segmental ostial ablation analyzed by computed tomography. *J Cardiovasc Electrophysiol*. 2003;14:150-155.
55. Lemola K, Sneider M, Desjardins B, et al. Effects of left atrial ablation of atrial fibrillation on size of the left atrium and pulmonary veins. *Heart Rhythm*. 2004;1:576-581.
56. Packer DL, Keelan P, Munger TM, et al. Clinical presentation, investigation, and management of pulmonary vein stenosis complicating ablation for atrial fibrillation. *Circulation*. 2005;111:546-554.
57. Qureshi AM, Prieto LR, Latson LA, et al. Transcatheter angioplasty for acquired pulmonary vein stenosis after radiofrequency ablation. *Circulation*. 2003;108:1336-1342.
58. Saad EB, Rossillo A, Saad CP, et al. Pulmonary vein stenosis after radiofrequency ablation of atrial fibrillation: functional characterization, evolution, and influence of the ablation strategy. *Circulation*. 2003;108:3102-3107.
59. Tsao H-M, Wu M-H, Huang B-H, et al. Morphologic remodeling of pulmonary veins and left atrium after catheter ablation of atrial fibrillation: insight from long-term follow-up of three-dimensional magnetic resonance imaging. *J Cardiovasc Electrophysiol*. 2005;16:7-12.
60. Lemola K, Sneider M, Desjardins B, et al. Computed tomographic analysis of the anatomy of the left atrium and the esophagus: implications for left atrial catheter ablation. *Circulation*. 2004;110:3655-3660.
61. Tops LF, Krishnan SC, Schuijf JD, Schalij MJ, Bax JJ. Non-coronary applications of cardiac multidetector row computed tomography. *JACC Cardiovasc Imaging*. 2008;1:94-106.
62. Tops LF, Schalij MJ, Bax JJ. Imaging and atrial fibrillation: the role of multi-modality imaging in patient evaluation and management of atrial fibrillation. *Eur Heart J*. 2010;31:542-551.
63. Dong J, Calkins H, Solomon SB, et al. Integrated electroanatomic mapping with three-dimensional computed tomographic images for real-time guided ablations. *Circulation*. 2006;113:186-194.
64. Dong J, Dickfeld T, Dalal D, et al. Initial experience in the use of integrated electroanatomic mapping with three-dimensional MR/CT images to guide catheter ablation of atrial fibrillation. *J Cardiovasc Electrophysiol*. 2006;17:459-466.
65. Kistler PM, Earley MJ, Harris S, et al. Validation of three-dimensional cardiac image integration: use of integrated CT image into electroanatomic mapping system to perform catheter ablation of atrial fibrillation. *J Cardiovasc Electrophysiol*. 2006;17:341-348.
66. Kistler PM, Rajappan K, Jahngir M, et al. The impact of CT image integration into an electroanatomic mapping system on clinical outcomes of catheter ablation of atrial fibrillation. *J Cardiovasc Electrophysiol*. 2006;17:1093-1101.
67. Mlkaelian BJ, Malchano ZJ, Neuzil P, et al. Images in cardiovascular medicine. Integration of 3-dimensional cardiac computed tomography images with real-time electroanatomic mapping to guide catheter ablation of atrial fibrillation. *Circulation*. 2005;112:e35-e36.
68. Rubenstein J, Kadish A. Three-dimensional image integration: a first experience with guidance of atrial fibrillation ablations. *J Cardiovasc Electrophysiol*. 2006;17:467-468.
69. Tops LF, Bax JJ, Zeppenfeld K, et al. Fusion of multislice computed tomography imaging with three-dimensional electroanatomic mapping to guide radiofrequency catheter ablation procedures. *Heart Rhythm*. 2005;2:1076-1081.
70. Daccarett M, Segerson NM, Golker J, et al. Blinded correlation study of three-dimensional electro-anatomical image integration and phased array intra-cardiac echocardiography for left atrial mapping. *Europace*. 2007;9:923-926.
71. Noseworthy PA, Malchano ZJ, Ahmed J, Holmvang G, Ruskin JN, Reddy VY. The impact of respiration on left atrial and pulmonary venous anatomy: implications for image-guided intervention. *Heart Rhythm*. 2005;2:1173-1178.
72. den Uijl DW, Tops LF, Tolosana JM, et al. Real-time integration of intracardiac echocardiography and multislice computed tomography to guide radiofrequency catheter ablation for atrial fibrillation. *Heart Rhythm*. 2008;5:1403-1410.
73. Packer DL, Johnson SB, Kolasa MW, Bunch TJ, Henz BD, Okumura Y. New generation of electro-anatomic mapping: full intracardiac ultrasound image integration. *Europace*. 2008;10(Suppl 3):iii35-iii41.
74. Ordovas K, Reddy G, Higgins C. MRI in nonischemic acquired heart disease. *J Magn Reson Imaging*. 2008;27:1195-1213.
75. Weinsaft JW, Klem I, Judd RM. MRI for the assessment of myocardial viability. *Cardiol Clin*. 2007;25:35-56.
76. Moon J, Reed E, Sheppard M, et al. The histologic basis of late gadolinium enhancement cardiovascular magnetic resonance in hypertrophic cardiomyopathy. *J Am Coll Cardiol*. 2004;43:2260-2264.
77. Peters DC, Wylie JV, Hauser TH, et al. Detection of pulmonary vein and left atrial scar after catheter ablation with three-dimensional navigator-gated delayed enhancement MR imaging: initial experience. *Radiology*. 2007;243:690-695.
78. McGann CJ, Kholmovski EG, Oakes RS, Blauer JJE, et al. New magnetic resonance imaging-based method for defining the extent of left atrial wall injury after the ablation of atrial fibrillation. *J Am Coll Cardiol*. 2008;52:1263-1271.
79. Badger TJ, Adjei-Poku YA, Burgon NS, et al. Initial experience of assessing esophageal tissue injury and recovery using delayed-enhancement MRI after atrial fibrillation ablation. *Circ Arrhythm Electrophysiol*. 2009;2:620-625.
80. Peters DC, Wylie JV, Hauser TH, et al. Recurrence of atrial fibrillation correlates with the extent of post-procedural late gadolinium enhancement: a pilot study. *JACC Cardiovasc Imaging*. 2009;2:308-316.
81. Reddy VY, Schmidt EJ, Holmvang G, Fung M. Arrhythmia recurrence after atrial fibrillation ablation: can magnetic resonance imaging identify gaps in atrial ablation lines? *J Cardiovasc Electrophysiol*. 2008;19:434-437.

82. Oakes RS, Badger TJ, Kholmovski EG, et al. Detection and quantification of left atrial structural remodeling with delayed-enhancement magnetic resonance imaging in patients with atrial fibrillation. *Circulation*. 2009;119:1758-1767.
83. Cappato R, Calkins H, Chen SA, et al. Updated worldwide survey on the methods, efficacy and safety of catheter ablation for human atrial fibrillation. *Circ Arrhythm Electrophysiol*. 2010;3:32-38.
84. Badger TJ, Oakes RS, Daccarett M, et al. Temporal left atrial lesion formation after ablation of atrial fibrillation. *Heart Rythm J*. 2009;6:161-168.
85. Chen MS, Marrouche NF, Khaykin Y, et al. Pulmonary vein isolation for the treatment of atrial fibrillation in patients with impaired systolic function. *J Am Coll Cardiol*. 2004;43:1004-1009.
86. Gillinov AM, Bakaeen F, McCarthy PM, et al. Surgery for paroxysmal atrial fibrillation in the setting of mitral valve disease: a role for pulmonary vein isolation? *Ann Thorac Surg*. 2006;81:19-26; discussion 27-28.
87. Gillinov AM, McCarthy PM, Blackstone EH, et al. Surgical ablation of atrial fibrillation with bipolar radiofrequency as the primary modality. *J Thorac Cardiovasc Surg*. 2005;129:1322-1329.
88. Kilicaslan F, Verma A, Saad E, et al. Transcranial Doppler detection of microembolic signals during pulmonary vein antrum isolation: implications for titration of radiofrequency energy. *J Cardiovasc Electrophysiol*. 2006;17:495-501.
89. Pappone C, Rosanio S, Oreto G, et al. Circumferential radiofrequency ablation of pulmonary vein ostia: a new anatomic approach for curing atrial fibrillation. *Circulation*. 2000;102:2619-2628.
90. Fahmy TS, Mlcochova H, Wazni OM, et al. Intracardiac echo-guided image integration: optimizing strategies for registration. *J Cardiovasc Electrophysiol*. 2007;18:276-282.
91. Wazni OM, Rossillo A, Marrouche NF, et al. Embolic events and char formation during pulmonary vein isolation in patients with atrial fibrillation: impact of different anticoagulation regimens and importance of intracardiac echo imaging. *J Cardiovasc Electrophysiol*. 2005;16:576-581.
92. Kolandaivelu A, Lardo AC, Halperin HR. Cardiovascular magnetic resonance guided electrophysiology studies. *J Cardiovasc Magn Reson*. 2009;11:21.
93. Vijayakumar S, Kholmovski EG, MacLeod RS, et al. Visualizing acute RF ablation lesions in the heart using non-contrast MRI at 3T. Poster Presentation. International Society for Magnetic Resonance in Medicine, Honolulu, HI, 2009.

CHAPTER 5

PERFORMANCE OF VOLTAGE MAPPING

Substrate mapping provides in-procedure feedback and guidance for the ablation of cardiac arrhythmias. With substrate mapping, it is assumed that the electrograms acquired from a given location are representative of the local electrophysiological properties. However, many factors influence the generation of an electrogram. For the catheter, considerations such as the size and spacing of electrodes, the type of reference used, contact with the tissue, and the orientation of the catheter with respect to the tissue an wavefront may affect electrogram morphology. For the tissue, the fiber orientation, the direction of impulse propagation, and the presence and size of abnormal substrate also may affect EGM morphology. The combined influence of these factors is sufficient to cast doubt on the particular meaning of any electrogram observed to have unique or abnormal properties. Consequently, it is imperative to characterize the effect of these various factors on the performance of substrate mapping for identifying arrhythmogenic myocardium. This chapter contains the results of a study previously published in the *Journal of Cardiovascular Electrophysiology* titled, "Sensitivity and Specificity of Substrate Mapping: An In Silico Framework for the Evaluation of Electroanatomical Substrate Mapping Strategies" [171]. This study focuses on voltage mapping, one type of substrate mapping, and the effect of various geometric factors on the ability of voltage mapping to detect abnormal myocardium. This work appears in the published format with permission from the journal.

Sensitivity and Specificity of Substrate Mapping: An *In Silico* Framework for the Evaluation of Electroanatomical Substrate Mapping Strategies

JOSHUA J.E. BLAUER, B.S.,*,† DARRELL SWENSON, PH.D.,*,† KOJI HIGUCHI, M.D.,* GERNOT PLANK, PH.D.,‡ RAVI RANJAN, M.D., PH.D.,* NASSIR MARROUCHE, M.D.,* and ROB S. MACLEOD, PH.D.*,†

From the *CARMA Center, University of Utah, Salt Lake City, Utah, USA; †Department of Bioengineering, University of Utah, Salt Lake City, Utah, USA; and ‡Institute of Biophysics, Medical University of Graz, Graz, Austria

Geometric Factors in Voltage Mapping. ***Background:*** **Voltage mapping is an important tool for characterizing proarrhythmic electrophysiological substrate, yet it is subject to geometric factors that influence bipolar amplitudes and thus compromise performance. The aim of this study was to characterize the impact of catheter orientation on the ability of bipolar amplitudes to accurately discriminate between healthy and diseased tissues.**

Methods and Results: **We constructed a 3-dimensional, *in silico*, bidomain model of cardiac tissue containing transmural lesions of varying diameter. A planar excitation wave was stimulated and electrograms were sampled with a realistic catheter model at multiple positions and orientations. We carried out validation studies in animal experiments of acute ablation lesions mapped with a clinical mapping system. Bipolar electrograms sampled at higher inclination angles of the catheter with respect to the tissue demonstrated improvements in both sensitivity and specificity of lesion detection. Removing low-voltage electrograms with concurrent activation of both electrodes, suggesting false attenuation of the bipolar electrogram due to alignment with the excitation wavefront, had little effect on the accuracy of voltage mapping.**

Conclusions: **Our results demonstrate possible mechanisms for the impact of catheter orientation on voltage mapping accuracy. Moreover, results from our simulations suggest that mapping accuracy may be improved by selectively controlling the inclination of the catheter to record at higher angles with respect to the tissue.** *(J Cardiovasc Electrophysiol, Vol. 25, pp. 774-780, July 2014)*

bipolar electrogram, computer-based model, electroanatomical mapping, voltage mapping

Introduction

Cardiac substrate mapping is a class of electroanatomical mapping in which proarrhythmic tissues are identified based on features of the local electrograms (EGMs). EGM features commonly interrogated for signs of pathology include signal amplitude, the power spectrum, and fractionation ("voltage," "DF," and "CFAE" mapping, respectively).[1-3] A common thread among these mapping techniques is the frequent reliance on bipolar EGMs which are valued in clinical electrophysiology for their sensitivity to local electrical properties. However, various geometric factors, e.g., perpendicular alignment of the electrode pair relative to the direction of the advancing activation wave, may influence bipolar EGM morphology and thus impact the accuracy of substrate mapping.

In voltage-based substrate mapping, the peak-to-peak amplitude of bipolar EGMs, typically from a single, representative activation sequence, is recorded and displayed on a geometric representation of the chamber being mapped. Multiple studies have demonstrated that diseased tissues, i.e., scarred or fibrotic, produce smaller bipolar amplitudes (BPAs) than are observed in healthy tissues.[1,4] However, studies using voltage mapping to localize lesions have reported both over- and underestimation of lesion size.[5-8] The plausible sources of these errors in voltage mapping are manifold but one possibility is the variability in BPAs that arises due to geometric uncertainty in electrode placement and orientation. Recently, Otomo *et al.* explored the effect of transmural ablation lesions on EGMs recorded with a mapping catheter oriented either perpendicular or parallel to the cardiac wall at the ablation site.[9] Their findings clearly demonstrated that EGM morphology changes due to the geometric positioning of the catheter. We have extended this line of inquiry using experiments and *in silico* studies, and to our knowledge, no previous study has systematically linked the effects of the geometric parameters on BPAs to the accuracy of voltage mapping–based detection of myocardial injury or disease.

A thorough and precise study of the effects of geometric parameters including catheter size, orientation, placement, and electrode configuration on the localization of cardiac

This project was supported by grants from the National Center for Research Resources (5P41RR012553–15) and the National Institute of General Medical Sciences (8 P41 GM103545–15) from the National Institutes of Health.

Dr. Marrouche reports participation on research grants/other research support and serving as a consultant/advisory board member of eCardio and Estech; honoraria relevant to this topic from Biotronik, Boston Scientific, and Boehringer Ingelheim; stock ownership in UMS, Cardiac Designs, Arapeen Medical, Marrek, and Sentro Med. Other authors: No disclosures.

Address for correspondence: Joshua J.E. Blauer, B.S., University of Utah, 72 South Central Campus Drive, WEB 3750, SCI Institute, Salt Lake City, UT 84112, USA. Fax: 801-585-6513; E-mail: blauer@sci.utah.edu

Manuscript received 21 February 2014; Revised manuscript received 2 April 2014; Accepted for publication 21 April 2014.

doi: 10.1111/jce.12444

tissue lesions is not practical using purely experimental approaches. Even with large mammal models it is not currently feasible to capture and control all the relevant parameters with adequate accuracy. In contrast, an approach based on computational modeling and simulation provides complete control over all relevant parameters and the ability to mimic the conditions in the heart. The requirements of such an *in silico* study include the ability to create realistic models of the myocardium and electrodes, to solve the associated bioelectric spread of excitation and extra-cardiac potentials, and to display and analyze the results quantitatively. The numerical methods and software for such a modeling pipeline are now available[10-12] and well enough refined to serve as a reliable platform for such a study.

The specific aims of our study were to identify and quantify the impact of some known but clinically uncontrolled geometric factors on cardiac substrate mapping. We used a myocardial slab in which we introduced lesions and then simulated the spread of activation through the tissue. We then introduced a geometrically realistic model of a clinical mapping and ablation catheter and simulated catheter placement at different sites and orientations relative to the tissue surface. By imposing a range of thresholds to distinguish between normal and subnormal bipolar voltage amplitudes, including accepted clinical thresholds, we predicted the sites of lesions, compared the results to the known locations, and then created receiver operating characteristic (ROC) curves. Based on this metric of performance, we could then identify the critical sources of error and determine the resulting bounds on precision for this ubiquitous technique in clinical cardiac electrophysiology.

Methods

Computational Model

We executed a bidomain simulation of the spread of activation through an electrically isotropic slab model of atrial myocardium with the Cardiac Arrhythmia Research Package software.[13] The model geometry was a $50 \times 50 \times 5$ mm slab composed of isotropic hexahedral elements with 0.18 mm edge length. The slab was completely immersed in a bath that was 3 mm deep on all sides except for the mapping surface, where the bath was 10 mm deep. Within the myocardial slab, we incorporated cylindrically shaped, transmural lesions of 4, 6, 8, and 10 mm diameter. One edge of the geometry was stimulated to produce a planar wavefront, and, according to standard practice, we scaled conductivities to produce physiologically realistic conduction velocities (0.56 m/s). The Courtemanche-Ramirez-Nattel cell model of atrial myocyte kinetics[14] simulated the excitation of normal myocardium whereas lesions were modeled as passive volume conductors.

A realistic catheter geometry (8 F diameter, 4 mm long tip, 2 mm long distal ring electrode with 2 mm interelectrode spacing) was used to sample the electric potential on the simulated heart surface at 1 kHz sampling frequency. A random sampling of 1,000 points on the surface of the tissue (738 on normal tissue, 190 on lesions, and 72 removed from analysis due to stimulus artifact in the EGMs), all at least 5 mm from the slab edge, determined the placement of the simulated catheter tip. The sampling of points was weighted such that the density of points on lesions was 3 times higher than that of normal tissues. With the catheter tip fixed at each of these 928 surface points (Fig. 1A), we then tilted the catheter through 116 uniformly distributed orientations in 3 dimensions (Fig. 1B). At each location and orientation of the catheter, we computed the extracellular potentials at the electrodes for the entire time series to reconstruct unipolar and bipolar EGMs (Fig. 1C).

There were 2 parameters in this study that we assumed would affect performance. The first was the angle of the catheter shaft relative to the tissue, defined as the inclination angle. A value of zero corresponded to all electrodes of the catheter lying flat on the tissue surface and a value of 90 degrees to a full perpendicular catheter orientation (Fig. 1A). We evaluated the sensitivity and specificity of lesion detection through the full range of catheter inclination angles. The second parameter of interest was the orientation of the bipolar electrodes relative to the activation wave front. However, curvature in the wave front caused by the lesions impeded consistent calculation of the angle between the bipolar electrode axis and the wavefront. To overcome this limitation we used the difference in activation times, annotated at the maximum negative slope of the distal and proximal unipolar EGMs,[15] as a marker of wave front arrival,[9] a metric we term ΔLAT, or absolute difference in local activation time expressed as:

$$\Delta\mathrm{LAT}(\mathrm{M}_1 - \mathrm{M}_2) = \mathrm{LAT}(\mathrm{M}_1) - \mathrm{LAT}(\mathrm{M}_2),$$

where M_1 and M_2 correspond to the 2 unipolar electrode sites. Small values of ΔLAT indicate (near) simultaneous arrival of activation at both electrodes, i.e., that the wave front direction is approximately perpendicular to the axis of the catheter. Given the anticipated error under such conditions, we evaluated the sensitivity and specificity of lesion detection when EGMs with small ΔLAT were removed from analysis.

Animal Model

Simulations provide considerably more control over relevant parameters than experiments, but they also require validation. While the scope of validation by experiment was inherently limited in this study, we were able to generate data to support our approach from dedicated animal studies approved by the University of Utah Institutional Animal Care and Use Committee. The details of this experimentation were previously reported by Ranjan *et al.* and are revisited in detail in the Supporting Information[16] Briefly, voltage mapping of swine right atria was performed before and after the creation of point ablation lesions. Gross pathological examination and analysis of the spatial characteristics of low-voltage regions facilitated estimation of the extent of injury surrounding lesions and calculation of sensitivities and specificities for voltage mapping.

Statistical Methods

All repeated measurements are expressed as mean $\pm$ standard deviation. Student's *t*-test, accompanied by the Holm-Bonferroni method for multiple comparisons, was used to test for significance. Significance was achieved at values of $P < 0.05$.

Sensitivity and specificity are reported as true positive ratio (TPR) and false positive ratio (FPR = 1-specificity), respectively, as defined by a standard confusion matrix.

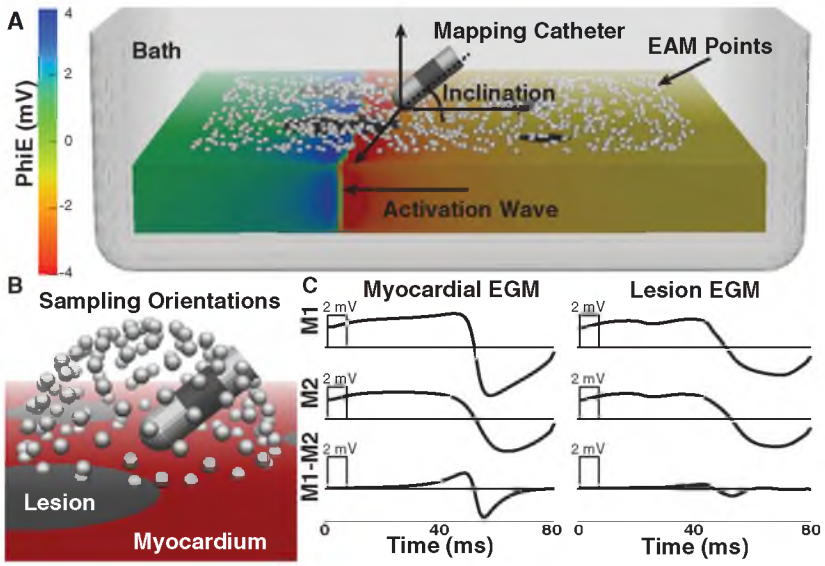

Figure 1. *In silico model of electroanatomical substrate mapping. A. Three-dimensional slab model with activation wave propagating from right to left and extracellular potentials displayed with color on the mesh. The white spheres show randomly selected points on the surface where the catheter tip was positioned for the recording of EGMs. The catheter, displayed at an inclination of ≈ 30 degrees, is representative of devices used clinically (8 F, 4 mm tip, 2 mm spacing). B. Illustration of the catheter positions used to sample electrograms. White spheres represent 116 transformations of the proximal electrode around the surface point. C. Representative electrograms acquired from same location in model before (L), and after simulated lesions were included in the model (R). EAM = electroanatomical map; EGMs = electrograms; PhiE = extracellular potential; M1 and M2 = unipolar signals from distal and proximal electrodes, respectively.*

Briefly, postablation points within the range of impact of each lesion were expected to show low voltage. Conversely, points sampled outside of the region impacted by ablation were anticipated to demonstrate normal bipolar amplitudes. A range of voltage thresholds for defining low voltage (0.25–3.0 mV) was tested to calculate receiver operating characteristic (ROC) curves for both models. We also used the Matthew's correlation coefficient (MCC), a performance metric for summarizing a confusion matrix in a single value.[17-19] MCC values range from −1 to +1, with a value of +1 indicating perfect correlation, or prediction. In this study, MCC was used to assess the performance of substrate mapping through a range of voltages.

Results

Computational Model

Figure 2 shows the mean bipolar amplitude, over the 116 recording orientations, at each mapping site from the lesion model. For all points, the mean bipolar amplitude for EGMs recorded on lesions, 2.00 ± 1.01 mV (n = 22,040), was significantly lower than BPAs from healthy tissue, 3.24 ± 0.91 mV (n = 85,608).

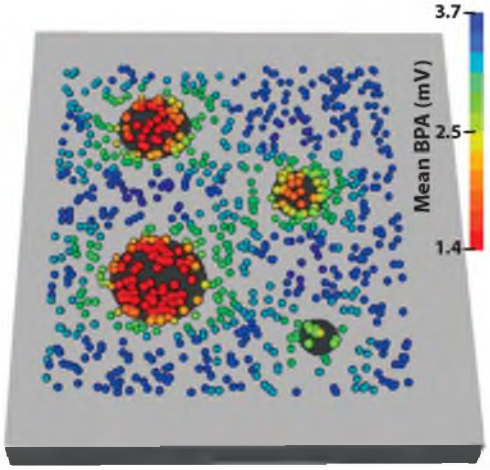

Figure 2. *Mean of 116 BPAs recorded at each mapping site. Bipolar amplitudes were recorded at 928 locations (colored spheres) on the lesion model (normal tissue is colored light gray and lesions are black). The mean of all bipolar amplitudes recorded at each of 928 sites (n = 116) determines sphere color.*

Comparison of Voltage Mapping Accuracy in Computational and Experimental Models

The fidelity of lesion detection with voltage-based substrate mapping, for both the *in silico* and *in vivo* models, was assessed by computing sensitivity, specificity, and MCC values over a range of physiologically realistic low-voltage thresholds ranging from 0.25 to 3.0 mV in increments of 0.25 mV. ROC curves and plots of MCC as a function of low-voltage threshold demonstrated a similar dependence of both models on threshold selection, an example of which is shown in Figure 3. As might be anticipated, varying the voltage threshold for lesion detection demonstrated

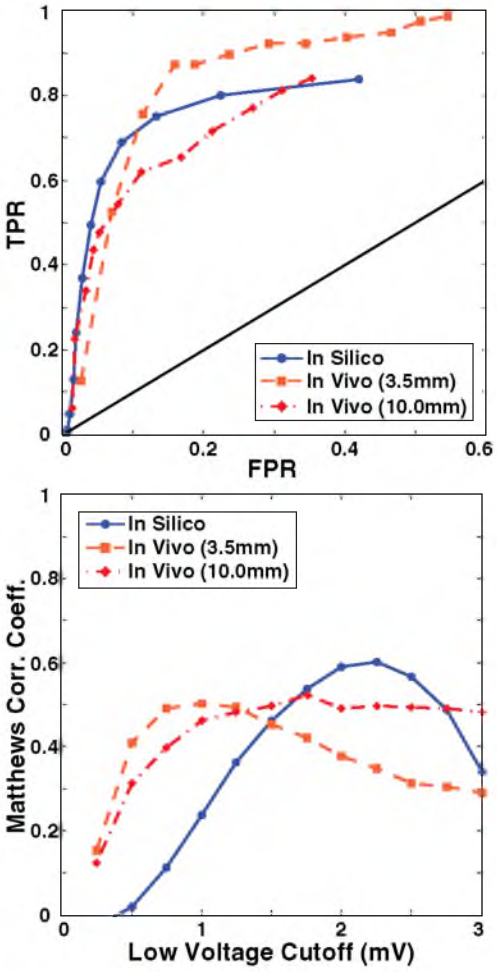

Figure 3. *Baseline evaluation of lesion detection accuracy. Top: Baseline TPR and FPR of lesion detection for the in vivo and in silico models were calculated at voltage cutoffs ranging from 0.25 to 3.0 mV. Bottom: MCC plotted as a function of the low-voltage cutoff illustrates the performance of substrate mapping in each model at a given voltage. TPR = true positive ratio; FPR = false positive ratio; MCC = Matthew's correlation coefficient. For a high quality, full color version of this figure, please see Journal of Cardiovascular Electrophysiology's website: www.wileyonlinelibrary.com/journal/jce*

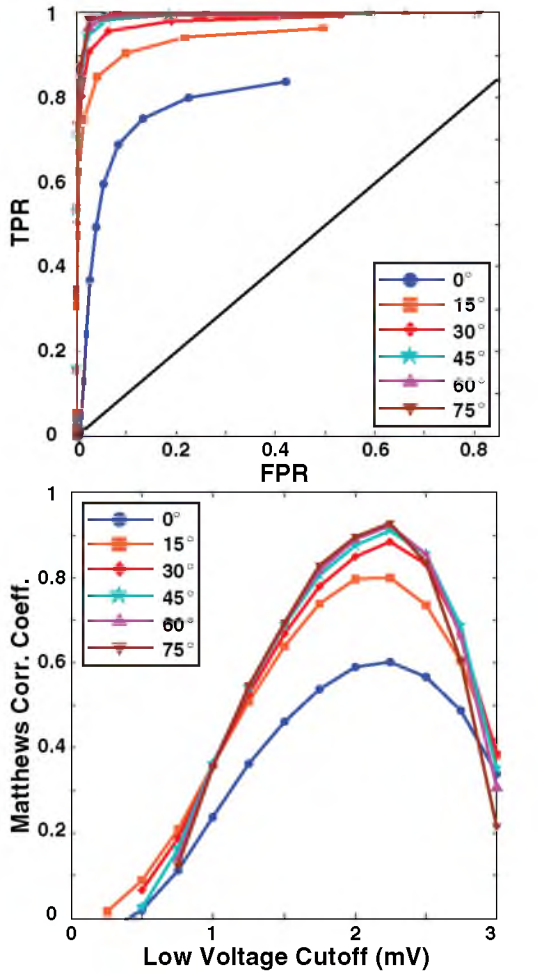

Figure 4. *Effect of inclination angle on in silico voltage mapping accuracy. The upper panel contains ROC curves that demonstrate the sensitivity and specificity of voltage mapping as BPAs recorded at low inclination angles are removed by increments of 15 degrees. The lower panel contains plots of Matthew's correlation coefficient which show the effect of progressively removing low inclination recordings on the performance of voltage mapping as a function of the low-voltage threshold. The blue curves, marked with circles, indicate the baseline conditions shown in the previous figure. For a high quality, full color version of this figure, please see Journal of Cardiovascular Electrophysiology's website: www.wileyonlinelibrary.com/journal/jce*

tradeoffs in sensitivity and specificity of the ROC curves. For the *in vivo* measurements, limiting the expected extent of low-voltage tissue to the 3.5 mm radius region of directly ablated myocardium resulted in relatively higher sensitivity and lower specificity compared to a more relaxed boundary that accounted for low voltages caused by injury responses surrounding lesion (10 mm radius). Results from the *in silico* model showed similar characteristics to the *in vivo* model, but with a generally improved specificity and higher voltages for lesions and normal tissues (Fig. 3). The following sections expand on this overall characterization of substrate mapping accuracy. Specifically, we evaluated the results under variations in inclination angle of the catheter and ΔLAT of the EGMs.

Effect of Catheter Inclination Angle on Lesion Detection

Figure 4 contains ROC curves in which bipolar EGM recordings acquired at low inclination angles were progressively removed, in increments of 15 degrees, from the sensitivity analysis. As the figure shows, such removal of low inclination EGMs, i.e., those for which the proximal electrode is near the cardiac surface, dramatically improved the ROC performance and the peak MCC values. For example, removing all EGMs with an inclination of less than 30 degrees improved the TPR and FPR over baseline by 21.8% and 6.0%, respectively, and the peak MCC value from

0.60 to 0.91. Improvements beyond 30 degrees were only incremental.

Effect of Catheter Orientation with Respect to Activation Wave on Lesion Detection

It is generally known that variations in alignment of the activation wave and the bipolar electrodes can alter the shape and amplitude of bipolar EGMs, reducing BPAs when the wavefront arrives at both electrodes simultaneously. To evaluate the effect of this parameter on the accuracy of lesion detection, we employed the same strategy as in the previous section by successively removing from consideration EGMs with small ΔLAT values (0, 1, and 2 milliseconds). As described in the Methods section, ΔLAT is an indirect metric of alignment between activation wavefront and electrode axis. The fact that this metric is based on signal morphology also allows application to both simulated and measured EGMs and we included both in this evaluation.

Figure 5 shows ROC and MCC curves following removal of recordings with |ΔLAT| of $\leq$ 0, 1, and 2 milliseconds compared to baseline results. For both the *in silico* and *in vivo* models, we detected little change in overall accuracy, as measured by the amplitude of the associated MCC, by removing low ΔLAT values. This finding was confirmed visually in Figure 5 by the observation that the ROC curves superimposed closely for all cases. Note that in the curves based on *in vivo* measurements, we applied separately the 3.5 mm and 10 mm assumptions for injury proximity to the lesion.

Discussion

Voltage mapping is a valuable clinical tool for the identification of arrhythmogenic myocardial tissue. However, the use of bipolar EGMs introduces geometric factors that may cause errors in the classification of diseased and healthy tissues. Previous studies have sought to determine optimal BPA voltage thresholds for identifying diseased tissue,[1,8] but were unable to consider the effect of these geometric factors on mapping accuracy. This study systematically explored the influence of electrode inclination angle and orientation on the ability of voltage mapping to detect changes in the myocardial substrate. Our findings elucidate possible mechanisms for improper classification of tissue type and suggest novel recording strategies that could improve voltage mapping accuracy.

The first factor whose role in lesion detection we investigated was the inclination angle of the catheter relative to the endocardial surface. Considering only BPAs recorded at inclinations above 30 degrees improved the quality of substrate classification by 51.7% (MCC of 0.6 to 0.91). At higher inclination angles, the bipolar electrode pair maintained common-mode rejection while reducing potentially confounding electric potentials sensed by the proximal electrode when located nearer the cardiac surface. Our simulations suggest that ensuring an inclination angle of >30 degrees could substantially improve lesion localization. Recent advances in catheter tracking and sensing, e.g., contact force measurement technology or real time MRI catheter tracking, are emerging technologies that could enable such control of catheter angle.[20-22]

The second geometric parameter we considered was the orientation of the catheter with respect to the activation wavefront. Perpendicular alignment of the electrode pair with the direction of the activation wave front may cause artifactual attenuation of the bipolar amplitudes resulting in healthy tissue being classified as scar.[23] While such errors would appear to be avoidable through directed electrode placement, robust determination of orientation of the catheter to the activation wave is not currently feasible in clinical cardiac mapping. We attempted to use signal processing to reduce the associated errors by identifying low-voltage bipolar EGMs with near simultaneous activation in their respective unipolar signals and removing them from consideration.[9] Our strategy assumed that small ΔLAT EGMs would disproportionately produce false positive, low-voltage recordings. However, in both the *in silico* and *in vivo* models, the removal of small ΔLAT EGMs had a mostly harmful effect on voltage mapping performance. Further examination of this finding revealed that small ΔLATs also frequently occurred when the catheter was at high inclination angles with respect to the tissue. Thus, true low-voltage EGMs recorded at higher inclination angles were improperly removed, because of their small ΔLATs, causing a decrease in sensitivity that offset any gains in specificity. While false low voltages caused by wavefront-EGM alignment tend to have small ΔLAT values, the reverse is not consistently true. However, these findings are specific to the electrode configuration and distribution of catheter orientations employed in this study. It is possible that other mapping devices, or distributions of catheter orientation, e.g., both bipolar electrodes always in tissue contact, may reveal utility for bipolar EGM discrimination based on the ΔLAT value.

Simulation allowed precise definition of the lesion boundaries in the model in a way that was not possible in our *in vivo* experimental studies (see Supporting Information). Gross pathological evaluation from the experiments did provide confirmation of lesion presence and size, however, BPA varies around the boundaries of lesions in ways that still inhibit precise *post hoc* determination. To deal with such variations, we assumed 2 regions around the lesions (radii of 3.5 mm and 10 mm) that contained low-voltage EGMs and evaluated the performance of measured signals separately for these 2 cases. With these assumptions, we attempted to incorporate into the analysis the variable and unpredictable effects of acute factors, beyond necrosis and tissue death, that are known to impact the amplitude of bipolar EGMs, e.g., stunning and edema. As noted, performance under these 2 assumptions was different in expected ways and provided a realistic basis for comparison with—and validation of—the results from simulations.

Calculation of MCC in this study returned a metric of accuracy in the detection of lesions as a function of threshold voltage. Through the various permutations of parameters, we found that the best BPA threshold remained relatively stable varying from 2.0 to 2.25 mV. This consistency supports the notion that establishing a carefully chosen voltage threshold is both feasible and useful to classify tissue type in clinical practice. However, because these findings were based on porcine and computational models, any extension of these values to clinical mapping studies is limited. Rather, we focused on evaluating factors that affect the performance of any low-voltage threshold as a discriminator of tissue type.

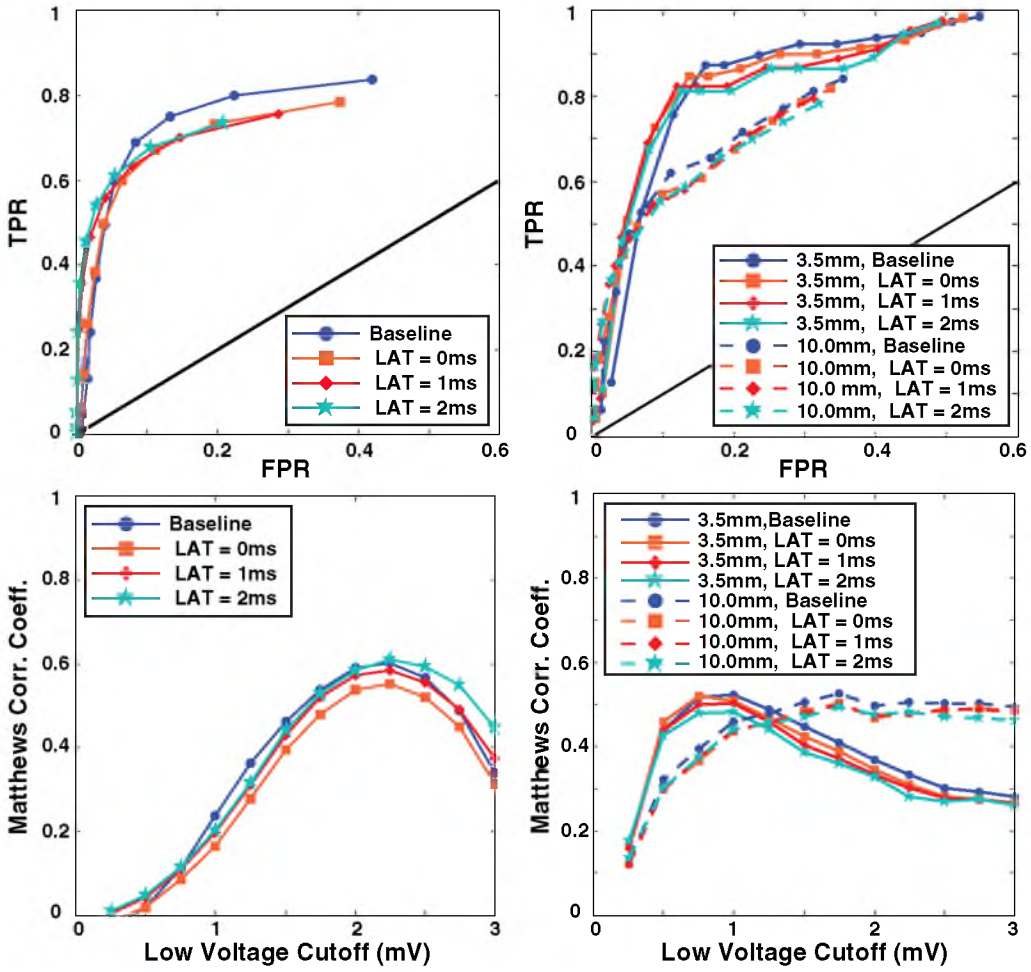

Figure 5. *Effect of simultaneous electrode activation on the accuracy of voltage mapping in silico (left column) and in vivo (right column). The top panels in both columns contain ROC curves from which EGMs with low ΔLAT values, indicating perpendicular alignment of the wavefront direction and the bipolar axis, were removed. The lower panels contain Matthew's correlation coefficient as a function of low-voltage threshold for the same EGMs. For a high quality, full color version of this figure, please see Journal of Cardiovascular Electrophysiology's website: www.wileyonlinelibrary.com/journal/jce*

Finally, the 3-dimensional (3-D) slab geometry we used is a simplified computational model that does not incorporate such factors as variation in wall thickness, or curvature of cardiac tissue. As such, a future step will be to incorporate more realistic geometric and tissue features into such a model. Even with such a simple model, we have illustrated in a novel way the impacts of realistic constraints of bipolar EGM-based cardiac mapping and validated some of those results with experiments. Extending the study to a more realistic, 3-D geometric model is straightforward so that this study can also serve as a feasibility test and motivator for additional complexity.

Conclusion

This study explored the utility of computational models for evaluating complex clinical scenarios that cannot be replicated in experiments. The specific case for this study was evaluating geometric parameters for their role in inducing uncertainty in cardiac mapping. The *in vivo* measurements provided qualitative validation of part of the simulations, instilling confidence that other simulation results were also valid. Our findings suggest that for parameters that are too difficult to control in experiments, e.g., inclination angle, simulation provides a tractable and powerful means to lend insight into the interactions of these factors. Furthermore, the results of this study support our initial hypothesis that different catheter orientations substantially impact the accuracy of diagnostic recordings, and suggest that controlling for optimal orientation would greatly improve the characterization of diseased myocardial substrates. Future confirmation of these findings could lead to improvements in catheter design and mapping technique. Such improvements in substrate characterization could extend the utility of voltage mapping to a variety of substrate-based arrhythmogenic cardiomyopathies.

Acknowledgments: The authors thank Christopher Gloschat for technical assistance.

References

1. Marchlinski FE, Callans DJ, Gottlieb CD, Zado E: Linear ablation lesions for control of unmappable ventricular tachycardia in patients with ischemic and nonischemic cardiomyopathy. Circulation 2000;101:1288-1296.
2. Nademanee K, McKenzie J, Kosar E, Schwab M, Sunsaneewitayakul B, Vasavakul T, Khunnawat C, Ngarmukos T: A new approach for catheter ablation of atrial fibrillation: Mapping of the electrophysiologic substrate. J Am Coll Cardiol 2004;43:2044-2053.
3. Sanders P, Berenfeld O, Hocini M, Jaïs P, Vaidyanathan R, Hsu L-F, Garrigue S, Takahashi Y, Rotter M, Sacher F, Scavée C, Ploutz-Snyder R, Jalife J, Haïssaguerre M: Spectral analysis identifies sites of high-frequency activity maintaining atrial fibrillation in humans. Circulation 2005;112:789-797.
4. Oakes RS, Badger TJ, Kholmovski EG, Akoum N, Burgon NS, Fish EN, Blauer J, Rao SN, DiBella EVR, Segerson NM, Daccarett M, Windfelder J, McGann CJ, Parker D, MacLeod RS, Marrouche NF: Detection and quantification of left atrial structural remodeling with delayed-enhancement magnetic resonance imaging in patients with atrial fibrillation. Circulation 2009;119:1758-1767.
5. Codreanu A, Odille F, Aliot E, Marie P-Y, Magnin-Poull I, Andronache M, Mandry D, Djaballah W, Régent D, Felblinger J, de Chillou C: Electroanatomic characterization of post-infarct scars. J Am Coll Cardio 2008;52:839-842.
6. Wijnmaalen AP, van der Geest RJ, van Huls van Taxis CFB, Siebelink H-MJ, Kroft LJM, Bax JJ, Reiber JHC, Schalij MJ, Zeppenfeld K: Head-to-head comparison of contrast-enhanced magnetic resonance imaging and electroanatomical voltage mapping to assess post-infarct scar characteristics in patients with ventricular tachycardias: Real-time image integration and reversed registration. Eur Heart J 2011;32:104-114.
7. Perez-David E, Arenal Á, Rubio-Guivernau JL, del Castillo R, Atea L, Arbelo E, Caballero E, Celorrio V, Datino T, Gonzalez-Torrecilla E, Atienza F, Ledesma-Carbayo MJ, Bermejo J, Medina A, Fernández-Avilés F: Noninvasive identification of ventricular tachycardia-related conducting channels using contrast-enhanced magnetic resonance imaging in patients with chronic myocardial infarction. J Am Coll Cardiol 2011;57:11.
8. Spears DA, Suszko AM, Dalvi R, Crean AM, Ivanov J, Nanthakumar K, Downar E, Chauhan VS: Relationship of bipolar and unipolar electrogram voltage to scar transmurality and composition derived by magnetic resonance imaging in patients with nonischemic cardiomyopathy undergoing VT ablation. Heart Rhythm 2012;9:1837-1846.
9. Otomo K, Uno K, Fujiwara H, Isobe M, Iesaka Y: Local unipolar and bipolar electrogram criteria for evaluating the transmurality of atrial ablation lesions at different catheter orientations relative to the endocardial surface. Heart Rhythm 2010;7:1291-1300.
10. MacLeod RS, Stinstra JG, Lew S, Whitaker RT, Swenson DJ, Cole MJ, Krüger J, Brooks DH, Johnson CR: Subject-specific, multiscale simulation of electrophysiology: A software pipeline for image-based models and application examples. Phil Trans R Soc A 2009;367:2293-2310.
11. Relan J, Pop M, Delingette H, Wright GA, Ayache N, Sermesant M: Personalization of a cardiac electrophysiology model using optical mapping and MRI for prediction of changes with pacing. IEEE Trans Biomed Eng 2011;58:3339-3349.
12. Camara O, Sermesant M, Lamata P, Wang L, Pop M, Relan J, De Craene M, Delingette H, Liu H, Niederer S, Pashaei A, Plank G, Romero D, Sebastian R, Wong KCL, Zhang H, Ayache N, Frangi AF, Shi P, Smith NP, Wright GA: Inter-model consistency and complementarity: Learning from ex-vivo imaging and electrophysiological data towards an integrated understanding of cardiac physiology. Prog Biophys Mol Bio 2011;107:122-133.
13. Vigmond EJ, Hughes M, Plank G, Leon LJ: Computational tools for modeling electrical activity in cardiac tissue. J Electrocardiol 2003;36:69-74.
14. Courtemanche M, Ramirez RJ, Nattel S: Ionic targets for drug therapy and atrial fibrillation-induced electrical remodeling: Insights from a mathematical model. Cardiovasc Res 1999;42:477-489.
15. Spach MS, Dolber PC: Relating extracellular potentials and their derivatives to anisotropic propagation at a microscopic level in human cardiac muscle. Evidence for electrical uncoupling of side-to-side fiber connections with increasing age. Circ Res 1986;58:356-371.
16. Ranjan R, Kholmovski EG, Blauer J, Vijayakumar S, Volland NA, Salama ME, Parker DL, MacLeod R, Marrouche NF: Identification and acute targeting of gaps in atrial ablation lesion sets using a real-time magnetic resonance imaging system. Circ Arrhythm Electrophysiol 2012;5:1130-1135.
17. Matthews BW: Comparison of the predicted and observed secondary structure of T4 phage lysozyme. Biochim Biophys Acta 1975;405:442-451.
18. Baldi P, Brunak S, Chauvin Y, Andersen CAF, Nielsen H: Assessing the accuracy of predition algorithms for classification: An overview. Bioinformatics 2000;16:412-424.
19. Jurman G, Riccadonna S, Furlanello C: A Comparison of MCC and CEN error measures in multi-class prediction. PLoS One 2012;7:e41882-e41886.
20. Yokoyama K, Nakagawa H, Shah DC, Lambert H, Leo G, Aeby N, Ikeda A, Pitha JV, Sharma T, Lazzara R, Jackman WM: Novel contact force sensor incorporated in irrigated radiofrequency ablation catheter predicts lesion size and incidence of steam pop and thrombus. Circ Arrhythm Electrophysiol 2008;1:354-362.
21. Guttman MA, Ozturk C, Raval AN, Raman VK, Dick AJ, DeSilva R, Karmarkar P, Lederman RJ, McVeigh ER: Interventional cardiovascular procedures guided by real-time MR imaging: An interactive interface using multiple slices, adaptive projection modes and live 3D renderings. J Magn Reson Imaging 2007;26:1429-1435.
22. Vergara GR, Vijayakumar S, Kholmovski EG, Blauer J, Guttman MA, Gloschat C, Payne G, Vij K, Akoum NW, Daccarett M, McGann CJ, MacLeod RS, Marrouche NF: Real-time magnetic resonance imaging-guided radiofrequency atrial ablation and visualization of lesion formation at 3 Tesla. Heart Rhythm 2011;8:295-303.
23. Brunckhorst CB, Delacretaz E, Soejima K, Maisel WH, Friedman PL, Stevenson WG: Impact of changing activation sequence on bipolar electrogram amplitude for voltage mapping of left ventricular infarcts causing ventricular tachycardia. J Interv Card Electrophysiol 2005;12:137-141.

Supporting Information

Additional supporting information may be found in the online version of this article at the publisher's website:

Figure 1. *In vivo* model of electroanatomical substrate mapping. A. Voltage maps acquired in a porcine right atrium pre- and postablation displaying bipolar amplitude. The purple spheres represent ablation points, all other points represent measurement sites colored according to bipolar amplitude.

Figure 2. Evolution of BPA with respect to distance from ablation site. Left—postablation points (red) and preablation points (blue) are plotted based on their BPA and distance from the centroid of the nearest ablation site. Right—mean and error bars (3 standard deviations) of the pre- (blue) and postablation (red) voltage maps as a function of distance from ablation sites based on kernel regression analysis.

Supplemental Material

Methods: Description of Animal Model Studies

University of Utah Institutional Animal Care and Use Committee approval was obtained for all animal experimentation. Five juvenile swine weighing 30 to 35 kgs were sedated with a cocktail of Telazol 4.4 mg/kg, Ketamine 2.2 mg/Kg and Xylazine 2.2 mg/Kg intra-muscularly and were placed on mechanical ventilation. Anesthesia was maintained with intravenous injections of 30-40 mg/Kg of pentobarbital. The femoral veins and arteries were accessed via cut down technique. 11 Fr. sheaths (St. Jude Medical, Austin, TX) were placed in the right and left femoral vein and were used to insert a mapping and ablation catheter. A 6 Fr. sheath was placed in the right femoral artery and was used for blood pressure monitoring and obtaining periodic arterial samples for blood gas analysis.

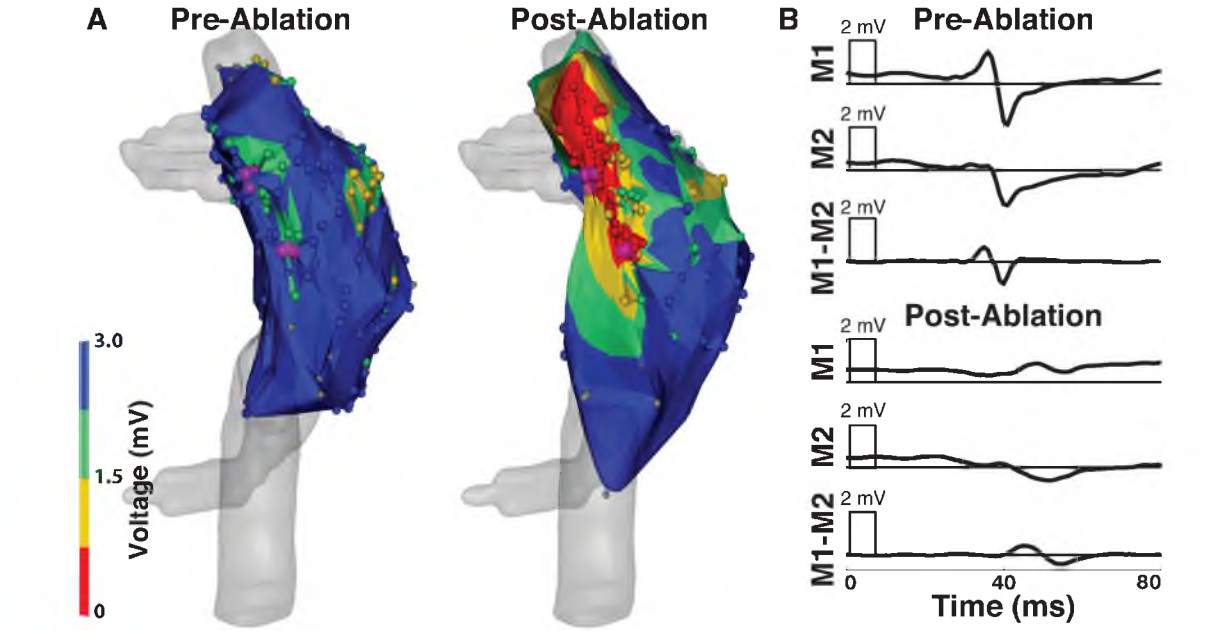

Figure 1: In vivo model of electroanatomical substrate mapping. A. Voltage maps acquired in a porcine right atrium pre- and postablation displaying bipolar amplitude. The purple spheres represent ablation points, all other points represent measurement sites colored according to bipolar amplitude. B. Representative electrograms acquired from the same location in the right atrium pre- and postablation. EAM - electroanatomical map, M1 and M2 - unipolar electrograms from the distal and proximal electrodes of a mapping catheter, M1-M2 - bipolar electrogram.

Anesthetized animals were moved to the electrophysiology lab with fluoroscopy (Artis Zeego, Siemens USA, Malvern, PA) and a CARTO XP electroanatomical mapping system (Biosense Webster, Diamond Bar, CA). A non-irrigated 4 mm tip NaviStar (Biosense Webster, Diamond

Bar, CA) catheter was used for electro- anatomical mapping. Baseline voltage maps were acquired and followed by the creation of two ablation lesions approximately 1 cm apart by delivering RF energy at 30 W for 30 seconds each in a temperature-controlled mode (60° C cutoff). During ablation we acquired mapping points every 5 to 10 seconds to ensure the catheter did not move. The center of each successfully ablated regions in the electroanatomical maps was estimated by calculating the centroid of all points acquired during the ablation. Immediately following the final ablation, the entire RA was remapped with particular emphasis on the areas surrounding the ablation sites with 142 ± 59 (min = 72, max = 194) points acquired per map (Figure 1A). The bipolar amplitude, ΔLAT, and Euclidean distance from the nearest ablation lesion center were calculated for each mapping point. Following the ablation and mapping studies, we intravenously injected each swine with 2,3,5-Triphenyl-2H-tetrazolium chloride (2% TTC), which demarcates ablated and infarcted tissues by staining live tissue red[1,2]. This step was immediately followed by lethal injection of intravenous potassium chloride.

Methods: Estimating the Extent of Ablation Injury

Ablation of cardiac tissue is known to cause immediate changes to the electrophysiological properties of directly targeted regions as well as surrounding tissues. These changes include cell death through membrane rupture, protein denaturing, stunning, and edema, all of which are known to affect BPAs to some degree[3-6]. Due to these factors it is challenging to appropriately demarcate which low voltages are due to actual injury (true positives), and those that arise because of factors unrelated to the health of the myocardial substrate (false positives). Consequently, we evaluated the extent of ablation injury, first, by gross pathological examination of the lesion sets, and, second, by analysis of postablation BPAs surrounding the lesion sites. The gross pathological analysis provided a stringent bound of ablation impact within which low voltage BPAs were strongly expected. We selected the loose bound based on analysis of the spatial transition of BPAs from low to normal voltages as distance from the lesion increased. These two bounds (described in more detail below) characterize the range of sensitivities and specificities that might be achieved with voltage mapping.

Gross Pathology of Ablation Lesions Lesion formation was confirmed by gross pathological assessment of the RA tissue. Lesion size was recorded based on two orthogonal measurements of the edge to edge diameter. Specifically, we acquired photographs of each lesion set, including a reference metric ruler, with a digital camera (Canon,Tokyo, Japan). The image analysis software GraphicConverter X v7.6.1 (Lemkesoft GmbH, Peine, Germany) was used to convert pixel size to millimeters via the reference ruler and then measure the lesion diameter with digital calipers using the boundary of the TTC staining. If the lesion shape was eccentric, its two principal axes were measured, otherwise axis orientation was arbitrary.

Kernel Regression Analysis Low voltage BPAs in the postablation maps were observed frequently beyond the anticipated burn radius (≈ 3-4 mm, Figure 2). We assumed that these low voltages were associated with the acute but transient injury responses to ablation. To estimate the outer range of low voltage BPAs, we used an approach known as kernel regression which is a non- parametric technique for estimating the conditional expectation of a random variable[7,8]. Software implementations of this technique are available in the open source statistical analysis package, R (The R Project for Statistical Computing, http://www.r-project.org). We used kernel

regression to analyze the relationship between BPAs (pre- and postablation) and the site of EGM acquisition relative to the lesion center. The mean BPA and ± 3 standard deviations were calculated for the pre- and postablation maps and the distance at which the respective error bars crossed was assigned as the loose boundary for expected low voltages (Figure 2).

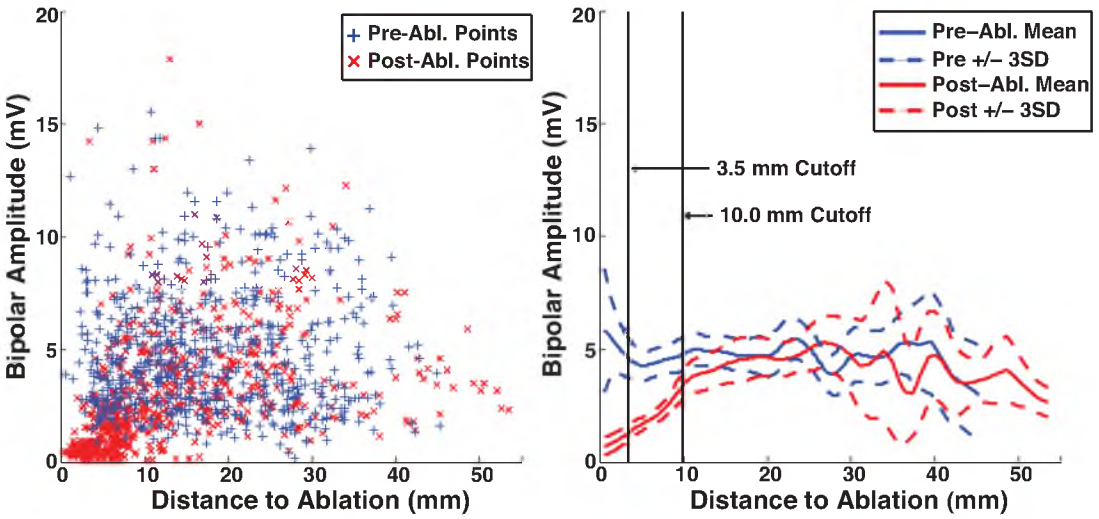

Figure 2: Evolution of BPA with respect to distance from ablation site. Left – Postablation points (red) and preablation points (blue) are plotted based on their BPA and distance from the centroid of the nearest ablation site. Right – Mean and error bars (3 standard deviations) of the pre- (blue) and postablation (red) voltage maps as a function of distance from ablation sites based on kernel regression analysis. The 3.5 mm cutoff represents the mean radius of lesions as measured by gross pathology. The 10.0 mm cutoff is the point at which the pre- and post ablation error bars cross in the kernel regression analysis.

Results: Animal Model

We performed electroanatomical mapping, ablation, and gross pathological analysis in all animals. There were no low voltage regions, i.e., areas with multiple, closely spaced low voltage recordings, in the preablation mapping of the swine right atria. The mean preablation bipolar amplitude was 4.74 ± 2.62 mV (n = 666). Following ablation, low voltage BPAs were observed in proximity to all attempted ablation sites (for an example, see Figure 1B). The mean diameter of all lesions was 7.3 ± 1.6 mm (n = 20 measures of 10 lesions, max = 10.1 mm, min = 4.5 mm). The lesions were mostly circular in shape with only one lesion presenting an anisotropy ratio greater than 2:1. Reasoning that tissue directly targeted by ablation would have the greatest likelihood of displaying low BPAs we estimated these regions based on the mean radius of the lesions from the gross pathological analysis and chose 3.5 mm from the lesion center as the stringent boundary. BPAs acquired within the stringent bound showed significantly lower voltages, 0.84 ± 1.64 mV (n = 78), than EGMs acquired outside the 3.5 mm stringent bound (3.38 ± 2.58 mV, n = 632). Figure 2 illustrates the spatial transition of post-ablation BPAs from low voltage at points near ablation centers to normal voltage at points remote from ablation. The

error bars (± 3 standard deviation) of the pre- and postablation kernel regression plots intersected at 10 mm from the lesion center. We selected this distance as the loose bound for the expectation of low voltages surrounding an ablation lesion. BPAs within the loose bound (10.0 mm from the lesion center) had significantly lower voltages (1.78 ± 1.71 mV, n =351), than bipolar EGMs acquired outside the 10 mm threshold (4.39 ± 2.71 mV, n = 359).

References

1. Kim RJ, Fieno DS, Parrish TB, Harris K, Chen EL. Relationship of MRI delayed contrast enhancement to irreversible injury, infarct age, and contractile function. *Circulation*. 1999;100:1992-2002.

2. Weiss C, Stewart M, Franzen O, Rostock T, Becker J, Skarda JR, Meinertz T, Willems S. Transmembraneous irrigation of multipolar radiofrequency ablation catheters: induction of linear lesions encircling the pulmonary vein ostium without the risk of coagulum formation? *J Interv Card Electrophysiol*. 2004;10:199–209.

3. Schwartzman D, Ren JF, Devine WA, Callans DJ. Cardiac swelling associated with linear radiofrequency ablation in the atrium. *J Interv Card Electrophysiol*. 2001;5:159–166.

4. Wood MA, Fuller IA. Acute and chronic electrophysiologic changes surrounding radiofrequency lesions. *Journal of Cardiovasc Electrophysiol,* 2002;*13:56-61.*

5. Knowles BR, Caulfield D, Cooklin M, Rinaldi CA, Gill J, Bostock J, Razavi R, Schaeffter T, Rhode KS. 3-D visualization of acute RF ablation lesions using MRI for the simultaneous determination of the patterns of necrosis and edema. *IEEE Trans Biomed Eng*. 2010;57:1467–1475.

6. McGann C, Kholmovski E, Blauer J, Vijayakumar S, Haslam T, Cates J, DiBella E, Burgon N, Wilson B, Alexander A, Prastawa M, Daccarett M, Vergara G, Akoum N, Parker D, MacLeod R, Marrouche N. Dark regions of no-reflow on late gadolinium enhancement magnetic resonance imaging result in scar formation after atrial fibrillation ablation. *J Am Coll Cardio*. 2011;58:177–185.

7. Racine JS, Li Q. Nonparametric estimation of regression functions with both categorical and continuous Data. *Journal of Econometrics*. 2004;119:99–130.

8. Li Q, Racine JS. Cross-validated local linear nonparametric regression. *Statistica Sinica*. 2004;14:485–512.

CHAPTER 6

CONDUCTION VELOCITY MAPPING

Many metrics of electrogram morphology used for substrate mapping are indirectly associated with mechanisms of arrhythmogenesis. For example, low voltage electrograms likely indicate scarred or otherwise abnormal tissues, but in many cases, scarring can have an anti-arrhythmogenic affect, as seen with scarring created during ablation procedures. Conduction velocity (CV) is an electrophysiological measure that is directly related to arrhythmogenic mechanisms (see Section 2.2.4). However, in current clinical practice, there are no established techniques for robust characterization of CV properties. This inability to robustly characterize CV properties of the cardiac substrate is primarily attributable to the anisotropic nature of conduction in the heart. In other words, recording of sinus activation in the heart cannot elucidate the anisotropy of conduction. In experimental studies, conduction anisotropy is measured by pacing from dense electrode arrays or measurement systems from which the spread of activation can be captured. Although clinical systems are capable of pacing-based stimulation of the myocardium, current clinical multielectrode arrays lack sufficient spatial sampling density to fully characterize the spread of an activation impulse away from the pacing site. This chapter presents novel approaches we have developed to facilitate robust CV property characterization with a clinical loop catheter using a repetitious stimulation and recording protocol. A final hinderance that this paper addresses is an approach for normalization of CV measures from multiple stimulus sites to account for variations in the CV properties that occur as an activation impulse moves away from a stimulus site, i.e., an increase in CV as the wavefront curvature decreases. This work was presented as a conference paper in the proceedings of Computing in Cardiology 2014 [172]. It is presented here in its published form with permission.

Controlled Activation for Interrogation of the Electrophysiological Substrate

Joshua JE Blauer[1,2,3], Fred Han[1], Ravi Ranjan[1,2], Nassir F Marrouche[1], Rob S MacLeod[1,2,3]

[1] CARMA Center, University of Utah, Salt Lake City, UT, USA
[2] Dept. of Bioengineering, University of Utah, Salt Lake City, UT, USA
[3] SCI Institute, University of Utah, Salt Lake City, UT, USA

Abstract

Ectopic activation and conduction may give rise to arrhythmias when a diseased myocardial substrate exists. Electrophysiological mapping studies that record electrical properties of the heart in sinus rhythm may fail to uncover pro-arrhythmic substrates that are triggered by ectopy. In this study we use simulation and experimental models of clinical, trackable, loop catheters to interrogate regions of myocardium by stimulating and recording with multiple activation patterns. Longitudinal and traverse conduction velocities of the tissue were acquired from the pacing protocol. Artifacts resulting from variable distance between the recording electrodes and pacing site were also detected and removed. This study demonstrates that the mapping of local tissue properties with variable activation patterns is feasible and can expose features of the electrophysiological substrate that can not be recovered during sinus conduction.

1. Introduction

The onset and entrenchment of atrial fibrillation (AF) is strongly associated with remodeling of the atrial myocardial substrate. As a results, as remodeling progresses, ablation strategies based solely on compartmentalization lose efficacy. Consequently, great clinical interest has centered on substrate mapping strategies that can identify proarrhythmic tissues for targeted therapy. In this scenario intracardiac electrogram (EGM) parameters such as voltage amplitude and presence and degree of fractionation are employed as markers of tissue with abnormal conduction properties [1, 2]. However, traditional mapping strategies for AF, whether recorded in sinus rhythm or AF, have neglected the effect of variable activation patterns on EGM parameters of interest.

A key feature of an ectopically triggered beat in the heart is that the resulting activation does not follow the same conduction patterns as a normal sinus beat. Thus, it is even conceivable that sinus conduction may mask the remodeled and pro-arrhythmic substrates that can only be exposed by extrasystole. In this study, we demonstrate the feasibility of mapping electrophysiological substrate features using varied activation patterns by pacing and recording within the same region of heart using a clinical loop catheter.

To demonstrate the feasibility of substrate mapping with controlled activation patterns, we selected conduction velocity (CV) as our initial parameter of interest. Conduction velocity is an important factor in the initiation of re-entry and is affected by substrate remodeling (heterogeneity and slowing) [3]. We explored factors associated with measurement of CV in this manner, and evaluated the information such measurements provide about myocardial substrate.

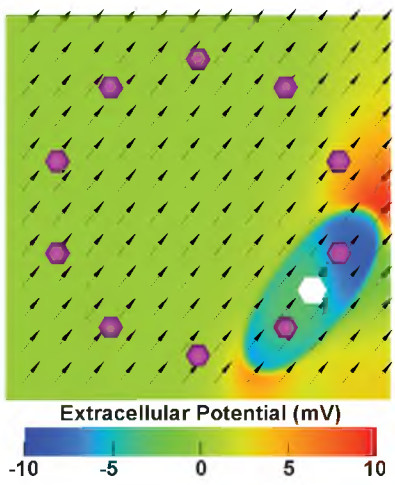

Figure 1. Anisotropic conductivity model of excitation propagation initiated by loop catheter pacing. Extracellular potential of this model is shown 10 ms after the start of pacing from the white hexagonal region. The purple spheres indicate the position of recording electrodes. The black arrows indicate the fiber orientation of the model.

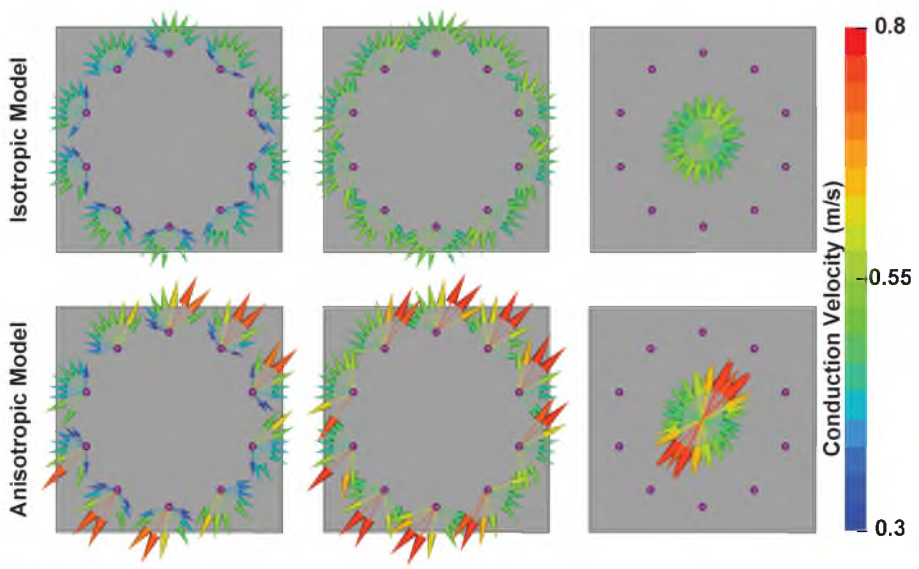

Figure 2. Characterization of local conduction properties with loop catheter. Left Column – Vectors at recording electrodes (purple spheres) point away from pacing site. Length and color correspond to conduction velocity (CV). Center Colum – CV vectors normalized to fixed distance from pacing site. Right Column – Compact representation of regional conduction.

2. Methods

This study incorporated computation modeling and direct recording of electrograms in large mammal experiments. In both cases, a pacing protocol involving stimulation from bipolar electrodes on a 10 pole loop catheter was performed to interrogate the conduction properties of the tissue. Specifically, a depolarization wave was activated by pacing from each pair of adjacent electrodes on the loop catheter, *i.e.*, 1-2, 2-3,...,9-10, to stimulate the region contained by the loop with 9 different activation patterns. EGMs from the non-pacing electrodes were acquired for each activation pattern and from them, activation times were determined from unipolar EGMs by computing the maximum negative slope, or from bipolar EGMs by a nonlinear energy operator [4]. CV was calculated as the distance, from the pacing site to the recording electrode, over the time to activation. CVs and directions from the respective studies were visualized using SCIRun[5].

2.1. Simulation

We implemented a 3-dimensional bidomain simulation of the spread of activation from pacing sites on slab models of atrial tissue with the Cardiac Arrhythmia Research Package (CARP) software [6]. The models were a 26.0×26.0×3.0 mm slab composed of isotropic hexahedral elements with 0.1 mm edge length immersed in 1.0 mm of bath surrounding all slab surfaces. For each activation pattern, we computed complete activation of the slab using the Courtemanche-Ramirez-Nattel cell model of atrial myocyte kinetics [7]. Pseudo-EGMs were generated at each electrode (1 kHz sampling frequency) for the entire 50 ms of simulation. Model conductivities were varied to produce both isotropic and anisotropic models (Figure 1).

2.2. Characterization of Conduction

The relationship between conduction velocity and the distance of the recording electrode from the pacing site was plotted and fit by linear regression. The slope of this regression was then used to normalize all CVs as though they had been recorded 20 mm from the pacing site.

CVs and their respective directions of conduction were compared to the fiber orientation of the computational models. Specifically, the angle between the fiber axis and directions of minimum and maximum conduction velocity were qualitatively assessed for correlation.

2.3. In Vivo Experimentation

The feasibility of pacing and recording from a single loop catheter for assessment of conduction velocities was tested during experimentation on a single canine. A 10 pole trackable circular mapping catheter (Lasso Nav, Biosense Webster, Diamond Bar, CA)was introduced into

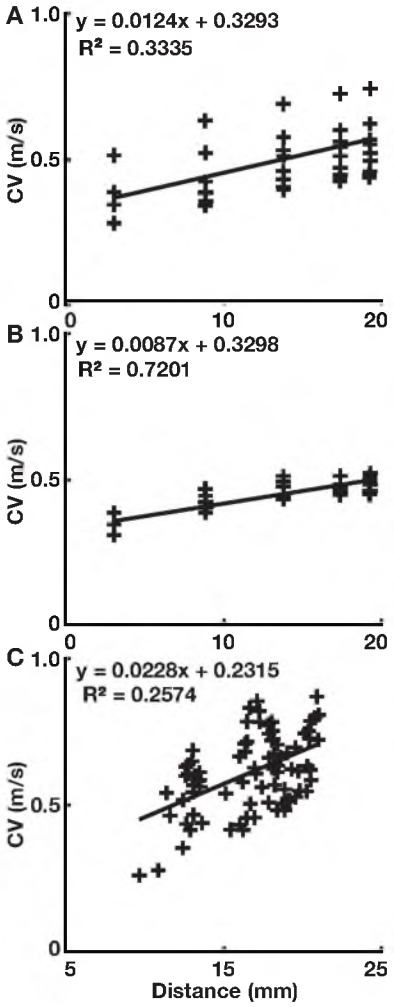

Figure 3. Linear regression of CV versus distance of the recording electrode from the pacing site. The slope for the anisotropic (top), isotropic (center) computational models, and *in vivo* model (bottom) was used to normalize all CV measurements to 20 mm from the pacing site.

the right atrium via percutaneous access of the femoral vein. The electrode array was placed in the high right atrium on the lateral wall and positioned such that clear EGMs were visible on all channels. Pacing was achieved with 600 ms cycle length, 10 mA, and 2 ms pulse width stimulation. Myocardial capture was confirmed then location and electrogram recordings were acquired with a CARTO 3 electrophysiological recording system.

3. Results

3.1. Simulation

Activation times were found for all loop catheter electrodes in the computational model. CV and the direction of conduction were plotted as color-mapped vectors over the model (Figure 2, Left column), where both the color and magnitude correspond to the CV. In both the isotropic and anisotropic models CVs measured from electrodes in proximity to the pacing site showed slower CVs than observed at distant recording electrodes.

3.2. Characterization of Conduction

Figure 3 shows a linear regression of conduction velocity as a function of conduction distance. In the center column of Figure 2, the CVs are normalized to a fixed distance (20 mm) by the slopes of the respective regressions. In the isotropic model (top row of Figure 2) the pre-normalization vectors (leftmost column) demonstrate anisotropy of CVs inconsistent with the spread of activation in the model. The normalized vectors (middle column), in contrast, indicate a uniform spread of activation that is consistent with the model conductivities. Anisotropy is apparent before normalization in the CVs of the anisotropic model, however, the CVs from electrode to electrode are inconsistent, even when oriented in the same direction, due to variable proximity of the recording electrodes to the paced sites. The normalization improves the consistency of CVs among vectors pointing in the same direction (visible in the center and right column of the second row of Figure 2). In the anisotropic model, the direction of highest CV lay along the fiber orientation (see Figure 1). As a compact representation of the conduction properties, the normalized vectors from each recording site were projected onto a point at the center of the loop catheter (Figure 2, right column).

3.3. In Vivo Experimentation

The pacing protocol to stimulate myocardial tissue with multiple activation patterns was successfully carried out at 2 locations in the canine model. Activation times were acquired on a median of 5 (min = 3, max = 6) bipolar channels for each pacing site. The number of interpretable EGMs was limited due to pacing artifact that saturated channels near the pacing site or by channels with no detectable activation signals. Similar to the simulation results, CV also increased with distance of the recording electrode from the pacing site. Figure 4 shows the result of normalizing and plotting CV vectors from measurements from two locations on the RA of the animal.

Figure 4. Compact representation of inter-loop conduction properties of right atrium at two sites. Both sites were interrogated with multiple activation patterns by bipolar pacing between electrodes around the loop. Normalized CV vectors indicate direction and velocity of conduction.

4. Discussion

Our study based on simulation and animal experimentation shows that interrogation of regions of myocardium with multiple activation patterns can elucidate basic conduction properties of that tissue, *e.g.*, CV and anisotropy, in a way that corrects for possible artifacts from the location of the pacing site. The results of such evaluations of the myocardial substrate may be useful to establish patient specific ablation strategies for arrhythmias like AF.

The rate of conduction from a focal pacing site is not constant even in the immediate area around the pacing site, and increases as the depolarization wave propagates outward [3]. Consequently, electrodes in proximity to the pacing site will observe relatively slower conduction than distant electrodes. The normalization by distance we propose allows for inter-electrode comparison of CVs and improves the characterization of local conduction properties. The maximum conduction distance for these models was about 20 mm and the **acceleration** of conduction remained relatively constant over these distances.

Previous studies have reported using loop catheters to record CV from planar wavefronts during sinus conduction [8], however, their results have been indicative of conduction in the longitudinal direction only, *i.e.*, parallel to the predominate fiber orientation. More generally, wavefronts initiated by local pacing have longitudinal and transverse aspects that permit characterization of the anisotropy of conduction. The findings of this study demonstrate how both longitudinal and transverse CVs may be recovered with this protocol.

The primary tenet of this controlled activation pattern mapping protocol is that sinus conduction is inherently stable and not prone to arrhythmogenesis. Thus, electroanatomical substrate mapping of tissue properties during sinus rhythm may fail to identify pro-arrhythmic substrates that are unmasked by ectopy and non-sinus conduction. However, this protocol is a preliminary effort and further considerations, *e.g.*, CV restitution, may be required to robustly identify tissues with arrhythmogenic conduction properties. Robust characterization of the atrial conduction substrate may facilitate better understanding of the mechanisms behind AF initiation and provide better targets for therapeutic interventions.

References

[1] Marchlinski FE, Callans DJ, Gottlieb CD, Zado E. Linear ablation lesions for control of unmappable ventricular tachycardia in patients with ischemic and nonischemic cardiomyopathy. Circulation Mar 2000;101(11):1288–96.

[2] Nademanee K, McKenzie J, Kosar E, Schwab M, Sunsaneewitayakul B, Vasavakul T, Khunnawat C, Ngarmukos T. A new approach for catheter ablation of atrial fibrillation: mapping of the electrophysiologic substrate. J Am Coll Cardiol Jun 2004;43(11):2044–53.

[3] Kléber AG, Rudy Y. Basic mechanisms of cardiac impulse propagation and associated arrhythmias. Physiological Reviews April 2004;84(2):431–488.

[4] Nguyen MP, Schilling C, Dössel O. A new approach for automated location of active segments in intracardiac electrograms. World Congress on Medical Physics 2010;.

[5] SCIRun: A Scientific Computing Problem Solving Environment, Scientific Computing and Imaging Institute (SCI), Download from: http://www.scirun.org.

[6] Vigmond EJ, Hughes M, Plank G, Leon LJ. Computational tools for modeling electrical activity in cardiac tissue. J Electrocardiol 2003;36 Suppl:69–74.

[7] Courtemanche M, Ramirez RJ, Nattel S. Ionic targets for drug therapy and atrial fibrillation-induced electrical remodeling: insights from a mathematical model. Cardiovasc Res May 1999;42(2):477–89.

[8] Weber FM, Schilling C, Seemann G, Luik A, Schmitt C, Lorenz C, Dössel O. Wave-direction and conduction-velocity analysis from intracardiac electrograms–a single-shot technique. IEEE Transactions on Biomedical Engineering October 2010;57(10):2394–2401.

Address for correspondence:

Joshua JE Blauer – blauer@sci.utah.edu

CHAPTER 7

MEAN LAPLACIAN EGM

The Mean Laplacian EGM study is closely related to the previous chapter. As previously discussed, conduction velocity (CV) and the anisotropy of conduction are important indicator of proarrhythmic potential. One pervasive limitation of CV measurement, however, is the necessity of determining activation times for every electrode measuring impulse propagation. This study presents a novel strategy for measuring CV and conduction anisotropy, without the requirement of activation time assignment, by assessing the mean Laplacian electrogram as computed over a clinically feasible electrode array.

7.1 Abstract

The velocity and anisotropy of conduction are important parameters when evaluating pro-arrhythmia risk. However, methods to quantify these parameters in a fast and reliable way are not currently available in the clinical electrophysiology laboratory.

The purpose of this study was to develop a method that allows for fast and reliable estimation of cardiac conduction and anisotropy.

Experimental data were obtained by electrical mapping of isolated guinea pig hearts using a multi-electrode array. Computer simulations were performed in a 3-dimensional bi-domain model incorporating tissue anisotropy. For both experimental and simulated data, conduction velocities (CV) and anisotropy were calculated and compared to distinct features of the mean Laplacian electrogram (MLE) which is a spatial average of Laplacian electrograms.

The QRS region of the MLE showed two distinct peaks. In animal experiments, the temporal locations of the peaks were sensitive to pharmacological manipulation of conduction. Importantly, the first and second peak correlated well with longitudinal (r=-0.52) and transverse (r=-0.82) CV, respectively. The simulations demonstrated that the MLE was dependent on the angle of rotation of the electrode array relative to fiber orientation. Mathematical analysis resulted in an optimized array design without rotational dependence.

The simulations were further used to link the morphology of the optimized MLE to the spatial development of the wavefront, resulting in highly accurate descriptors of longitudinal and transverse CV as well as anisotropy.

We have developed a novel signal, the mean Laplacian electrogram, that enables fast and reliable estimation of conduction velocity and anisotropy.

7.2 Introduction

The conductive properties of cardiac tissue are an important part of the arrhythmogenic substrate. Various diseases, e.g. ischemia, infarction, and fibrosis, alter the conductive properties of the myocardium creating favorable conditions for ectopy and reentry [84, 173, 174]. Specifically, cardiomyopathies that cause a decrease in conduction velocity (CV) favor arrhythmogenesis by decreasing the critical wavelength necessary to foster reentry [53]. However, the CV of an excitation wave moving through myocardial tissue will depend on the alignment of the wave direction and the underlying orientation of the muscle fibers [39, 40, 175]. Conduction along the fiber direction (longitudinal) will progress much faster than conduction across the fibers (transverse). Although this anisotropy is a normal feature of cardiac conduction, abnormal anisotropy may result in conduction block and the generation of reentrant arrhythmias [176, 177, 178].

Changes to the anisotropy of CV have been observed with aging and in conjunction with cardiomyopathies that promote microfibrosis and remodeling of gap junction expression and localization [179, 135]. In the experimental laboratory, multidetector arrays, e.g., plaque electrodes or optical mapping systems, facilitate the creation of activation maps at high temporal and spatial resolution that track the spread of activation through the myocardium [58]. Such approaches allow calculation of longitudinal CV (CVL), transverse CV (CVT), and thus anisotropy [33]. However, these techniques are not easily adaptable for clinical use. Currently, no technique is available that allows for fast and reliable estimation of CV and anisotropy in clinical EP studies. Robust clinical characterization of CV and anisotropy during minimally invasive electrophysiology (EP) studies would be a valuable in characterizing proarrhythmic substrates in patients.

Laplacian electrograms (LEs) are typically computed from a grid of unipolar electrodes (UEs) in an approximation of the second order spatial gradient of the surface potential, which results in a local estimate of current sources or sinks [84]. One consequence of this approximation is that potentials from remote sources are cancelled out and only the local information is preserved, allowing for robust detection of cardiac activation times [59, 32]. From these complementary features, we speculated that a signal based on spatial averaging

of LEs might provide information about the local spread of activation and anisotropy of CV.

Here, we describe a novel method to combine information from a grid of UEs into a single signal, the mean Laplacian electrogram (MLE). We explore the hypothesis that distinct features of the QRS region of the MLE signal correlate directly with local cardiac conduction velocities in the underlying tissue. We also perform computer simulations in order to elucidate the electrophysiological underpinnings of the signal.

7.3 Methods

All animal procedures were carried out according to the Guide for the Care and Use of Laboratory Animals published by the US National Institutes of Health (NIH Publication No. 85-23, revised 1996) and were approved by the Institutional Animal Care and Use Committee of the University of Utah (Protocol No. 09-09008).

7.3.1 Experimental Procedures

The experimental procedure has been described in detail previously [180]. Briefly, Langendorff perfused guinea pig hearts were electrically mapped by recording UEs from the anterior epicardial surface. The recording electrodes were ordered in a regular 8 by 8 grid with 2 mm interelectrode spacing. One of the four central electrodes was used to pace the heart at a cycle length of 300 ms. The signals were high- and low-pass filtered at 0.03 and 500 Hz, respectively, and digitally sampled at 4 kHz. Hearts were perfused with a solution consisting of 1.25 mM CaCl2, 140 mM NaCl, 4.5 mM KCl, 5.5 mM dextrose, 0.7 mM MgCl2, and 10 mM HEPES (pH 7.4). Conduction was slowed by adding either 1 μM flecainide (USP, Rockville, MD) or 30-50 μM carbenoxolone (Sigma-Aldrich, St. Louis, MO) to the perfusate.

7.3.2 Simulation Procedures

All simulations were performed using a 3-dimensional bidomain slab model of electrically anisotropic myocardial tissue created using the SCIRun problem solving environment [181] and implemented using the Cardiac Arrhythmia Research Package (CARP) software [20]. The dimensions of the slab were 26x26x3 mm and it was composed of isotropic hexahedral elements with 0.1 mm edge length immersed in 1.0 mm of bath solution surrounding all slab surfaces. The excitable properties of the model were based on the cellular model of Courtemanche et al. [24] Conduction velocity and anisotropy were varied by scaling the longitudinal and transverse conductivities independently. Extracellular potentials corre-

sponding to UEs were computed at different locations and evaluated at a sampling rate of 1 kHz.

7.3.3 Data Analysis

Conduction velocities (CV) were calculated based on activation time maps as described previously [180]. Local Laplacian potentials were calculated according to Janse et al. [84] with the exception of a unit conversion. Local Laplacian electrograms (LE) were calculated for electrodes for which there were at least 7 surrounding electrodes that could be included in the calculation. This restriction excluded the outermost electrodes in the grid and the pacing electrode, resulting in a total of 35 LEs. The 35 LEs were then averaged to obtain a single signal, which we refer to as the mean Laplacian electrogram (MLE). The temporal locations of the two separate peaks in the QRS region of the experimentally measured MLE were parameterized by the time to peak onset (TP) of each peak. By analogy to activation time assignment in a UE, the TP was defined as the time from the pacing artifact to the maximum negative downstroke of the relevant peak (Fig. 7.1 C).

7.3.4 Statistical Procedures

All statistical calculations were performed using R (v3.0.2; http://www.R-project.org), specifically the functions 'stats' (v3.0.2), 'boot' (v1.3-9), 'smatr' (v3.4-3) and 'simpleboot' (v1.1-3). The correlation between the two measures of conduction (CV vs TP) was quantified using the sample Pearson correlation coefficient (r). Bootstrap distributions of the r-values were generated based on 5000 bootstrap replicates and 95 % confidence intervals (CI, bias-corrected and accelerated) were estimated. A correlation was deemed significant if the CI did not include 0 and was labeled according to the r-value as very strong ($r>0.8$), strong ($0.8>r>0.6$), moderate ($0.6>r>0.4$), or weak ($r<0.4$). For experimental data, differences in means were compared using Welch's t-test. Unless otherwise specified, experimental data are summarized by the mean and standard deviation (SD). For the simulation data, CV estimates obtained with the standard vector based approach were compared directly with the MLE approach by means of a type II linear regression (major axis) analysis [182] and 95 % CIs were estimated for the fitted parameters (slope and intercept). If the CI for the slope included 1, it was taken to indicate no significant bias between variables.

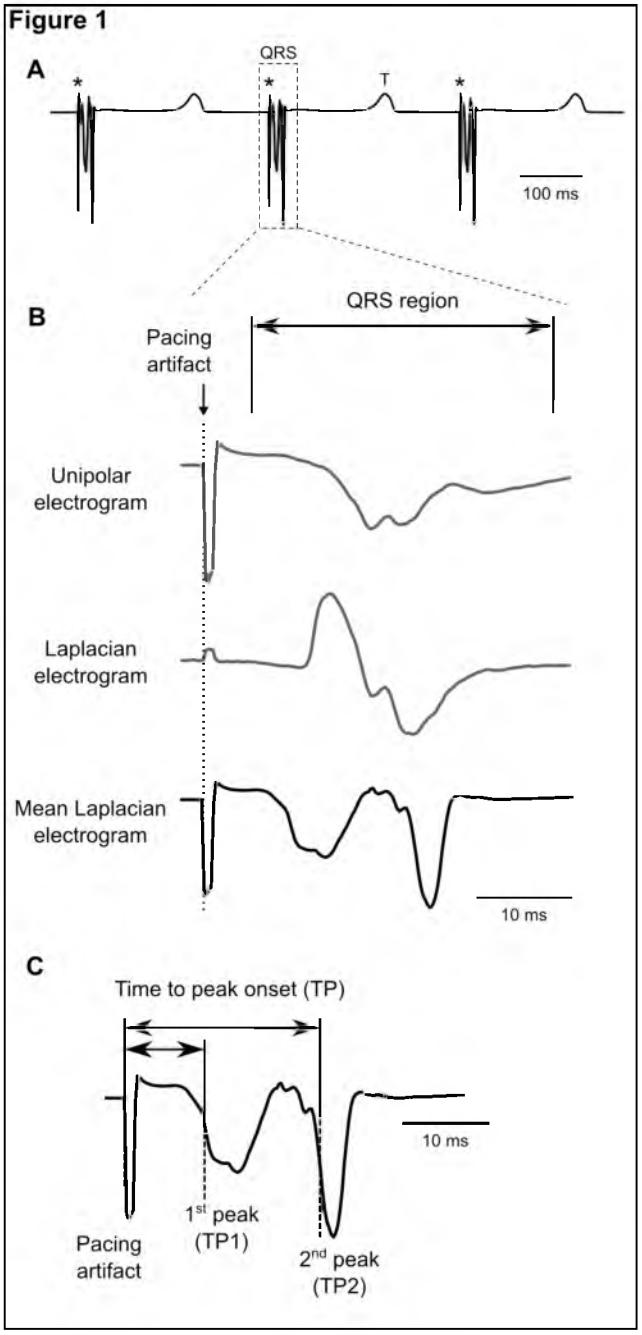

Fig. 7.1. Representative unipolar, Laplacian, and mean Laplacian electrograms. A. Example of an MLE recorded from the ventricles of a guinea pig heart during three paced beats is shown. Asterisks indicate the pacing stimuli. The QRS complex and T-wave of the second beat are labeled. B. Unipolar, Laplacian and Mean Laplacian electrograms corresponding to the boxed region in A are shown on an expanded timescale for comparison. Note the distinct two peaks in the MLE. C. Illustration of the quantification of the temporal location of the peaks in the MLE. See details in the text.

7.4 Results

7.4.1 Quantification of Conductivity from the MLE

The aim of this study was to develop a novel and reliable estimate of conduction velocity and anisotropy in cardiac tissue that can be implemented in the clinical EP laboratory. To this end, we have explored the properties of the mean Laplacian electrogram (MLE), which is the average of multiple LEs. Fig. 7.1 A shows an MLE recorded from a guinea pig heart during epicardial pacing from the center of the recording array. A total of three beats are shown and it can be seen that the MLE displays recognizable deflections similar to a QRS complex and a T-wave. Fig. 7.1 B shows the QRS region of a representative UE, the LE for the same electrode, and the resulting MLE for comparison. The MLE displays two very distinct downward deflections which we refer to as peaks. As a first step to understand the origin of the peaks in this spatially averaged signal, the temporal locations of the peaks were quantified by the time to peak onset (TP) defined as the time from the pacing artifact to the maximum negative downstroke of the peaks. Thus, TP1 and TP2 refer to the temporal locations of the first and second peak, respectively.

As the LE represents local current singularities (positive deflections are current sources and negative deflections are current sinks) in the tissue underneath the recording electrode, we surmised that the peaks in the QRS region of the MLE represented the major current sinks in the tissue under the recording array. This leads to the hypothesis that the peaks are representative of the principal components of current flow in the tissue and thus that their temporal location would be sensitive to changes in CV. To test this hypothesis experimentally, we pharmacologically slowed conduction using flecainide, a sodium channel blocker, or carbenoxolone, a gap junction uncoupler, in guinea pig hearts. Fig. 7.2 A shows activation time isochrone maps from a representative heart recorded under control (top) and flecainide (bottom) conditions. Conduction slowing in the presence of flecainide is evident from the closer spacing of the isochrones compared to the control. The corresponding MLEs are shown in Fig. 7.2 B and, in line with our hypothesis, the temporal locations of both peaks are shifted to the right. Next, we investigated whether the temporal location of the peaks correlated with transverse and longitudinal components of conduction velocity. In Fig. 7.2 C, CVL is plotted against TP1 (open squares) and CVT is plotted against TP2 (filled squares) for control (n=15), flecainide (n=5), and carbenoxolone (n=8) conditions. Importantly, for the correlation analysis to be valid, data values need to be independent so that the analysis presented in Fig. 7.2 C includes only unpaired data. For the same reason, longitudinal and transverse data were analyzed separately. For CVL versus TP1, the correlation coefficient

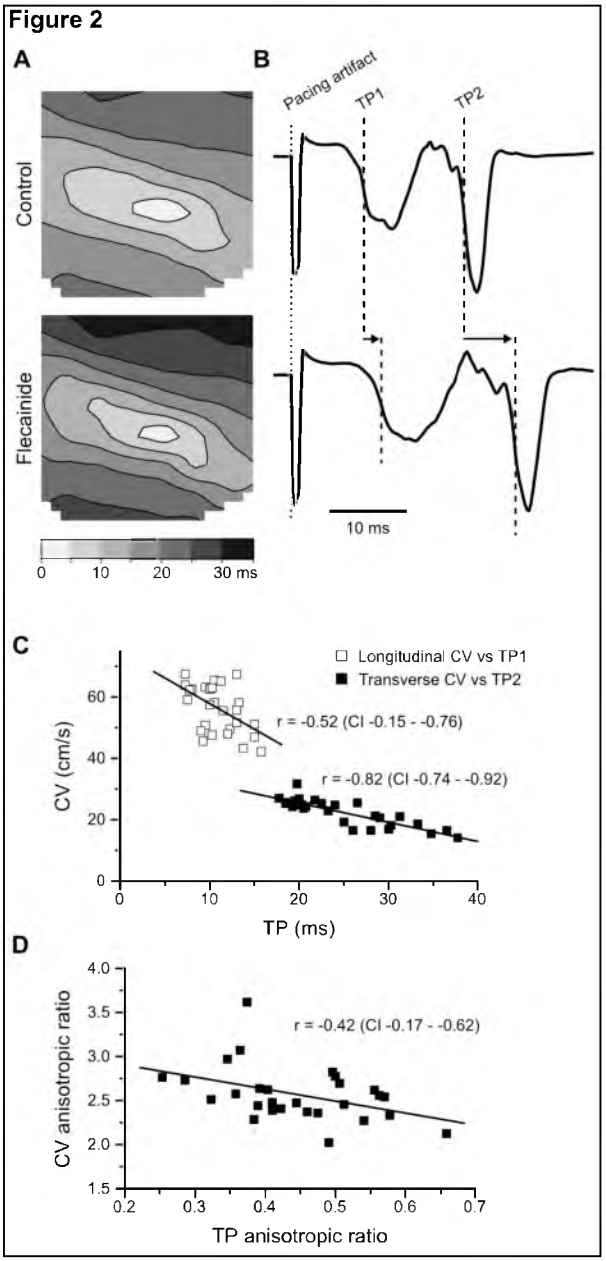

Fig. 7.2. Conduction velocity and anisotropy correlates with features of the MLE. A. Representative activation time isochrone maps recorded from a guinea pig heart under control or flecainide conditions. The closer spacing of isochronal lines with flecainide demonstrates slowing of conduction. B. MLEs corresponding to the maps in A. Note that the temporal location of both peaks are shifted to the right as indicated by the shift in TP1 and TP2. C. Plot of CV calculated from the maps in A versus TP1 (for longitudinal CV) and TP2 (for transverse CV). The corresponding correlation coefficients and CIs are indicated. D. Plot of anisotropy based on CV versus anisotropy based on TP. The corresponding correlation coefficients and CIs are indicated. Please note that the regression lines (ordinary least squares regression) in C and D are for visual purposes only.

was moderate (r=-0.52 (CI -0.15–0.76)) while correlation between CVT and TP2 was strong (r=-0.82 (CI -0.74–0.92)). The relationship between CV anisotropy (ratio of CVL to CVT) and the ratio of TP1 to TP2 is shown in Fig. 7.2 D. Although the correlation was only moderate (r=-0.42 (CI -0.17–0.62)), which is likely due to the variation in TP1 (see Fig. 7.2 C), it is significant and supports the hypothesis that the peaks in the QRS region of the MLE capture the conductive properties of the tissue.

To evaluate whether the MLE-derived measurements could also be used to detect conduction slowing directly, we performed a comparison of experiments in which paired data (n=13) were available for both control and pharmacologically slowed conduction. First, evaluating conduction velocity in the standard way, significant reductions of 21±6% (p<0.001) and 30±10% (p<0.001) were detected for CVL and CVT, respectively (Fig. 7.3) A). These numbers compared well against changes in TP1 and TP2 of 20±18% (p=0.003) and 40±20% (p<0.001), respectively, demonstrating that the MLE can be used to detect conduction slowing (Fig. 7.3 B).

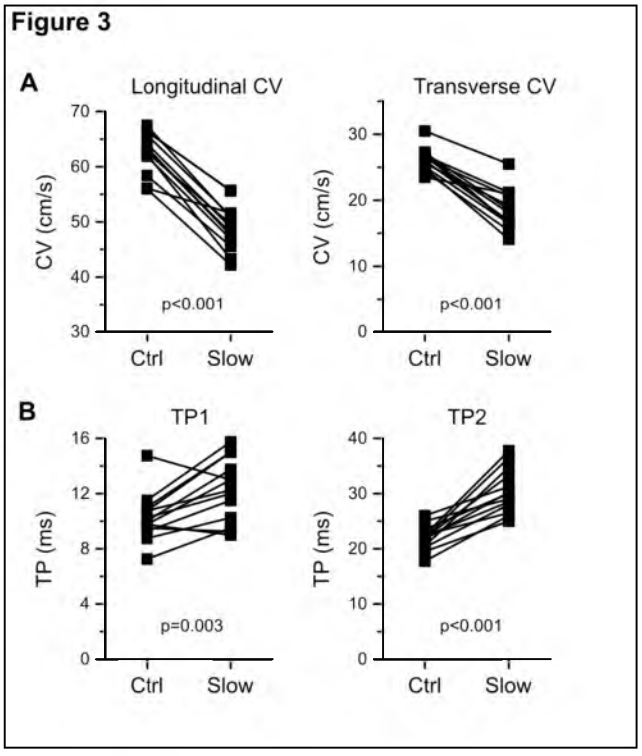

Fig. 7.3. Detection of conduction slowing. The graphs show paired comparisons of longitudinal CV (A), transverse CV (B), TP1 (C), and TP2 (D) under control conditions and under conditions of pharmacologically induced conduction slowing. P-values from Welch's t-test are indicated.

7.4.2 Reproduction of the MLE by Computer Simulations

To better understand the electrophysiological origin and meaning of the MLE, we performed computer simulations of a slab model of cardiac tissue and reconstructed the signals from a 8x8 electrode grid similar to the one used in the ex vivo experiments. Fig. 7.4 A (top panel) shows the activation time map from a representative simulation and corresponding MLE with the electrode array rotated in two different angles with respect to fiber orientation (denoted 0 and 45 degrees, top and bottom panels, respectively). Interestingly, for the 0 degree orientation, which is very close to the orientation of the array in the ex vivo measurements, the reconstructed MLE similarly displayed two distinct peaks. However, rotation of the electrode array resulted in a more complex morphology of the MLE. As the reason for this rotational dependence was not immediately clear, we reexamined the mathematics behind the calculation of the MLE. Since each individual LE is calculated using a 3x3 coefficient stencil (Fig. 7.4 B) the LE can effectively be considered a weighted linear combination of the nine electrodes included in the stencil. Consequently, as the MLE is a simple spatial average of the LEs, it too can be obtained directly from a linear combination of electrodes. Thus, instead of calculating the MLE as the average of 35 LEs, the corresponding mathematical expression can be rearranged and simplified substantially (see Supplemental Material). The resulting expression can be organized in a matrix representation including all electrodes on the grid. The equivalent 8x8 coefficient stencil is shown in Fig. 7.4 C. Interestingly, the stencil revealed that the central electrodes do not contribute to the MLE (coefficients of zero) and that there is a markedly heterogeneous contribution among the electrodes with non-zero coefficients. This unequal contribution of especially the corner electrodes explains the rotational dependence of the MLE based on the 8x8 electrode array.

7.4.3 Development of a Clinically Adaptable Electrode Configuration

For clinically practical purposes, it would be advantageous to derive a circular configuration of the electrodes, as such a design can more easily be implemented in a catheter-based solution than a rectilinear grid.

A potential solution can be obtained by considering only the electrodes with non-zero coefficients in the stencil shown in Fig. 7.4 C. Conceptually, these non-zero electrodes are identical to two squares with electrodes along the sides: An outer square with electrode coefficients of positive sign and an inner square with electrode coefficients of negative sign. Transforming the shape of the squares into two concentric circles results in a design similar to the one shown in Fig. 7.5. In Fig. 7.5 A, the localization and coefficients of two concentric

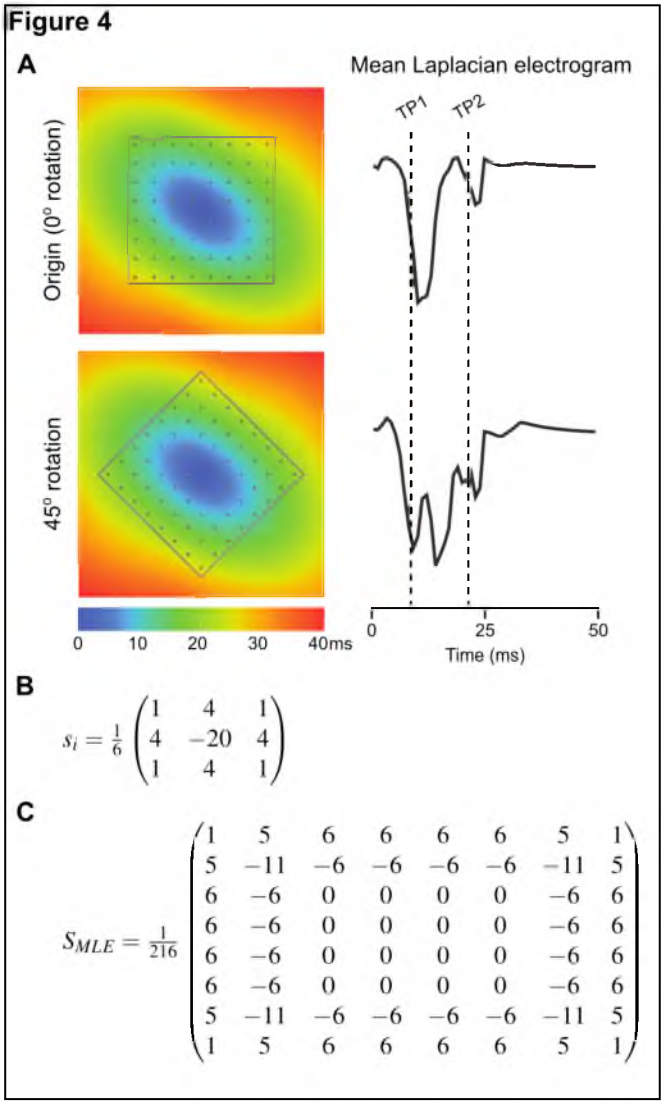

Fig. 7.4. Reconstruction of the MLE in a bidomain simulation of conduction. A. Representative simulated activation time maps and corresponding MLEs with the 8x8 recording array rotated at different angles with respect to fiber orientation. Notice the fractionation of the MLE as the array is rotated 45 degrees. B. Matrix representation of the 3x3 coefficient stencil used to calculate the Laplacian electrogram for each of the 36 central electrodes. C. Matrix representation of the equivalent 8x8 coefficient stencil of the MLE. Notice the resulting cancellation of the central coefficients and the heterogenous weight of the corner coefficients.

rings (dual ring array) with 20 electrodes each are indicated along with the formula for calculating the corresponding MLE. The resulting MLE can be calculated as the sum of the potentials recorded on the outer ring minus the sum of the potentials recorded on the inner ring. Potentially, such an electrode configuration can be implemented on a fixed diameter circular recording catheter, as suggested on the diagram in Fig. 7.5 B.

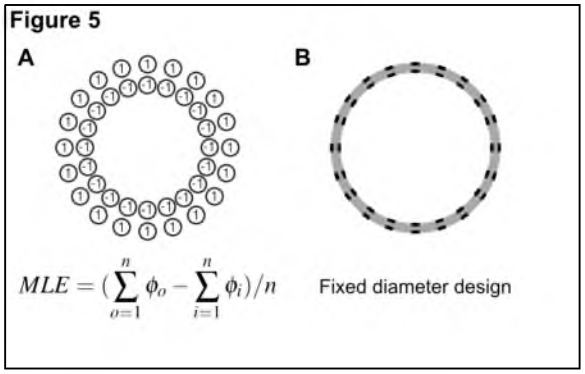

Fig. 7.5. Representation of the revised rotationally independent recording configuration. A. The recording electrodes are organized in two concentric rings of different diameter (Dual Ring Array). Analogous to the coefficient stencil in 4C, the electrodes on the inner ring have a negative coefficients (-1) and the electrodes on the outer ring positive coefficients (+1). The corresponding MLE is calculated by subtracting the sum of the inner electrodes (ϕ_i) from the sum of the outer electrodes (ϕ_o) as indicated by the formula. B. Tentative design of a fixed diameter recording array with the inner and outer electrodes placed on the same ring.

We turned again to simulations to evaluate the dual ring array (DRA) configuration. A representative simulated activation time map is shown in Fig. 7.6 A with the DRA electrode configuration overlaid. The corresponding MLE, calculated using the formula in Fig. 7.5 A, is shown in Fig. 7.6 B. In contrast to the MLE based on the 8x8 grid configuration, the two peaks are much less distinct. A first major peak can easily be recognized. However, a second peak is hard to discern with confidence. This was not entirely unexpected as the distinct peaks were a feature of the heterogeneous coefficients assigned to the electrodes on the 8x8 grid (Fig. 7.4 C). To improve the interpretation of the features of the MLE signal, we compared the temporal evolution of the signal to isopotential maps during the first 25 ms of the simulation. The comparison showed that the location of the major peak (P1) corresponded to the time when the propagating wavefront first passed the outer ring electrodes (Fig. 7.6 C) longitudinally relative to the fiber direction. Similarly, a second peak (P2) coincided with the end of the wavefront passing the last of the inner electrodes (Fig. 7.6 D) transverse to the fiber orientation. As the end of the wavefront passed the last electrodes on the outer ring, the MLE crossed the isoelectric line (Fig. 7.6 E; zero crossing (ZC)) also along the transverse direction. Importantly, knowing the exact location of the wavefront and thus the distance from the pacing site corresponding to these MLE landmarks allowed us to directly estimate longitudinal CV (from P1) and transverse CV (from P2 or ZC).

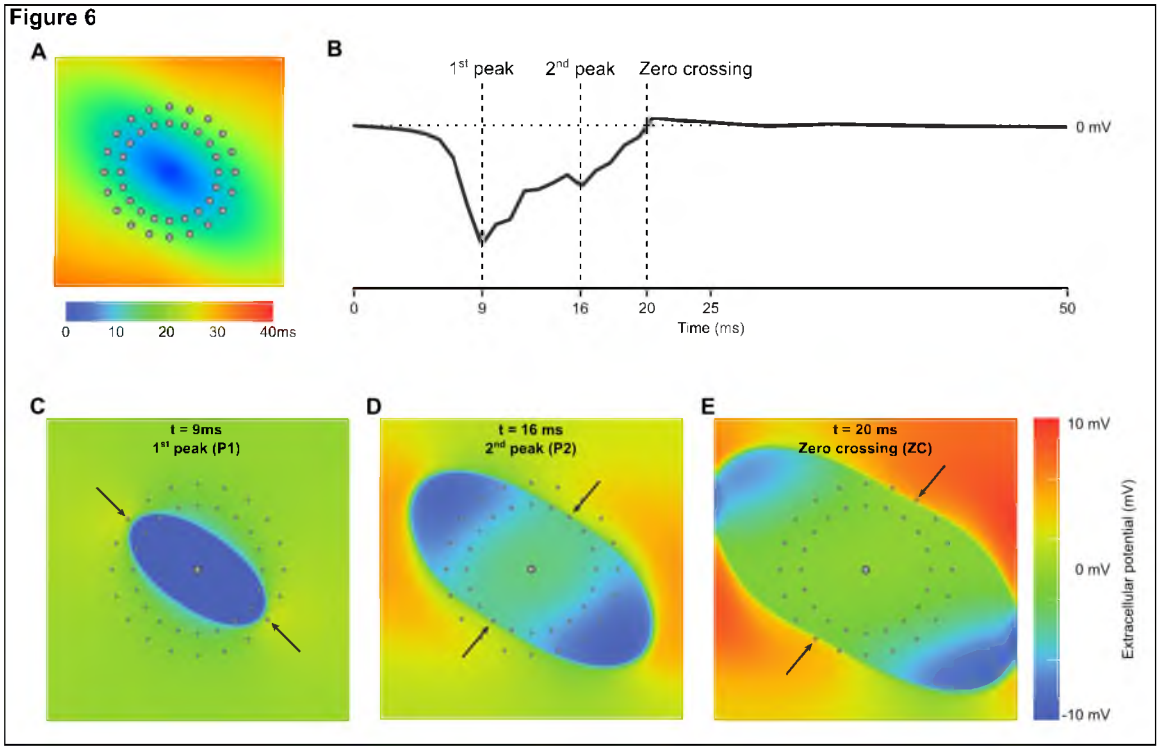

Fig. 7.6. Simulation of MLEs based on the Dual Ring Array. A. Simulated activation time map with the position of the DRA electrodes indicated. B. The MLE corresponding to the map in A. The temporal location of the first and second peaks as well as the zero crossing are indicated. C-E. Isopotential maps corresponding to the time points of the first peak (C), the second peak (D), and the zero crossing (E). The arrows point to the electrodes closest to the propagating wavefront at each time point. The pacing site is indicated as a larger dot in the center of the maps in C-E.

We performed a series of 20 simulations in which longitudinal and transverse conductivities were varied to produce a range of conduction velocities . The simulations were repeated with DRA configurations of 10, 15, and 20 electrodes on each ring as well as at three angles of rotation for each DRA configuration. For CVL versus P1, CVT versus P2, and CVT versus ZC, the correlations were quantified for each angle of each DRA configuration, giving a total of 9 correlation coefficients for each combination. Fig. 7.7 A shows the resulting correlation coefficients. The graph demonstrates that P1 and ZC consistently correlate very strongly with the traditional measures of CV ($r>0.95$ for all correlations) while P2 is less reliable. In general, it was more difficult to identify the second peak in the MLEs while the first peak and the zero crossing were easily identified, which is reflected in the variability of the correlation coefficients. Importantly, for the best performing MLE landmarks, P1 and ZC, the correlations were fairly insensitive to both the number of electrodes and angle of

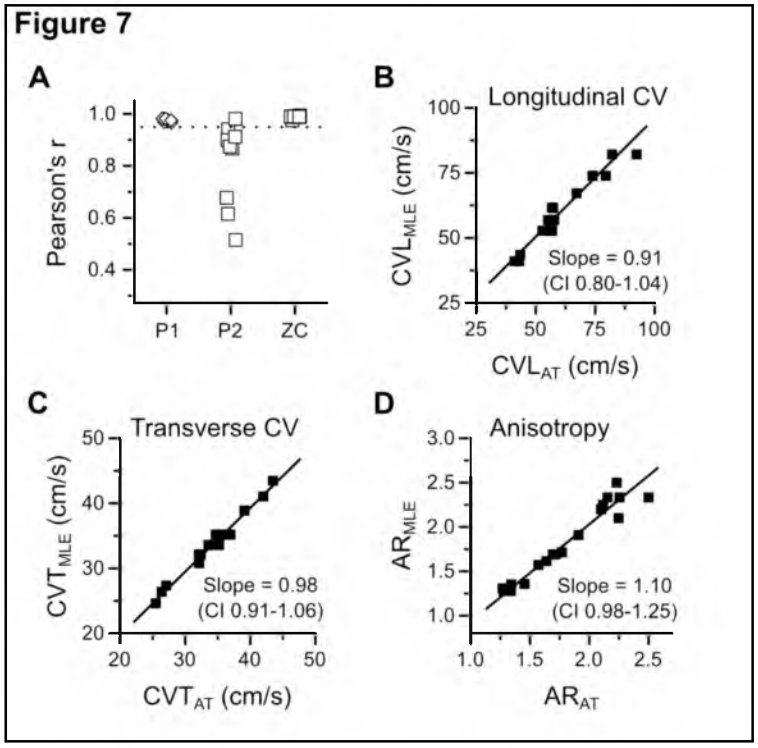

Fig. 7.7. Comparison of CV and anisotropy estimates for the DRA-based MLE and activation time map methods. A. Plot of correlation coefficients describing the relationship between CV calculated from activation time maps versus different features of the MLE. The dotted line indicates r=0.95. P1, first peak. P2, second peak, ZC, zero crossing. B-D. Plots of the relationship between CV calculated from activation time maps versus CV calculated from the MLE for longitudinal CV (B), transverse CV (C), and conduction anisotropy (D). The solid lines represent the type II (major axis) regression line. The line slope and the corresponding CI is indicated for each regression.

rotation. For both P1 and ZC, we further performed a type II linear regression to estimate the potential bias in CV compared to the traditional method of CV estimation (Fig. 7.6 B and C). Compared to CVL and CVT, P1 and ZC respectively showed no significant bias, i.e., the slope of the regression line was not different from 1 (P1, slope=0.91 (CI 0.80-1.04); ZC, slope=0.98 (CI 0.91-1.06)). Additionally, the ratio of P1 to ZC estimates of CV also correlated very strongly with CV anisotropy (ratio of CVL to CVT) (r>0.95 for all correlations) and showed no significant bias (slope=1.10 (CI 0.98-1.25), Fig. 7.6 D). Taken together, the simulation results indicate that the DRA based MLE can be used to robustly estimate longitudinal and transverse conduction velocities and the resulting anisotropy from a single signal without the need of assigning activation times to multiple individual UEs.

7.5 Discussion

The MLE is a novel strategy for extracting fundamental features of action potential propagation in cardiac tissue. The estimation of CVs through pacing and activation mapping has been extensively studied in clinical and experimental settings [39, 33, 41] and one persistent complication is the difficulty of assigning activation times to complex and/or noisy UEs. Using high-resolution plaque electrodes permits the application of signal processing techniques, such as computation of LEs, after which activation times can be more readily determined [59, 32]. However, plaque electrodes and high-resolution mapping both present challenges for routine clinical electrophysiology procedures. Similarly, the measurement of both CVL and CVT to estimate conduction anisotropy is theoretically feasible using current multielectrode mapping systems. However, the addition of multiple channels from which activation times must be determined and then analyzed as a whole to compute CVL and CVT compounds the previous problem making clinical adoption prohibitive, and as yet unrealized. The approach of the MLE permits rapid characterization of electrophysiological features of impulse propagation over the spatial domain of the mapping array.

Our analysis of the experimental data demonstrates that the morphological features of the MLE are closely related to discrete events in the propagation of excitation that occurs following local pacing of the myocardium. The temporal location of the two primary peaks appear to correlate well with longitudinal and transverse components of conduction. The computer simulations were able to reproduce our experimental data and added the finding that the MLE morphology was heavily dependent on the rotation of recording array with respect to fiber direction. By serendipity, this aspect was not identified in the experimental data, very likely due to a fairly robust placement of the array in all of the experiments. We were able to trace the source of the rotational dependence mathematically to the heterogeneous weighing of the contribution of the electrodes located in the corners of the array. Furthermore, through the simulations, we were able to develop a dual-ring electrode configuration and identify the optimal hallmarks of the MLE to extract measures of conduction. The dual-ring configuration should make the general approach more readily adaptable for clinical use.

The study clearly demonstrates the value of computation models for explicating complex electrophysiological phenomena and their relationship to recording arrays. The computational models utilized in this study clarified the interactions between wavefront propagation and the geometry of the plaque array that produce the characteristic features of the MLE. This ability to visualize and rapidly permute through many possible scenarios was critical

to the discovery of the rotational sensitivity of the plaque array, and development of the rotationally invariant DRA. Furthermore, experimental evaluation of the effect of a range of conductivities on the morphological features of the MLE would have been prohibitive. Given the ready availability of simulations software, the field is approaching a point when investigation of measured electrophysiological phenomena is incomplete without validation based on robust computation models.

At its most basic level, the MLE can be interpreted as a summation of electrograms acquired from an array of bipolar electrodes oriented radially around a pacing site (Fig. 7.5). The relatively simple array geometry and signal processing of the MLE makes it a promising tool for the characterization of cardiac conduction properties, i.e., CVs and anisotropy of conduction. The conversion of the MLE sampling array from a plaque array to the DRA configuration substantially improves the feasibility of deploying an MLE sensing array in a percutaneous electrophysiology study.

Clinical deployment of the MLE in patients with atrial fibrillation (AF) could facilitate assessment of substrate remodeling and its impact on impulse conduction in the atria. The AF atria are subjected to many remodeling processes that have been shown to impact impulse propagation [5]. Many of these remodeling processes appear to differentially impact the transverse aspect of myocytes to a greater extent than the longitudinal aspect [30]. In light of these observations, robust examination of the anisotropy of conduction could provide valuable insight into the state of AF induced remodeling. Of note, the experimental findings of this study are based on ventricular recordings from guinea pig ventricles. However, because of the potential for clinical application of this approach in the atria, the simulations were run using an atrial myocyte model and a tissue slab with thickness most akin to atrial tissue (3 mm). In spite of this difference, the basic morphology of the MLE was conserved between the experimental and simulation studies.

7.6 Conclusion

We have developed a method in which a novel single electrical signal, the mean Laplacian electrogram (MLE), constructed from a number of simultaneously recorded unipolar electrograms, can be used to quantify both velocity and anisotropy of conduction without the need to assign activation times to individual electrograms and without explicit knowledge of the spatial propagation of the wavefront. In consideration of the clinical feasibility, the simplicity of the signal analysis, and the value of robust characterization of conduction properties, the MLE is a promising addition to current substrate mapping strategies.

7.7 Acknowledgements

This work was supported by the Nora Eccles Treadwell Foundation (S.P.) and the Carlsberg Foundation (A.P.L.). Support for the development of SCIRun came from the National Institutes of Health (NIH) grant number P41GM103545.

7.8 Supplementary Material

The idea of the electrode array is to obtain an approximation to the surface Laplacian of the potential distribution, ϕ. Mathematically, this is represented for the continuous function ϕ(x,y) as

$$\nabla^2\phi = \frac{\partial^2\phi}{\partial x^2} + \frac{\partial^2\phi}{\partial y^2}. \tag{7.1}$$

From Taylor series, it is possible to determine discrete approximations to the surface Laplacian as the 3 x 3 stencil

$$S = \frac{1}{6}\begin{pmatrix} 1 & 4 & 1 \\ 4 & -20 & 4 \\ 1 & 4 & 1 \end{pmatrix}. \tag{7.2}$$

One obtains an approximation to the surface Laplacian by considering a 3 x 3 array of measured potential $\phi_{i,j}$

$$\Phi(i,j) = \begin{pmatrix} \phi_{i-1,j-1} & \phi_{i,j-1} & \phi_{i+1,j-1} \\ \phi_{i-1,j} & \phi_{i,j} & \phi_{i+1,j} \\ \phi_{i-1,j+1} & \phi_{i,j+1} & \phi_{i+1,j+1} \end{pmatrix}. \tag{7.3}$$

The approximation to the surface Laplacian is obtained from the Frobenius product of two matrices S and $\Phi(i,j)$, i.e., the Laplacian at the node (i,j) denoted L_{ij} is given by

$$L_{ij} = S : \Phi(i,j) \tag{7.4}$$

where the operator ':' represents the Frobenius product. In long hand, we have

$$L_{ij} = \frac{1}{6}(\phi_{i-1,j-1}+4\phi_{i,j-1}+\phi_{i+1,j-1}+4\phi_{i-1,j}-20\phi_{i,j}+4\phi_{i+1,j}+\phi_{i-1,j+1}+4\phi_{i,j+1}+\phi_{i+1,j+1}). \tag{7.5}$$

Finally, the MLE is determined as the average over all possible Lapalcian L_{ij}. That is, for an n x n potential electrode array,

$$MLE = \frac{1}{N} \sum_{i=2}^{n-1} \sum_{j=2}^{n-1} L_{ij} \tag{7.6}$$

for the Laplacians L_{ij} which exist and N is the total number of Laplacians which do exist. For example, for the 8 x 8 array currently in use, assuming that all 63 recording electrodes perform correctly, then 35 Laplacians can be obtained.

Hence for the 8 x 8 electrode array considered here, the coefficient stencil is given by

$$S_{MLE} = \frac{1}{216} \begin{pmatrix} 1 & 5 & 6 & 6 & 6 & 6 & 5 & 1 \\ 5 & -11 & -6 & -6 & -6 & -6 & -11 & 5 \\ 6 & -6 & 0 & 0 & 0 & 0 & -6 & 6 \\ 6 & -6 & 0 & 0 & 0 & 0 & -6 & 6 \\ 6 & -6 & 0 & 0 & 0 & 0 & -6 & 6 \\ 6 & -6 & 0 & 0 & 0 & 0 & -6 & 6 \\ 5 & -11 & -6 & -6 & -6 & -6 & -11 & 5 \\ 1 & 5 & 6 & 6 & 6 & 6 & 5 & 1 \end{pmatrix}. \tag{7.7}$$

To see why this is reasonable from a mathematical point of view, consider a continuous variation in potential, ϕ, over some two-dimensional domain Ω. The surface Laplacian is then

$$l(x, y, t) = \nabla^2 \phi = \frac{\partial^2 \phi}{\partial x^2} + \frac{\partial^2 \phi}{\partial y^2}. \tag{7.8}$$

Averaging the Laplacian over the region Ω is again equivalent to taking the integral over the region, hence

$$L(t) = \iint_{\Omega} l(x, y, t) dx dy = \iint_{\Omega} \nabla^2 \phi d\Omega = \oint_{\partial\Omega} \nabla \phi \cdot \mathbf{n} d\omega \tag{7.9}$$

which follows from the divergence theorem. Here $\partial\Omega$ represents the boundary of the region Ω, $\mathbf{n}$ is the outward point normal to Ω, and $d\omega$ represents a line element along the boundary $\partial\Omega$. Essentially, the average Laplacian can be obtained from a knowledge of the normal derivatives of the potentials around the boundary of the domain, regardless of the shape of the domain.

CHAPTER 8

CONCLUSIONS AND FUTURE WORK

Substrate mapping can identify arrhythmogenic tissues in which the morphology of electrograms indicates the condition of the local myocardium. Detection and localization of proarrhythmic features can then guide appropriate treatment. However, the current tools and metrics used for clinical substrate mapping are often inadequate to control critical system parameters and identify direct indicators of diseased tissues. Bidomain simulations can help address these limitations through evaluation of substrate mapping techniques. The implementation of such simulations forms the unifying premise of this dissertation. Through the three primary aims of this work, we have demonstrated the ability of multiscale computation models to: 1) assess factors that influence the performance of substrate mapping, 2) guide the development of novel substrate mapping strategies, and 3) explicate poorly understood phenomena in electrophysiological signals. In addition to these contributions, the use of such models provides direct benefits in terms of mitigated cost, reduced use of animal studies, and decreased time required for hypothesis testing.

8.1 Aim 1: Near-Field Electrograms

In the first study, bidomain simulations of a voltage mapping study were performed to assess geometric factors that influence the morphology of EGMs, and consequently the ability to detect diseased tissue based on a voltage threshold. This study confirmed the common assumption that improper electrode alignment with the wavefront of the activation impulse could produce low voltage EGMs. More interestingly, however, was the finding that particular electrode orientations, with respect to the tissue, were important to the performance of voltage mapping. Specifically, near-perpendicular orientation of the bipolar electrodes, relative to the cardiac tissue, demonstrated both insensitivity to the direction of the activation impulse and enhanced sensitivity and specificity for the detection of abnormal myocardium. This finding has significant implications for clinical operators who utilize voltage mapping strategies, but who lack tools capable of controlling this parameter. The

findings of this study are also likely to be relevant for other substrate mapping strategies that rely on the use of bipolar EGMs.

The improved accuracy for voltage mapping provided by perpendicular orientations can be interpreted in terms of EGM referencing. In current clinical cardiac electrophysiology, EGMs are acquired with one of two possible referencing schemes. The first, and most commonly used, is a bipolar reference. The other is a unipolar reference with Wilson's central terminal, or another distant electrode, acting as the anodal reference (see Section 2.4.2). As previously discussed, the concept of a unipolar EGM is a misnomer, and thus bipolar and unipolar references simply, if insufficiently, describe a spectrum in which the anodal electrode is either close to or relatively removed from the exploratory electrode. In the case of the perpendicularly oriented bipolar electrode pair, we have adopted the term "near-field unipolar EGM," or simply "near-field EGM," to describe the acquisition of an EGM with the distal electrode touching the tissue, and the reference electrode in the blood pool no closer to any cardiac tissue than the tissue being probed by the exploratory electrode. The beneficial properties of near-field EGMs include features typically associated with bipolar EGMs, i.e., common mode rejection of far-field signals and unipolar EGMs, i.e., consistent EGM morphology and insensitivity to the direction of wavefront propagation. These findings make near-field EGMs an attractive option for clinical electrophysiology, and in particular for substrate mapping procedures. However, immediate application of the near-field EGMs is prevented by persistent limitations in the control and guidance of the electrophysiological mapping catheter. Specifically, navigating a catheter to locations of interest throughout the heart is already a challenge that requires substantial training. Requiring the catheter to reach all locations at a perpendicular orientation may be infeasible for many locations in the heart. Moreover, robust confirmation of proper alignment is limited with current catheter navigation systems.

In response to the limited ability to acquire near-field EGMs with current clinical electrophysiological systems, we have conceived a novel diagnostic recording catheter that inherently acquires near-field EGMs wherever an exploratory electrode comes in contact with the myocardium. This catheter-based electrode array is similar to diagnostic mini-basket catheters in current clinical use. However, a simple modification to the basket array, in which a reference electrode is placed at the center of the basket, allows all EGMs to be acquired with near-field EGM referencing. With this design, the basket forms a protective barrier that prevents the central reference electrode from coming in contact with the cardiac tissue. Additionally, because the central electrode is equidistant from

the exploratory electrodes located on the splines of the basket, the reference is consistent for all channels. Patent protection for the perspective catheter concept has been initiated, and negotiations have begun with an industrial partner to develop a prototype of the device (Fig. 8.1).

Development of an electrode array in which the reference anode remains situated in the blood pool is a straightforward design specification. Validation of near-field electrograms as superior measurements for characterization of the cardiac electrophysiological substrate, however, requires careful consideration. Specifically, direct measure of a known cardiac substrate, i.e., scar tissue, must be acquired using standard clinical systems as well as the near-field electrogram recording system. Various experimental and clinical systems are available to create mappable substrates, including radio-frequency ablation or intracardiac injection of alcohol. Following the creation of scar tissue, an MRI can be used to characterize the location and extent of scaring. Finally, direct measurement of electrograms from the surface of the scarred tissue using typical clinical systems for comparison to near-field electrogram measurements would allow for comparison of the relative and absolute mapping accuracy.

Fig. 8.1. Concept for diagnostic catheter capable of acquiring near-field EGMs. This basket-type catheter contains a central reference electrode surrounded by splines containing multiple exploratory electrodes, which allows for clinical mapping with near-field EGMs.

8.2 Aim 2: Conduction Velocity Mapping

The second study provides an example of how multiscale modeling of cardiac electrophysiology can guide the development of novel mapping strategies. In this study, a bidomain model of atrial myocardium was implemented in which an action potential could be stimulated at multiple points around a representation of a clinical loop catheter. The intent of this pacing protocol was to stimulate the tissue with multiple activation patterns to elucidate the underlying properties of substrate, e.g., the fiber orientation or presence of conduction slowing. The primary challenge with such an approach is based on the acceleration of the action potential impulse as it propagates away from the pacing site due to changes in the wavefront curvature. Because the electrodes of the loop catheter are at variable distances from the pacing site, electrodes at greater distances detect higher conduction velocities (CV) than do closer electrodes. However, because the bidomain model has sufficient fidelity to capture this characteristic, we were able to determine, over the small distances encompassed by the loop array, that the change in conduction velocity with distance could be modeled and corrected for with a linear function. This finding was supported by measurements acquired from an experimental model and demonstrates the utility of multiscale models of cardiac electrophysiology.

Having shown that CVs can be measured from a loop catheter in the experimental model, and can be normalized according to the distance of the recording electrode from the pacing site, the next step for this project is to develop methods for reconstructing the local conduction properties and assessing how they vary depending on the activation pattern. In Chapter 6, we demonstrated that the normalized vectors can be projected to the center of the loop array. The collection of projected vectors contains a great deal of information about the local conduction properties, but it is difficult to interpret relevant information from this representation, i.e., longitudinal and transverse conduction velocity, or conduction anisotropy. One possible approach for simplifying this information is a dimensionality reduction-based approach known as singular value decomposition (SVD). Similar to other decomposition strategies, e.g., eigenvalue, or Fourier decomposition, an SVD of the vector data identifies the principal axes of variation in the data. This approach would theoretically identify, as the first principal axis, the direction in which action potential impulses conduct the fastest, i.e., the direction of longitudinal CV (Fig. 8.2). The next component, or axis, would then be perpendicular to the first axis and would provide an approximation of the transverse CV. This novel approach for evaluating cardiac conduction properties could be repeated throughout the heart and is feasible with current catheter technology.

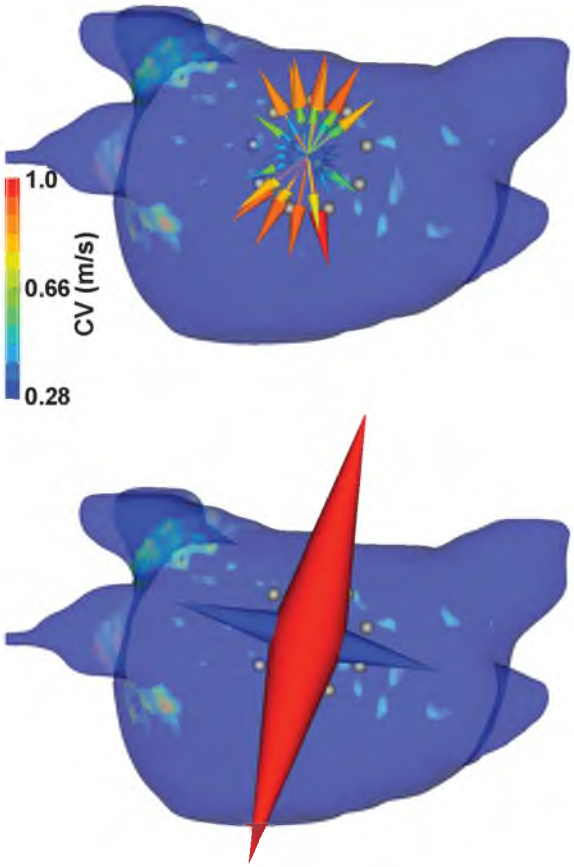

Fig. 8.2. Singular value decomposition (SVD) of conduction velocity vectors. Top - Conduction velocity (CV) vectors acquired with multiple activation pattern mapping protocol that have been normalized for distance from the pacing site and projected to the center of the loop array. Bottom - The first two principal axes recovered from SVD of CV vectors indicating the direction of longitudinal and transverse conduction (red and blue cones, respectively.)

8.3 Aim 3: Mean Laplacian Electrogram

The third study is a prime illustration of the ability of cardiac electrophysiological simulations to help clarify the mechanisms that govern the genesis of electrical signals from the heart. In the case of the mean Laplacian electrogram (MLE), it was readily apparent that the observed peaks were somehow related to the spread of activation across the recording array. However, it was not until the mathematical basis of the MLE acquisition was clarified and simulations were run that the morphology of the MLE could be thoroughly explained. Additionally, it was through permutation of model parameters that the impact of the plaque array's rotational asymmetry was established. With these pieces in place, it was possible to conceptualize the dual ring array (DRA) for simplified and clinically feasible sampling of the MLE.

The MLE is an attractive option for CV measurement, compared to the approach in the second study, because it obviates the need to identify activation times for multiple channels. Of course, the primary limitation of this approach is that no current clinical electrode arrays quite meet the DRA specifications. Future work on this project will be focused on extending the mathematics that allow acquisition of the MLE from a DRA array to an array in current clinical use.

The findings of these studies have shown the ability of multiscale modeling to sufficiently replicate cardiac electrophysiological processes in order to examine, interpret, and refine substrate mapping procedures. Consequently, not only do the findings from the individual aims contribute to the development of novel strategies for substate mapping, but the work as a whole provides a compelling argument for the use of simulations in the development and validation of electrophysiological diagnostics. Interestingly, the workflow of hypothesis testing, experimentation, and validation was found to be flexible in terms of whether simulation or experimentation came first. In the first two studies, computational models were used to develop and test new mapping strategies that were then tested in experimental animal studies. On the other hand, the MLE signal was first examined with experimental data and then validated with computational studies that elucidated the mechanism that drives the genesis of the MLE signal. Naturally, risks are associated with simulation studies, e.g., oversimplification of complex physiological processes or overfitting when a model lacks sufficient degrees of freedom. However, with this approach, in which experimental and computational studies are closely coupled and carried out in parallel, it may be possible to avoid many of these pitfalls. With the continued development of electrophysiological modeling systems, and the increasing complexity of signal processing applied to cardiac EGMs, we may well have reached a stage where characterization of electrical signals from the heart is incomplete until robust computational models can both replicate the behavior and explore factors, such as orientation with respect to the tissue (Aim 1) or rotational asymmetry (Aim 3), that may influence interpretation of the signals.

REFERENCES

[1] M. A. Allessie, J. Ausma, and U. Schotten, "Electrical, contractile and structural remodeling during atrial fibrillation." *Cardiovascular Research*, vol. 54, no. 2, pp. 230–246, May 2002.

[2] S. Nattel, B. Burstein, and D. Dobrev, "Atrial remodeling and atrial fibrillation: mechanisms and implications," *Circulation: Arrhythmia and Electrophysiology*, vol. 1, no. 1, pp. 62–73, Apr. 2008.

[3] W. G. Stevenson, J. N. Weiss, I. Wiener, and K. Nademanee, "Slow conduction in the infarct scar: relevance to the occurrence, detection, and ablation of ventricular reentry circuits resulting from myocardial infarction." *American heart journal*, vol. 117, no. 2, pp. 452–467, Feb. 1989.

[4] N. M. S. de Groot, R. P. M. Houben, J. L. Smeets, E. Boersma, U. Schotten, M. J. Schalij, H. Crijns, and M. A. Allessie, "Electropathological substrate of longstanding persistent atrial fibrillation patients With structural heart disease: epicardial breakthrough," *Circulation*, vol. 122, no. 17, pp. 1674–1682, Oct. 2010.

[5] M. A. Allessie, N. M. S. de Groot, R. P. M. Houben, U. Schotten, E. Boersma, J. L. Smeets, and H. J. Crijns, "Electropathological substrate of long-standing persistent atrial fibrillation in patients with structural heart disease: longitudinal dissociation," *Circulation: Arrhythmia and Electrophysiology*, vol. 3, no. 6, pp. 606–615, Dec. 2010.

[6] E. M. Aliot, W. G. Stevenson, J. M. Almendral-Garrote, F. Bogun, C. H. Calkins, E. Delacretaz, P. D. Bella, G. Hindricks, P. Jaïs, M. E. Josephson, J. Kautzner, G. N. Kay, K.-H. Kuck, B. B. Lerman, F. Marchlinski, V. Reddy, M.-J. Schalij, R. Schilling, K. Soejima, D. Wilber, European Heart Rhythm Association, European Society of Cardiology, and Heart Rhythm Society, "EHRA/HRS Expert consensus on catheter ablation of ventricular arrhythmias: developed in a partnership with the European Heart Rhythm Association (EHRA), a registered branch of the European Society of Cardiology (ESC), and the Heart Rhythm Society (HRS); in collaboration with the American College of Cardiology (ACC) and the American Heart Association (AHA)." *Europace*, vol. 11, no. 6, pp. 771–817, Jun. 2009.

[7] H. Calkins, K.-H. Kuck, R. Cappato, J. Brugada, A. J. Camm, S.-A. Chen, H. J. G. Crijns, R. J. Damiano, D. W. Davies, J. DiMarco, J. Edgerton, K. Ellenbogen, M. D. Ezekowitz, D. E. Haines, M. Haïssaguerre, G. Hindricks, Y. Iesaka, W. Jackman, J. Jalife, P. Jaïs, J. Kalman, D. Keane, Y.-H. Kim, P. Kirchhof, G. Klein, H. Kottkamp, K. Kumagai, B. D. Lindsay, M. Mansour, F. E. Marchlinski, P. M. McCarthy, J. L. Mont, F. Morady, K. Nademanee, H. Nakagawa, A. Natale, S. Nattel, D. L. Packer, C. Pappone, E. Prystowsky, A. Raviele, V. Reddy, J. N. Ruskin, R. J. Shemin, H.-M. Tsao, and D. Wilber, "2012 HRS/EHRA/ECAS Expert consensus statement on catheter and surgical ablation of atrial fibrillation: recommendations

for patient selection, procedural techniques, patient management and follow-up, definitions, endpoints, and research trial design," *Heart Rhythm*, vol. 9, no. 4, pp. 632–696.e21, Jan. 2012.

[8] R. J. Kim, D. S. Fieno, T. B. Parrish, K. Harris, E. L. Chen, O. Simonetti, J. Bundy, J. P. Finn, F. J. Klocke, and R. M. Judd, "Relationship of mri delayed contrast enhancement to irreversible injury, infarct age, and contractile function," *Circulation*, vol. 100, no. 19, pp. 1992–2002, Nov 1999.

[9] C. J. McGann, E. G. Kholmovski, R. S. Oakes, J. J. Blauer, M. Daccarett, N. Segerson, K. J. Airey, N. Akoum, E. Fish, T. J. Badger *et al.*, "New magnetic resonance imaging-based method for defining the extent of left atrial wall injury after the ablation of atrial fibrillation," *Journal of the American College of Cardiology*, vol. 52, no. 15, pp. 1263–1271, 2008.

[10] R. S. Oakes, T. J. Badger, E. G. Kholmovski, N. Akoum, N. S. Burgon, E. N. Fish, J. J. E. Blauer, S. N. Rao, E. V. R. DiBella, N. M. Segerson, M. Daccarett, J. Windfelder, C. J. McGann, D. Parker, R. S. MacLeod, and N. F. Marrouche, "Detection and quantification of left atrial structural remodeling with delayed-enhancement magnetic resonance imaging in patients with atrial fibrillation," *Circulation*, vol. 119, no. 13, pp. 1758–67, Apr 2009.

[11] C. McGann, N. Akoum, A. Patel, E. Kholmovski, P. Revelo, K. Damal, B. Wilson, J. Cates, A. Harrison, R. Ranjan, N. S. Burgon, T. Greene, D. Kim, E. V. R. DiBella, D. Parker, R. S. MacLeod, and N. F. Marrouche, "Atrial fibrillation ablation outcome is predicted by left atrial remodeling on MRI." *Circulation: Arrhythmia and Electrophysiology*, vol. 7, no. 1, pp. 23–30, Feb. 2014.

[12] D. M. Cassidy, J. A. Vassallo, J. M. Miller, D. S. Poll, A. E. Buxton, F. E. Marchlinski, and M. E. Josephson, "Endocardial catheter mapping in patients in sinus rhythm: relationship to underlying heart disease and ventricular arrhythmias." *Circulation*, vol. 73, no. 4, pp. 645–652, Apr. 1986.

[13] F. E. Marchlinski, D. J. Callans, C. D. Gottlieb, and E. Zado, "Linear ablation lesions for control of unmappable ventricular tachycardia in patients with ischemic and nonischemic cardiomyopathy," *Circulation*, vol. 101, no. 11, pp. 1288–96, Mar 2000.

[14] P. Sanders, J. B. Morton, N. C. Davidson, S. J. Spence, J. K. Vohra, P. B. Sparks, and J. M. Kalman, "Electrical remodeling of the atria in congestive heart failure: electrophysiological and electroanatomic mapping in humans." *Circulation*, vol. 108, no. 12, pp. 1461–1468, Sep. 2003.

[15] A. Verma, O. M. Wazni, N. F. Marrouche, D. O. Martin, F. Kilicaslan, S. Minor, R. A. Schweikert, W. Saliba, J. Cummings, J. D. Burkhardt, M. Bhargava, W. A. Belden, A. Abdul-Karim, and A. Natale, "Pre-existent left atrial scarring in patients undergoing pulmonary vein antrum isolation: an independent predictor of procedural failure," *J Am Coll Cardiol*, vol. 45, no. 2, pp. 285–92, Jan 2005.

[16] U. F. National Institutes of Health, National Department of Energy and N. S. F. Drug Administration, "Par-11-203: Predictive multiscale models for biomedical, biological, behavioral, environmental and clinical research (interagency u01)," Apr. 2011.

[17] P. Sanders, O. Berenfeld, M. Hocini, P. Jaïs, R. Vaidyanathan, L.-F. Hsu, S. Garrigue, Y. Takahashi, M. Rotter, F. Sacher, C. Scavée, R. Ploutz-Snyder, J. Jalife, and M. Haïssaguerre, "Spectral analysis identifies sites of high-frequency activity maintaining atrial fibrillation in humans," *Circulation*, vol. 112, no. 6, pp. 789–97, Aug 2005.

[18] O. Schmitt, "Biological information processing using the concept of interpenetrating domains," in *Information Processing in the Nervous System*, K. Leibovic, Ed. New York: Springer Verlag, 1969.

[19] L. Tung, "A bidomain model for describing ischemic myocardial DC potentials," Ph.D. dissertation, M.I.T., 1978.

[20] E. J. Vigmond, M. Hughes, G. Plank, and L. J. Leon, "Computational tools for modeling electrical activity in cardiac tissue," *J Electrocardiol*, vol. 36 Suppl, pp. 69–74, 2003.

[21] F. M. Weber, C. Schilling, G. Seemann, A. Luik, C. Schmitt, C. Lorenz, and O. Dössel, "Wave-direction and conduction-velocity analysis from intracardiac electrograms–a single-shot technique." *IEEE Transactions on Biomedical Engineering*, vol. 57, no. 10, pp. 2394–2401, Oct. 2010.

[22] N. C. Thompson, J. Stinnett-Donnelly, N. Habel, B. Benson, J. H. T. Bates, B. E. Sobel, and P. S. Spector, "Improved spatial resolution and electrogram wave direction independence with the use of an orthogonal electrode configuration," *Journal of Clinical Monitoring and Computing*, vol. 28, no. 2, pp. 157–163, Sep. 2013.

[23] C. H. Luo and Y. Rudy, "A model of the ventricular cardiac action potential. Depolarization, repolarization, and their interaction." *Circulation Research*, vol. 68, no. 6, pp. 1501–1526, Jun. 1991.

[24] M. Courtemanche, R. J. Ramirez, and S. Nattel, "Ionic targets for drug therapy and atrial fibrillation-induced electrical remodeling: insights from a mathematical model," *Cardiovasc Res*, vol. 42, no. 2, pp. 477–89, May 1999.

[25] R. Plonsey and R. C. Barr, *Bioelectricity a Quantitative Approach*, 3rd ed. Springer Science, 2007.

[26] M. Haissaguerre, P. Jais, D. C. Shah, A. Takahashi, M. Hocini, G. Quiniou, S. Garrigue, A. Le Mouroux, P. Le Métayer, and J. Clementy, "Spontaneous initiation of atrial fibrillation by ectopic beats originating in the pulmonary veins." *The New England journal of medicine*, vol. 339, no. 10, pp. 659–666, Sep. 1998.

[27] V. G. Fast and A. G. Kléber, "Role of wavefront curvature in propagation of cardiac impulse," *Cardiovascular Research*, vol. 33, no. 2, pp. 258–271, Feb. 1997.

[28] P. Sanders, J. B. Morton, N. C. Davidson, S. J. Spence, J. K. Vohra, P. B. Sparks, and J. M. Kalman, "Electrical remodeling of the atria in congestive heart failure: electrophysiological and electroanatomic mapping in humans." *Circulation*, vol. 108, no. 12, pp. 1461–1468, Sep. 2003.

[29] M. K. Stiles, B. John, C. X. Wong, P. Kuklik, A. G. Brooks, D. H. Lau, H. Dimitri, K. C. Roberts-Thomson, L. Wilson, P. De Sciscio, G. D. Young, and P. Sanders, "Paroxysmal lone atrial fibrillation is associated with an abnormal atrial substrate,"

Journal of the American College of Cardiology, vol. 53, no. 14, pp. 1182–1191, Apr. 2009.

[30] M. S. Spach and P. C. Dolber, "Relating extracellular potentials and their derivatives to anisotropic propagation at a microscopic level in human cardiac muscle. Evidence for electrical uncoupling of side-to-side fiber connections with increasing age." *Circulation Research*, vol. 58, no. 3, pp. 356–371, Mar. 1986.

[31] A. G. Kléber and Y. Rudy, "Basic mechanisms of cardiac impulse propagation and associated arrhythmias." *Physiological Reviews*, vol. 84, no. 2, pp. 431–488, Apr. 2004.

[32] B. B. Punske, Q. Ni, R. L. Lux, R. S. MacLeod, P. R. Ershler, T. J. Dustman, M. J. Allison, and B. Taccardi, "Spatial methods of epicardial activation time determination in normal hearts," *Annals of Biomedical Engineering*, vol. 31, no. 7, pp. 781–792, mar 2003.

[33] P. V. P. Bayly, B. H. B. KenKnight, J. M. J. Rogers, R. E. R. Hillsley, R. E. R. Ideker, and W. M. W. Smith, "Estimation of conduction velocity vector fields from epicardial mapping data." *Biomedical Engineering, IEEE Transactions on*, vol. 45, no. 5, pp. 563–571, May 1998.

[34] R. MacLeod and J. Blauer, "Atrial fibrillation," in *Multimodal Cardiovascular Imaging: Principles and Clinical Applications*, O. Pahlm and G. Wagner, Eds. McGraw-Hill, 2011, pp. 420–431.

[35] National Center for Health Statistics, "Deaths: final data for 2013," pp. 1–71, Dec. 2014.

[36] B. Hille, *Ion Channels of Excitable Membranes*, 3rd ed. Sinauer Associates Inc., 2001.

[37] D. M. Bers, "Calcium cycling and signaling in cardiac myocytes," *Annual Review of Physiology*, vol. 70, no. 1, pp. 23–49, Mar. 2008.

[38] H. J. Witchel, "Drug-induced hERG block and long QT syndrome." *Cardiovascular Therapeutics*, vol. 29, no. 4, pp. 251–259, Aug. 2011.

[39] M. H. Draper and M. Mya-Tu, "A comparison of the conduction velocity in cardiac tissues of various mammals." *Quarterly Journal of Experimental Physiology and Cognate Medical Sciences*, vol. 44, no. 1, pp. 91–109, Jan. 1959.

[40] T. Sano, N. Takayama, and T. Shimamoto, "Directional difference of conduction velocity in the cardiac ventricular syncytium studied by microelectrodes." *Circulation Research*, vol. 7, no. 2, pp. 262–267, Mar. 1959.

[41] D. E. Roberts, L. T. Hersh, and A. M. Scher, "Influence of cardiac fiber orientation on wavefront voltage, conduction velocity, and tissue resistivity in the dog." *Circulation Research*, vol. 44, no. 5, pp. 701–712, May 1979.

[42] Y. Kanzaki, F. Terasaki, M. Okabe, S. Fujita, T. Katashima, K. Otsuka, and N. Ishizaka, "Three-dimensional architecture of cardiomyocytes and connective tissue in human heart revealed by scanning electron microscopy." *Circulation*, vol. 122, no. 19, pp. 1973–1974, Nov. 2010.

[43] D. DiFrancesco, "Funny channels in the control of cardiac rhythm and mode of action of selective blockers," *Pharmacological Research*, vol. 53, no. 5, pp. 399–406, May 2006.

[44] H. F. Brown, D. DiFrancesco, and S. J. Noble, "How does adrenaline accelerate the heart?" *Nature*, vol. 280, no. 5719, pp. 235–236, Jul. 1979.

[45] D. DiFrancesco and C. Tromba, "Acetylcholine inhibits activation of the cardiac hyperpolarizing-activated current,i f," *Pflügers Archiv : European journal of physiology*, vol. 410, no. 1-2, pp. 139–142, 1987.

[46] P. A. Iaizzo. (2015, apr) Atlas of human cardiac anatomy. [Online]. Available: http://www.vhlab.umn.edu/atlas/

[47] E. J., "Observations of the physiology of purkinje tissue." *Am J Physiol.*, vol. 30, pp. 395–419, 1912.

[48] A. P. De Carvalho, W. C. De Mello, and B. F. Hoffman, "Electrophysiological evidence for specialized fiber types in rabbit atrium." *The American journal of physiology*, vol. 196, no. 3, pp. 483–488, Mar. 1959.

[49] R. H. Anderson, M. J. Janse, F. J. van Capelle, J. Billette, A. E. Becker, and D. Durrer, "A combined morphological and electrophysiological study of the atrioventricular node of the rabbit heart." *Circulation Research*, vol. 35, no. 6, pp. 909–922, Dec. 1974.

[50] M. A. McGuire, J. M. de Bakker, J. T. Vermeulen, A. F. Moorman, P. Loh, B. Thibault, J. L. Vermeulen, A. E. Becker, and M. J. Janse, "Atrioventricular junctional tissue. Discrepancy between histological and electrophysiological characteristics." *Circulation*, vol. 94, no. 3, pp. 571–577, Aug. 1996.

[51] K. P. Anderson, R. Walker, P. Urie, P. R. Ershler, R. L. Lux, and S. V. Karwandee, "Myocardial electrical propagation in patients with idiopathic dilated cardiomyopathy." *The Journal of clinical investigation*, vol. 92, no. 1, pp. 122–140, Jul. 1993.

[52] A. P. Henriquez, R. Vogel, B. J. Muller-Borer, C. S. Henriquez, R. Weingart, and W. E. Cascio, "Influence of dynamic gap junction resistance on impulse propagation in ventricular myocardium: a computer simulation study." *Biophysical Journal*, vol. 81, no. 4, pp. 2112–2121, Oct. 2001.

[53] G. R. Mines, "On circulating excitations in heart muscles and their possible relation to tachycardia and fibrillation," *Transactions of the Royal Society of Canada*, vol. 8, pp. 43–52, 1914.

[54] A. C. Linnenbank, J. M. T. de Bakker, and R. Coronel, "How to measure propagation velocity in cardiac tissue: a simulation study." *Frontiers in physiology*, vol. 5, p. 267, 2014.

[55] T. J. Herron, P. Lee, and J. Jalife, "Optical imaging of voltage and calcium in cardiac cells & tissues," *Circulation Research*, vol. 110, no. 4, pp. 609–623, Feb. 2012.

[56] B. J. Boukens and I. R. Efimov, "A century of optocardiography," *IEEE Reviews in Biomedical Engineering*, vol. 7, pp. 115–125, May 2014.

[57] M. S. Spach, R. C. BARR, G. A. SERWER, J. M. Kootsey, and E. A. JOHNSON, "Extracellular potentials related to intracellular action potentials in the dog purkinje system," *Circulation Research*, vol. 30, no. 5, pp. 505–519, May 1972.

[58] R. E. Ideker, W. M. Smith, S. M. Blanchard, S. L. Reiser, E. V. Simpson, P. D. Wolf, and N. D. Danieley, "The Assumptions of isochronal cardiac mapping." *Pacing and clinical electrophysiology : PACE*, vol. 12, no. 3, pp. 456–478, Mar. 1989.

[59] R. Coronel, F. J. Wilms-Schopman, J. R. de Groot, M. J. Janse, F. J. van Capelle, and J. M. de Bakker, "Laplacian electrograms and the interpretation of complex ventricular activation patterns during ventricular fibrillation." *Journal of Cardiovascular Electrophysiology*, vol. 11, no. 10, pp. 1119–1128, Oct. 2000.

[60] P. A. Wolf, R. D. Abbott, and W. B. Kannel, "Atrial fibrillation as an independent risk factor for stroke: the Framingham Study." *Stroke; a journal of cerebral circulation*, vol. 22, no. 8, pp. 983–988, Aug. 1991.

[61] C. T. January and J. M. Riddle, "Early afterdepolarizations: mechanism of induction and block. A role for L-type Ca2+ current." *Circulation Research*, vol. 64, no. 5, pp. 977–990, May 1989.

[62] J. Zeng and Y. Rudy, "Early afterdepolarizations in cardiac myocytes: mechanism and rate dependence." *Biophysical Journal*, vol. 68, no. 3, pp. 949–964, Mar. 1995.

[63] S. M. Pogwizd, K. Schlotthauer, L. Li, W. Yuan, and D. M. Bers, "Arrhythmogenesis and contractile dysfunction in heart failure: Roles of sodium-calcium exchange, inward rectifier potassium current, and residual beta-adrenergic responsiveness." *Circulation Research*, vol. 88, no. 11, pp. 1159–1167, Jun. 2001.

[64] H. J. Wellens, K. I. Lie, and D. Durrer, "Further observations on ventricular tachycardia as studied by electrical stimulation of the heart. Chronic recurrent ventricular tachycardia and ventricular tachycardia during acute myocardial infarction." *Circulation*, vol. 49, no. 4, pp. 647–653, Apr. 1974.

[65] M. E. Josephson, L. N. Horowitz, A. Farshidi, and J. A. Kastor, "Recurrent sustained ventricular tachycardia. 1. Mechanisms." *Circulation*, vol. 57, no. 3, pp. 431–440, Mar. 1978.

[66] J. M. de Bakker, F. J. van Capelle, M. J. Janse, A. A. Wilde, R. Coronel, A. E. Becker, K. P. Dingemans, N. M. van Hemel, and R. N. Hauer, "Reentry as a Cause of Ventricular Tachycardia in Patients with Chronic Ischemic Heart Disease: Electrophysiologic and Anatomic Correlation." *Circulation*, vol. 77, no. 3, pp. 589–606, Mar. 1988.

[67] G. W. H. Bailey, B. A. Braniff, E. W. Hancock, and K. E. Cohn, "Relation of left atrial pathology to atrial fibrillation in mitral valvular disease," *Annals of Internal Medicine*, vol. 69, no. 1, pp. 13–20, Jul. 1968.

[68] J. T. Bigger and B. N. Goldreyer, "The mechanism of supraventricular tachycardia." *Circulation*, vol. 42, no. 4, pp. 673–688, Oct. 1970.

[69] M. E. Josephson and J. A. Kastor, "Supraventricular tachycardia: mechanisms and management." *Annals of internal medicine*, vol. 87, no. 3, pp. 346–358, Sep. 1977.

[70] B. N. Goldreyer and A. N. Damato, "The essential role of atrioventricular conduction delay in the initiation of paroxysmal supraventricular tachycardia." *Circulation*, vol. 43, no. 5, pp. 679–687, May 1971.

[71] M. A. Allessie, F. I. M. BONKE, and F. J. G. SCHOPMAN, "Circus movement in rabbit atrial muscle as a mechanism of tachycardia," *Circulation Research*, vol. 33, no. 1, pp. 54–62, Jul. 1973.

[72] M. A. Allessie, F. I. Bonke, and F. J. Schopman, "Circus movement in rabbit atrial muscle as a mechanism of tachycardia. II. The role of nonuniform recovery of excitability in the occurrence of unidirectional block, as studied with multiple microelectrodes." *Circulation Research*, vol. 39, no. 2, pp. 168–177, Aug. 1976.

[73] ——, "Circus movement in rabbit atrial muscle as a mechanism of tachycardia. III. The "leading circle" concept: a new model of circus movement in cardiac tissue without the involvement of an anatomical obstacle." *Circulation Research*, vol. 41, no. 1, pp. 9–18, Jul. 1977.

[74] J. L. Smeets, M. A. Allessie, W. J. Lammers, F. I. Bonke, and J. Hollen, "The wavelength of the cardiac impulse and reentrant arrhythmias in isolated rabbit atrium. The role of heart rate, autonomic transmitters, temperature, and potassium." *Circulation Research*, vol. 58, no. 1, pp. 96–108, Jan. 1986.

[75] S. B. Knisley and B. C. Hill, "Effects of bipolar point and line stimulation in anisotropic rabbit epicardium: assessment of the critical radius of curvature for longitudinal block," *Biomedical Engineering, IEEE Transactions on*, vol. 42, no. 10, pp. 957–966, Oct. 1995.

[76] W. Einthoven, "The string salvanometer and the human electrocardiogram," *KNAW Proceedings*, 1903.

[77] ——, "The different forms of the human electrocardiogram and their signification." *The Lancet*, vol. 179, no. 4622, pp. 853–861, Mar. 1912.

[78] F. N. Wilson, F. D. Johnston, A. G. Macleod, and P. S. Barker, "Electrocardiograms that represent the potential variations of a single electrode," *American heart journal*, vol. 9, no. 4, pp. 447–458, Apr. 1934.

[79] W. G. Stevenson and K. Soejima, "Recording techniques for clinical electrophysiology." *Journal of Cardiovascular Electrophysiology*, vol. 16, no. 9, pp. 1017–1022, Sep. 2005.

[80] U. B. Tedrow and W. G. Stevenson, "Recording and interpreting unipolar electrograms to guide catheter ablation," *Heart Rhythm*, vol. 8, no. 5, pp. 791–796, May 2011.

[81] K. L. K. Venkatachalam, J. E. J. Herbrandson, and S. J. Asirvatham, "Signals and signal processing for the electrophysiologist: part II: signal processing and artifact." *Circulation: Arrhythmia and Electrophysiology*, vol. 4, no. 6, pp. 974–981, Dec. 2011.

[82] K. Otomo, K. Uno, H. Fujiwara, M. Isobe, and Y. Iesaka, "Local unipolar and bipolar electrogram criteria for evaluating the transmurality of atrial ablation lesions at different catheter orientations relative to the endocardial surface," *Heart Rhythm*, vol. 7, no. 9, pp. 1291–1300, Sep. 2010.

[83] C. B. Brunckhorst, E. Delacretaz, K. Soejima, W. H. Maisel, P. L. Friedman, and W. G. Stevenson, "Impact of changing activation sequence on bipolar electrogram amplitude for voltage mapping of left ventricular infarcts causing ventricular tachycardia," *J Interv Card Electrophysiol*, vol. 12, no. 2, pp. 137–41, Mar 2005.

[84] M. J. Janse, F. J. van Capelle, H. Morsink, A. G. Kléber, F. Wilms-Schopman, R. Cardinal, C. N. d'Alnoncourt, and D. Durrer, "Flow of "injury" current and patterns of excitation during early ventricular arrhythmias in acute regional myocardial ischemia in isolated porcine and canine hearts. Evidence for two different arrhythmogenic mechanisms." *Circulation Research*, vol. 47, no. 2, pp. 151–165, Aug. 1980.

[85] P. D. White and L. E. Viko, "Clinical observations of heart block," *Am. J. M. Sc.*, vol. 165, no. 5, pp. 659–666, May 1923.

[86] M. W., "ber die unvollstndige Strung der Erregungsberleitung zwischen Vorhof und Kammer des menschlichen Herzens [On the partial block of impulse conduction between atrium and ventricle of human hearts]." *Z Gesamte Exp Med.*, vol. 41, pp. 180–237, 1924.

[87] J. Morganroth, "Premature ventricular complexes. Diagnosis and indications for therapy." *JAMA: the journal of the American Medical Association*, vol. 252, no. 5, pp. 673–676, Aug. 1984.

[88] E. Carmeliet, "Cardiac ionic currents and acute ischemia: from channels to arrhythmias." *Physiological Reviews*, vol. 79, no. 3, pp. 917–1017, Jul. 1999.

[89] J. K. Kjekshus, P. R. Maroko, and B. E. Sobel, "Distribution of myocardial injury and its relation to epicardial ST-segment changes after coronary artery occlusion in the dog." *Cardiovascular Research*, vol. 6, no. 5, pp. 490–499, Sep. 1972.

[90] A. G. Kléber, "ST-segment elevation in the electrocardiogram: a sign of myocardial ischemia." *Cardiovascular Research*, vol. 45, no. 1, pp. 111–118, Jan. 2000.

[91] P. J. Zimetbaum and M. E. Josephson, "Use of the electrocardiogram in acute myocardial infarction," *The New England journal of medicine*, vol. 348, no. 10, pp. 933–940, Mar. 2003.

[92] B. Taccardi, "Distribution of heart potentials on the thoracic surface of normal human subjects." *Circulation Research*, vol. 12, pp. 341–352, Apr. 1963.

[93] B. Taccardi, B. B. Punske, R. L. Lux, R. S. MacLeod, P. R. Ershler, T. J. Dustman, and Y. Vyhmeister, "Useful lessons from body surface mapping." *Journal of Cardiovascular Electrophysiology*, vol. 9, no. 7, pp. 773–786, Jul. 1998.

[94] L. Gepstein, G. Hayam, and S. A. Ben-Haim, "A novel method for nonfluoroscopic catheter-based electroanatomical mapping of the heart. In vitro and in vivo accuracy results." *Circulation*, vol. 95, no. 6, pp. 1611–1622, Mar. 1997.

[95] D. C. Shah, P. Jaïs, M. Haïssaguerre, S. Chouairi, A. Takahashi, M. Hocini, S. Garrigue, and J. Clémenty, "Three-dimensional mapping of the common atrial flutter circuit in the right atrium," *Circulation*, vol. 96, no. 11, pp. 3904–3912, Dec. 1997.

[96] C. Knackstedt, P. Schauerte, and P. Kirchhof, "Electro-anatomic mapping systems in arrhythmias," *Europace*, vol. 10, no. Supplement 3, pp. iii28–iii34, Nov. 2008.

[97] F. Del Carpio Munoz, T. L. Buescher, and S. J. Asirvatham, "Three-dimensional mapping of cardiac arrhythmias: what do the colors really mean?" *Circulation: Arrhythmia and Electrophysiology*, vol. 3, no. 6, pp. e6–e11, Dec. 2010.

[98] K. Nademanee, J. McKenzie, E. Kosar, M. Schwab, B. Sunsaneewitayakul, T. Vasavakul, C. Khunnawat, and T. Ngarmukos, "A new approach for catheter ablation of atrial fibrillation: mapping of the electrophysiologic substrate," *J Am Coll Cardiol*, vol. 43, no. 11, pp. 2044–53, Jun 2004.

[99] S. M. Narayan, D. E. Krummen, K. Shivkumar, P. Clopton, W.-J. Rappel, and J. M. Miller, "Treatment of atrial fibrillation by the ablation of localized sources: Confirm (conventional ablation for atrial fibrillation with or without focal impulse and rotor modulation) trial," *J Am Coll Cardiol*, vol. 60, no. 7, pp. 628–36, Aug 2012.

[100] Y. Rudy and J. R. Silva, "Computational biology in the study of cardiac ion channels and cell electrophysiology." *Quarterly reviews of biophysics*, vol. 39, no. 1, pp. 57–116, Feb. 2006.

[101] E. J. Vigmond, R. Weber dos Santos, A. J. Prassl, M. Deo, and G. Plank, "Solvers for the cardiac bidomain equations." *Progress in Biophysics and Molecular Biology*, vol. 96, no. 1-3, pp. 3–18, Jan. 2008.

[102] R. L. Winslow, S. Cortassa, B. O'Rourke, Y. L. Hashambhoy, J. J. Rice, and J. L. Greenstein, "Integrative modeling of the cardiac ventricular myocyte." *Wiley interdisciplinary reviews. Systems biology and medicine*, vol. 3, no. 4, pp. 392–413, Jul. 2011.

[103] C. H. Luo and Y. Rudy, "A model of the ventricular cardiac action potential. Depolarization, repolarization, and their interaction." *Circulation Research*, vol. 68, no. 6, pp. 1501–1526, Jun. 1991.

[104] ——, "A dynamic model of the cardiac ventricular action potential. II. Afterdepolarizations, triggered activity, and potentiation." *Circulation Research*, vol. 74, no. 6, pp. 1097–1113, Jun. 1994.

[105] R. M. Shaw and Y. Rudy, "Ionic mechanisms of propagation in cardiac tissue. Roles of the sodium and L-type calcium currents during reduced excitability and decreased gap junction coupling." *Circulation Research*, vol. 81, no. 5, pp. 727–741, Nov. 1997.

[106] A. L. HODGKIN and A. F. HUXLEY, "A quantitative description of membrane current and its application to conduction and excitation in nerve." *The Journal of physiology*, vol. 117, no. 4, pp. 500–544, Aug. 1952.

[107] J. Cooper, R. J. Spiteri, and G. R. Mirams, "Cellular cardiac electrophysiology modeling with Chaste and CellML." *Frontiers in physiology*, vol. 5, p. 511, Jan. 2015.

[108] R. Plonsey, "Bioelectric sources arising in excitable fibers (ALZA lecture)." *Annals of Biomedical Engineering*, vol. 16, no. 6, pp. 519–546, 1988.

[109] A. E. Pollard, N. Hooke, and C. S. Henriquez, "Cardiac propagation simulation." *Critical reviews in biomedical engineering*, vol. 20, no. 3-4, pp. 171–210, 1992.

[110] K. McDowell, F. Vadakkumpadan, R. Blake, J. Blauer, G. Plank, R. MacLeod, and N. Trayanova, "Methodology for patient-specific modeling of atrial fibrosis as a substrate for atrial fibrillation," *Journal of Electrocardiology*, 2012.

[111] K. S. McDowell, F. Vadakkumpadan, R. Blake, J. Blauer, G. Plank, R. S. MacLeod, and N. A. Trayanova, "Mechanistic inquiry into the role of tissue remodeling in fibrotic lesions in human atrial fibrillation," *Biophysical journal*, vol. 104, no. 12, pp. 2764–2773, 2013.

[112] K. S. McDowell, S. Zahid, F. Vadakkumpadan, J. Blauer, R. S. MacLeod, and N. A. Trayanova, "Virtual electrophysiological study of atrial fibrillation in fibrotic remodeling." *PLoS ONE*, vol. 10, no. 2, p. e0117110, 2015.

[113] A. Neic, M. Liebmann, E. Hoetzl, L. Mitchell, E. J. Vigmond, G. Haase, and G. Plank, "Accelerating cardiac bidomain simulations using graphics processing units." *IEEE Transactions on Biomedical Engineering*, vol. 59, no. 8, pp. 2281–2290, Aug. 2012.

[114] A. S. Go, D. Mozaffarian, V. L. Roger, E. J. Benjamin, J. D. Berry, W. B. Borden, D. M. Bravata, S. Dai, E. S. Ford, C. S. Fox, S. Franco, H. J. Fullerton, C. Gillespie, S. M. Hailpern, J. A. Heit, V. J. Howard, M. D. Huffman, B. M. Kissela, S. J. Kittner, D. T. Lackland, J. H. Lichtman, L. D. Lisabeth, D. Magid, G. M. Marcus, A. Marelli, D. B. Matchar, D. K. McGuire, E. R. Mohler, C. S. Moy, M. E. Mussolino, G. Nichol, N. P. Paynter, P. J. Schreiner, P. D. Sorlie, J. Stein, T. N. Turan, S. S. Virani, N. D. Wong, D. Woo, M. B. Turner, and on behalf of the American Heart Association Statistics Committee and Stroke Statistics Subcommittee, "Heart disease and stroke statistics–2013 update: a report from the American Heart Association," *Circulation*, vol. 127, no. 1, pp. e6–e245, Jan. 2013.

[115] A. S. Go, E. M. Hylek, K. A. Phillips, Y. Chang, L. E. Henault, J. V. Selby, and D. E. Singer, "Prevalence of diagnosed atrial fibrillation in adults: national implications for rhythm management and stroke prevention: the AnTicoagulation and Risk Factors In Atrial Fibrillation (ATRIA) study," *JAMA: the journal of the American Medical Association*, vol. 285, no. 18, pp. 2370–2375, May 2001.

[116] M. H. Kim, S. S. Johnston, B.-C. Chu, M. R. Dalal, and K. L. Schulman, "Estimation of total incremental health care costs in patients with atrial fibrillation in the United States." *Circulation: Cardiovascular Quality and Outcomes*, vol. 4, no. 3, pp. 313–320, May 2011.

[117] D. G. Wyse, I. C. Van Gelder, P. T. Ellinor, A. S. Go, J. M. Kalman, S. M. Narayan, S. Nattel, U. Schotten, and M. Rienstra, "Lone atrial fibrillation: does it exist?" *Journal of the American College of Cardiology*, vol. 63, no. 17, pp. 1715–1723, May 2014.

[118] W. Evans and P. Swann, "Lone auricular fibrillation." *Heart*, vol. 16, no. 2, pp. 189–194, Apr. 1954.

[119] F. N. Brand, R. D. Abbott, W. B. Kannel, and P. A. Wolf, "Characteristics and prognosis of lone atrial fibrillation. 30-year follow-up in the Framingham Study." *JAMA: the journal of the American Medical Association*, vol. 254, no. 24, pp. 3449–3453, Dec. 1985.

[120] S. L. Kopecky, B. J. Gersh, M. D. McGoon, J. P. Whisnant, D. R. Holmes, D. M. Ilstrup, and R. L. Frye, "The natural history of lone atrial fibrillation. A population-based study over three decades." *The New England journal of medicine*, vol. 317, no. 11, pp. 669–674, Sep. 1987.

[121] E. M. Kallergis, C. A. Goudis, and P. E. Vardas, "Atrial fibrillation: A progressive atrial myopathy or a distinct disease?" *International Journal of Cardiology*, vol. 171, no. 2, pp. 126–133, Feb. 2014.

[122] V. Fuster, L. E. Rydén, D. S. Cannom, H. J. Crijns, A. B. Curtis, K. A. Ellenbogen, J. L. Halperin, J.-Y. Le Heuzey, G. N. Kay, J. E. Lowe, S. B. Olsson, E. N. Prystowsky, J. L. Tamargo, and S. Wann, "ACC/AHA/ESC 2006 Guidelines for the management of patients with atrial fibrillation—executive summary: a report of the American College of Cardiology/American Heart Association Task Force on practice guidelines and the European Society of Cardiology Committee for practice guidelines (Writing committee to revise the 2001 guidelines for the management of patients with atrial fibrillation) developed in collaboration with the European Heart Rhythm Association and the Heart Rhythm Society," *Journal of the American College of Cardiology*, vol. 48, no. 4, pp. 854–906, Aug. 2006.

[123] B. P. Knight, G. F. Michaud, S. A. Strickberger, and F. Morady, "Electrocardiographic differentiation of atrial flutter from atrial fibrillation by physicians." *Journal of Electrocardiology*, vol. 32, no. 4, pp. 315–319, Oct. 1999.

[124] C. Pappone, S. Rosanio, G. Oreto, M. Tocchi, F. Gugliotta, G. Vicedomini, A. Salvati, C. Dicandia, P. Mazzone, V. Santinelli, S. Gulletta, and S. Chierchia, "Circumferential radiofrequency ablation of pulmonary vein ostia: A new anatomic approach for curing atrial fibrillation." *Circulation*, vol. 102, no. 21, pp. 2619–2628, Nov. 2000.

[125] H. Oral, B. P. Knight, H. Tada, M. Ozaydin, A. Chugh, S. Hassan, C. Scharf, S. W. K. Lai, R. Greenstein, F. Pelosi, S. A. Strickberger, and F. Morady, "Pulmonary vein isolation for paroxysmal and persistent atrial fibrillation." *Circulation*, vol. 105, no. 9, pp. 1077–1081, Mar. 2002.

[126] N. F. N. Marrouche, T. T. Dresing, C. C. Cole, D. Bash, E. E. Saad, K. K. Balaban, S. V. S. Pavia, R. R. Schweikert, W. W. Saliba, A. A. Abdul-Karim, E. E. Pisano, R. R. Fanelli, P. P. Tchou, and A. A. Natale, "Circular mapping and ablation of the pulmonary vein for treatment of atrial fibrillation: impact of different catheter technologies." *Journal of the American College of Cardiology*, vol. 40, no. 3, pp. 464–474, Aug. 2002.

[127] N. F. Marrouche, "Phased-array intracardiac echocardiography monitoring during pulmonary vein isolation in patients with atrial fibrillation: impact on outcome and complications," *Circulation*, vol. 107, no. ¿21, pp. 2710–2716, Jun. 2003.

[128] M. C. Wijffels, C. J. Kirchhof, R. Dorland, and M. A. Allessie, "Atrial fibrillation begets atrial fibrillation. A study in awake chronically instrumented goats." *Circulation*, vol. 92, no. 7, pp. 1954–1968, Oct. 1995.

[129] C. W. White, R. E. Kerber, H. R. Weiss, and M. L. Marcus, "The effects of atrial fibrillation on atrial pressure-volume and flow relationships." *Circulation Research*, vol. 51, no. 2, pp. 205–215, Aug. 1982.

[130] C. A. Morillo, G. J. Klein, D. L. Jones, and C. M. Guiraudon, "Chronic rapid atrial pacing. Structural, functional, and electrophysiological characteristics of a new model of sustained atrial fibrillation." *Circulation*, vol. 91, no. 5, pp. 1588–1595, Mar. 1995.

[131] M. C. Wijffels, C. J. Kirchhof, R. Dorland, J. Power, and M. A. Allessie, "Electrical remodeling due to atrial fibrillation in chronically instrumented conscious goats: roles of neurohumoral changes, ischemia, atrial stretch, and high rate of electrical activation." *Circulation*, vol. 96, no. 10, pp. 3710–3720, Nov. 1997.

[132] U. Schotten, "Electrical and contractile remodeling during the first days of atrial fibrillation go hand in hand," *Circulation*, vol. 107, no. 10, pp. 1433–1439, Mar. 2003.

[133] L. Yue, J. Feng, R. Gaspo, G. R. Li, Z. Wang, and S. Nattel, "Ionic remodeling underlying action potential changes in a canine model of atrial fibrillation." *Circulation Research*, vol. 81, no. 4, pp. 512–525, Oct. 1997.

[134] L. Polontchouk, J. A. Haefliger, B. Ebelt, T. Schaefer, D. Stuhlmann, U. Mehlhorn, F. Kuhn-Regnier, E. R. De Vivie, and S. Dhein, "Effects of chronic atrial fibrillation on gap junction distribution in human and rat atria." *Journal of the American College of Cardiology*, vol. 38, no. 3, pp. 883–891, Sep. 2001.

[135] K. Sawa, G. Klein, Z. Szalay, S. Hein, E. P. Bauer, and J. Shaper, "Structural correlate of atrial fibrillation in human patients," *Cardiovascular Research*, vol. 54, pp. 361–379, 2002.

[136] M. Wilhelm, W. Kirste, S. Kuly, K. Amann, W. Neuhuber, M. Weyand, W. G. Daniel, and C. Garlichs, "Atrial distribution of connexin 40 and 43 in patients with intermittent, persistent, and postoperative atrial fibrillation." *Heart, lung & circulation*, vol. 15, no. 1, pp. 30–37, Feb. 2006.

[137] B. Burstein and S. Nattel, "Atrial fibrosis: mechanisms and clinical relevance in atrial fibrillation." *Journal of the American College of Cardiology*, vol. 51, no. 8, pp. 802–809, Feb. 2008.

[138] H. R. L. Fraser and R. W. D. Turner, "Auricular fibrillation," *British Medical Journal*, vol. 2, no. 4953, pp. 1414–1418, Dec. 1955.

[139] W. L. Henry, J. Morganroth, A. S. Pearlman, C. E. Clark, D. R. Redwood, S. B. Itscoitz, and S. E. Epstein, "Relation between echocardiographically determined left atrial size and atrial fibrillation." *Circulation*, vol. 53, no. 2, pp. 273–279, Feb. 1976.

[140] B. M. Psaty, T. A. Manolio, L. H. Kuller, R. A. Kronmal, M. Cushman, L. P. Fried, R. White, C. D. Furberg, and P. M. Rautaharju, "Incidence of and risk factors for atrial fibrillation in older adults." *Circulation*, vol. 96, no. 7, pp. 2455–2461, Oct. 1997.

[141] U. Schotten, H.-R. Neuberger, and M. A. Allessie, "The role of atrial dilatation in the domestication of atrial fibrillation," *Progress in Biophysics and Molecular Biology*, vol. 82, no. 1-3, pp. 151–162, May 2003.

[142] A. J. Sanfilippo, V. M. Abascal, M. Sheehan, L. B. Oertel, P. Harrigan, R. A. Hughes, and A. E. Weyman, "Atrial enlargement as a consequence of atrial fibrillation. A prospective echocardiographic study." *Circulation*, vol. 82, no. 3, pp. 792–797, Sep. 1990.

[143] B. D. Hoit, "Left atrial size and function," *Journal of the American College of Cardiology*, vol. 63, no. 6, pp. 493–505, Feb. 2014.

[144] P. R. Schvartzman and R. D. White, "Giant left atrium." *Circulation*, vol. 104, no. 6, pp. E28–9, Aug. 2001.

[145] J. W. Hurst, "Memories of patients with a giant left atrium." *Circulation*, vol. 104, no. 22, pp. 2630–2631, Nov. 2001.

[146] A. Boldt, "Fibrosis in left atrial tissue of patients with atrial fibrillation with and without underlying mitral valve disease," *Heart*, vol. 90, no. 4, pp. 400–405, Apr. 2004.

[147] J. Jalife and K. Kaur, "Atrial remodeling, fibrosis, and atrial fibrillation," *Trends in Cardiovascular Medicine*, pp. 1–10, Feb. 2015.

[148] S. Verheule, E. Tuyls, A. Gharaviri, S. Hulsmans, A. van Hunnik, M. Kuiper, J. Serroyen, S. Zeemering, N. H. L. Kuijpers, and U. Schotten, "Loss of continuity in the thin epicardial layer because of endomysial fibrosis increases the complexity of atrial fibrillatory conduction." *Circulation: Arrhythmia and Electrophysiology*, vol. 6, no. 1, pp. 202–211, Feb. 2013.

[149] T. J. Bunch and J. D. Day, "Adverse remodeling of the left atrium in patients with atrial fibrillation: when is the tipping point in which structural changes become permanent?" *Journal of Cardiovascular Electrophysiology*, pp. n/a–n/a, May 2015.

[150] W. J. Manning and D. I. Silverman, "Atrial anatomy and function postcardioversion: insights from transthoracic and transesophageal echocardiography." *Progress in Cardiovascular Diseases*, vol. 39, no. 1, pp. 33–46, Jul. 1996.

[151] P. Reant, S. Lafitte, P. Jaïs, K. Serri, R. Weerasooriya, M. Hocini, X. Pillois, J. Clémenty, M. Haïssaguerre, and R. Roudaut, "Reverse remodeling of the left cardiac chambers after catheter ablation after 1 year in a series of patients with isolated atrial fibrillation." *Circulation*, vol. 112, no. 19, pp. 2896–2903, Nov. 2005.

[152] N. F. Marrouche, D. Wilber, G. Hindricks, P. Jaïs, N. Akoum, F. Marchlinski, E. Kholmovski, N. Burgon, N. Hu, L. Mont, T. Deneke, M. Duytschaever, T. Neumann, M. Mansour, C. Mahnkopf, B. Herweg, E. Daoud, E. Wissner, P. Bansmann, and J. Brachmann, "Association of atrial tissue fibrosis identified by delayed enhancement MRI and atrial fibrillation catheter ablation: the DECAAF study." *JAMA*, vol. 311, no. 5, pp. 498–506, Feb. 2014.

[153] G. Malasana, J. D. DAY, J. P. Weiss, B. G. Crandall, T. L. Bair, H. T. May, J. S. Osborn, J. L. Anderson, J. B. Muhlestein, D. L. Lappe, J. Nelson, and T. J. BUNCH, "A strategy of rapid cardioversion minimizes the significance of early recurrent atrial tachyarrhythmias after ablation for atrial fibrillation." *Journal of Cardiovascular Electrophysiology*, vol. 22, no. 7, pp. 761–766, Jul. 2011.

[154] T. J. Bunch, H. T. May, T. L. Bair, D. L. Johnson, J. P. Weiss, B. G. Crandall, J. S. Osborn, J. L. Anderson, J. B. Muhlestein, D. L. Lappe, and J. D. DAY, "Increasing time between first diagnosis of atrial fibrillation and catheter ablation adversely affects long-term outcomes." *Heart Rhythm*, vol. 10, no. 9, pp. 1257–1262, Sep. 2013.

[155] S. Nattel, "New ideas about atrial fibrillation 50 years on," *Nature*, vol. 415, no. 6868, pp. 219–226, 2002.

[156] M. Vaquero, D. Calvo, and J. Jalife, "Cardiac fibrillation: from ion channels to rotors in the human heart." *Heart Rhythm*, vol. 5, no. 6, pp. 872–879, Jun. 2008.

[157] A. C. Skanes, R. Mandapati, O. Berenfeld, J. M. Davidenko, and J. Jalife, "Spatiotemporal periodicity during atrial fibrillation in the isolated sheep heart." *Circulation*, vol. 98, no. 12, pp. 1236–1248, Sep. 1998.

[158] G. K. MOE and J. A. Abildskov, "Atrial fibrillation as a self-sustaining arrhythmia independent of focal discharge," *American heart journal*, vol. 58, no. 1, pp. 59–70, Jul. 1959.

[159] M. Allessie, W. Lammers, F. Bonke, and J. Hollen, "Experimental evaluation of moes multiple wavelet hypothesis of atrial fibrillation." in *Cardiac Electrophysiology and Arrhythmias*, J. Jalife and D. P. Zipes, Eds. Orlando: Grune & Stratton, 1985, pp. 265–275.

[160] K. T. Konings, C. J. Kirchhof, J. R. Smeets, H. J. Wellens, O. C. Penn, and M. A. Allessie, "High-density mapping of electrically induced atrial fibrillation in humans." *Circulation*, vol. 89, no. 4, pp. 1665–1680, Apr. 1994.

[161] G. Y. H. Lip and D. A. Lane, "Stroke prevention in atrial fibrillation: a systematic review." *JAMA*, vol. 313, no. 19, pp. 1950–1962, May 2015.

[162] W. Haverkamp, A. Martinez-Rubio, C. Hief, A. Lammers, S. Mühlenkamp, T. Wichter, G. Breithardt, and M. Borggrefe, "Efficacy and safety of d,l-sotalol in patients with ventricular tachycardia and in survivors of cardiac arrest." *Journal of the American College of Cardiology*, vol. 30, no. 2, pp. 487–495, Aug. 1997.

[163] S. H. Hohnloser, "Proarrhythmia with class III antiarrhythmic drugs: types, risks, and management." *The American journal of cardiology*, vol. 80, no. 8A, pp. 82G–89G, Oct. 1997.

[164] W. Haverkamp, G. Breithardt, A. J. Camm, M. J. Janse, M. R. Rosen, C. Antzelevitch, D. Escande, M. Franz, M. Malik, A. Moss, and R. Shah, "The potential for QT prolongation and pro-arrhythmia by non-anti-arrhythmic drugs: clinical and regulatory implications. Report on a Policy Conference of the European Society of Cardiology." *Cardiovascular Research*, pp. 219–233, Aug. 2000.

[165] D. G. Wyse, A. L. Waldo, J. P. DiMarco, M. J. Domanski, Y. Rosenberg, E. B. Schron, J. C. Kellen, H. L. Greene, M. C. Mickel, J. E. Dalquist, S. D. Corley, and Atrial Fibrillation Follow-up Investigation of Rhythm Management (AFFIRM) Investigators, "A comparison of rate control and rhythm control in patients with atrial fibrillation." *The New England journal of medicine*, vol. 347, no. 23, pp. 1825–1833, Dec. 2002.

[166] M. C. E. F. Wijffels and H. J. G. M. Crijns, "Rate versus rhythm control in atrial fibrillation." *Cardiology clinics*, vol. 22, no. 1, pp. 63–69, Feb. 2004.

[167] J. L. Cox, T. E. Canavan, R. B. Schuessler, M. E. Cain, B. D. Lindsay, C. Stone, P. K. Smith, P. B. Corr, and J. P. Boineau, "The surgical treatment of atrial fibrillation. II. Intraoperative electrophysiologic mapping and description of the electrophysiologic basis of atrial flutter and atrial fibrillation." *The Journal of Thoracic and Cardiovascular Surgery*, vol. 101, no. 3, pp. 406–426, Mar. 1991.

[168] S. M. Prasad, H. S. Maniar, C. J. Camillo, R. B. Schuessler, J. P. Boineau, T. M. Sundt III, J. L. Cox, and R. J. Damiano Jr, "The Cox maze III procedure for atrial fibrillation: long-term efficacy in patients undergoing lone versus concomitant procedures," *The Journal of Thoracic and Cardiovascular Surgery*, vol. 126, no. 6, pp. 1822–1827, Dec. 2003.

[169] I. M. Robbins, E. V. Colvin, T. P. Doyle, W. E. Kemp, J. E. Loyd, W. S. McMahon, and G. N. Kay, "Pulmonary vein stenosis after catheter ablation of atrial fibrillation." *Circulation*, vol. 98, no. 17, pp. 1769–1775, Oct. 1998.

[170] H.-S. Mun, B. Joung, J. Shim, H. J. Hwang, J. Y. Kim, M.-H. Lee, and H.-N. Pak, "Does additional linear ablation after circumferential pulmonary vein improve clinical outcome in patients with paroxysmal atrial fibrillation? Prospective randomised study," *Heart*, pp. heartjnl–2011–301 107, Jan. 2012.

[171] J. J. Blauer, D. Swenson, K. Higuchi, G. Plank, R. Ranjan, N. Marrouche, and R. S. MacLeod, "Sensitivity and specificity of substrate mapping: an in silico framework for the evaluation of electroanatomical substrate mapping strategies," *Journal of Cardiovascular Electrophysiology*, 2014.

[172] J. Blauer, F. Han, R. Ranjan, N. Marrouche, and R. MacLeod, "Controlled activation for interrogation of the electrophysiological substrate," in *Computing in Cardiology, 2014*, vol. 41. IEEE, 2014, pp. 189–192.

[173] M. J. Schalij, W. J. Lammers, R. P. L, and A. M. A, "Anisotropic conduction and reentry in perfused epicardium of rabbit left ventricle," *Am J Physiol*, vol. 263, pp. H1466–1478, 1992.

[174] R. Wilders, M. B. Wagner, D. A. Golod, R. Kumar, Y. G. Wang, W. N. Goolsby, R. W. Joyner, and H. J. Jongsma, "Effects of anisotropy on the development of cardiac arrhythmias associated with focal activity." *Pflüg Arch Eur J Physiol*, vol. 441, no. 2-3, pp. 301–312, Dec. 2000.

[175] B. Taccardi, E. Macchi, R. L. Lux, P. R. Ershler, S. Spaggiari, S. Baruffi, and Y. Vyhmeister, "Effect of myocardial fiber direction on epicardial potentials." *Circulation*, vol. 90, no. 6, pp. 3076–90, Dec. 1994.

[176] M. S. Spach, W. T. r. Miller, D. B. Geselowitz, R. C. Barr, J. M. Kootsey, and E. A. Johnson, "The discontinuous nature of propagation in normal canine cardiac muscle. Evidence for recurrent discontinuities of intracellular resistance that affect the membrane currents." *Circulation Research*, vol. 48, no. 1, pp. 39–54, Jan. 1981.

[177] M. Delmar, D. C. Michaels, T. Johnson, and J. Jalife, "Effects of increasing intercellular resistance on transverse and longitudinal propagation in sheep epicardial muscle." *Circulation Research*, vol. 60, no. 5, pp. 780–785, May 1987.

[178] C. de Diego, F. Chen, Y. Xie, R. K. Pai, L. Slavin, J. Parker, S. T. Lamp, Z. Qu, J. N. Weiss, and M. Valderrbano, "Anisotropic conduction block and reentry in neonatal rat ventricular myocyte monolayers." *Am J Physiol Heart Circ Physiol*, vol. 300, no. 1, pp. H271–8, Jan 2011.

[179] M. S. Spach, P. C. Dolber, and J. F. Heidlage, "Influence of the passive anisotropic properties on directional differences in propagation following modification of the sodium conductance in human atrial muscle. A model of reentry based on anisotropic

discontinuous propagation." *Circulation Research*, vol. 62, no. 4, pp. 811–832, Apr. 1988.

[180] A. P. Larsen, K. J. Sciuto, A. P. Moreno, and S. Poelzing, "The voltage-sensitive dye di-4-anepps slows conduction velocity in isolated guinea pig hearts." *Heart Rhythm*, vol. 9, no. 9, pp. 1493–1500, Nov 2012.

[181] R. S. MacLeod, J. G. Stinstra, S. Lew, R. T. Whitaker, D. J. Swenson, M. J. Cole, J. Krger, D. H. Brooks, and C. R. Johnson, "Subject-specific, multiscale simulation of electrophysiology: a software pipeline for image-based models and application examples." *Philos Transact A Math Phys Eng Sci*, vol. 13, no. 367, pp. 2293–310, Jun. 2009.

[182] D. I. Warton, I. J. Wright, D. S. Falster, and M. Westoby, "Bivariate line-fitting methods for allometry." *Biol Rev*, vol. 81, no. 2, pp. 259–91, May 2006.